IMPACT OF ENVIRONMENTAL CONDITIONS ON FIBERGLASS-REINFORCED POLYURETHANE FOAM COMPOSITES

A Thesis
Submitted to the Graduate Faculty
of the
North Dakota State University
of Agriculture and Applied Science

By

Aron Mark Fisk

In Partial Fulfillment of the Requirements
for the Degree of
MASTER OF SCIENCE

Major Department:
Mechanical Engineering

November 2010

Fargo, North Dakota

North Dakota State University
Graduate School

Title

Impact of Environmental Conditions on

Fiberglass Reinforced Polyurethane Foam Composites

By

Aron Fisk

The Supervisory Committee certifies that this ***disquisition*** complies with North Dakota State University's regulations and meets the accepted standards for the degree of

MASTER OF SCIENCE

SUPERVISORY COMMITTEE:

North Dakota State University Libraries Addendum

To protect the privacy of individuals associated with the document, signatures have been removed from the digital version of this document.

Date

Signature

ABSTRACT

Fisk, Aron Mark, M.S., Department of Mechanical Engineering, College of Engineering and Architecture, North Dakota State University, November 2010. Impact of Environmental Conditions on Fiberglass-reinforced Polyurethane Foam Composites. Major Professor: Dr. Chad A. Ulven.

Incorporating reinforcement within a polymer (i.e. composite) can obtain substantial performance increases. However, composites may be susceptible to conditions that could have a significant impact on their performance. The objective of this study was to characterize SpaceAge Synthetics (SAS) fiberglass-reinforced rigid, closed-cell polyurethane foam (PU) after subjected to various environmental conditions.

SAS composites were characterized as a function of material composition after conditioned to extreme temperatures, moisture, ultraviolet irradiation (UV), or a combination thereof. The experimental process involved accelerated conditioning to further induce property changes and assure long-term integrity.

Empirical expressions for SAS composites were generated to represent performance changes for different environmental conditions. Increasing temperature 93 °C from ambient showed an 18% decrease in strength and 24% decrease in stiffness for a 450 kg/m^3 foam density reinforced with 7.6% fiber volume fraction. This performance loss resulted from the ductility of the polymer increasing with temperature. Decreasing temperature 68 °C from ambient showed a 56% increase in strength and 26% increase in stiffness. When SAS composites were subjected to moisture at room temperature, no statistical difference was observed after being exposed to 100% RH for 72 h duration. These mechanical performance analyses included varying material parameters such as: foam density, fiber content, void content, and thickness. The addition of heat to the 100% RH moisture drastically reduced mechanical performance up to 33% in strength and 22% in stiffness.

Ultraviolet irradiation caused chemical changes within the SAS composites, which was first noted by the pronounced color shift within the yellowness index (YI). Additional reinforcement near the surface created a 269% lower shift in YI. It was observed that initially cross-linking occurred while at the same time chain scission was occurring at a larger rate. Fourier Transform Infrared Spectroscopy proved that UV penetrated 0.25 mm within the surface, showing the effects occur mainly on the surface.

Finally, SAS composites exhibited a 31% increase in strength and a 12% increase in stiffness with a post cure process. Post curing for 4 h at 100 °C raised the glass transition temperature from 119 °C to 128 °C. The performance increase was attributed from the post cure process inducing additional cross-linking within polymer chains.

ACKNOWLEDGMENTS

To my adviser, Dr. Chad A. Ulven, I want to express my appreciation for his valuable advice, assistance, and continuous guidance throughout this research project and in the preparation of this thesis. It was an honor being his graduate student.

My sincere appreciation is also extended to Dr. Ghodrat Karami, Dr. Fardad Azarmi, and Dr. Scott Pryor. I thank all of them for the assistance, advice, time contribution to this committee, and efforts for reading and correcting the thesis.

I must thank Heidi Docktor, Dr. Venkata S. Chevali, and other members of our research group for the lab and equipment help within this project. I would also like to thank SpaceAge Synthetics for the materials and financial support of this research project.

Special thanks must be given to my parents, Mark and Julie Fisk, for their love, sincere support, and understanding that made the fulfillment of this work possible.

TABLE OF CONTENTS

LIST OF TABLES

LIST OF FIGURES

CHAPTER 1. INTRODUCTION

Polyurethane (PU) foam has a vast range of applications due to its many different forms. It can be formed into an open cell structure, being more flexible and resilient, or a closed-cell structure molded into rigid parts [1]. This versatility in properties has led to a rapid increase in the use of PU, making it a common material in many applications. Polyurethane can be either a thermoset or thermoplastic, with thermosets being more essential [1]. Thermoplastic and thermoset PU differ where thermoplastics have covalent bonds joining atoms together in the polymer chains, whereas thermosets have covalent bonds joining the atoms together and polymer chains [1]. This additional joined polymer chains is known as cross-linking. For that reason, a thermoset PU will be more rigid than a thermoplastic PU by further restricting the long-range molecular motion, which also increases the glass transition temperature.

The polymerization process of polymeric materials introduces reversible and irreversible effects due to the exothermic reaction, chemical changes during processing, and mismatch in coefficients of thermal expansion of the constituents [2]. The processing could also induce residual stresses and warpage. After fabrication, polymer materials operate in a variety of environmental conditions that could have pronounced impact on their performance [2]. It is imperative for polymers to retain critical properties during use, and therefore one needs to know how the environmental conditions impact the polymeric material. Environmental factors influencing the mechanical behavior of PU foam could be correlated to hot/cold temperatures, moisture, ultraviolet (UV) light, mechanical loads, and combinations thereof [1,9]. These conditions can degrade the polymer similarly to corrosion in metals. The effects are significant on some polymers and minimal on others, because there are many underlying factors in which the polymer responds to various environmental conditions [1].

1.1. Scope of the Study

This study investigates closed-cell, rigid PU foam as the matrix material for fiberglass-reinforced polymer matrix composites. A composite consists of two or more distinct constituents having considerably different properties. These different constituent material properties provide significantly different properties to the composite [3]. One of the phases is typically stiffer and stronger which is called the reinforcement, whereas the less stiff and weaker phase is usually known as the matrix [2]. Manmade composites occurred early as the Israelites using straw-reinforced clay bricks as recorded in the book of Exodus in the Old Testament [3].

In this work, environmental conditions were investigated with fiberglass-reinforced rigid PU foam through means of mechanical experimentation. The composite materials were characterized after being exposed to moisture, UV light, extreme temperatures, or a combination of all three. Polyurethane foam density, panel thickness, and reinforcement orientation were varied to identify the effects various environmental conditions have on performance as a function of exposure duration or temperature. Fourier transform infrared spectroscopy (FTIR), differential scanning caliorimetry (DSC), and thermal gravimetric analysis (TGA) were used to characterize the degree of degradation of the composite, glass transition temperature, degree of cure, and decomposition temperature.

The characterization process involved accelerated testing to further induce property changes and assure long-term integrity [4]. For SAS, it is crucial to formulate products that can withstand weathering and light exposure. Accelerated weathering and light stability tests are widely used for research and development, quality control, and material classification. These accelerated tests provide a means of fast and reproducible results [5] to characterize long term exposure.

This research topic arose from U.S. Navy / SpaceAge Synthetics Spartan Scout project. SpaceAge Synthetics (SAS) subcontracts some of the testing, material characterization, and

design to North Dakota State University. The project involves designing and testing of parts that have the potential to be used by the U.S. Navy in the Spartan Scout, an unmanned vessel shown in Figure 1. The problem with the Spartan Scout is that the weight of the vessel is too heavy for the cranes on the carrier to lift the vessel into the sea. SpaceAge Synthetics materials integrate lightweight structures while having high specific strength and stiffness. It is these strong, lightweight structures that give the advantage to be used in the Navy over many existing monolithic structures, where the intention is to reduce weight while maintaining strength and integrity.

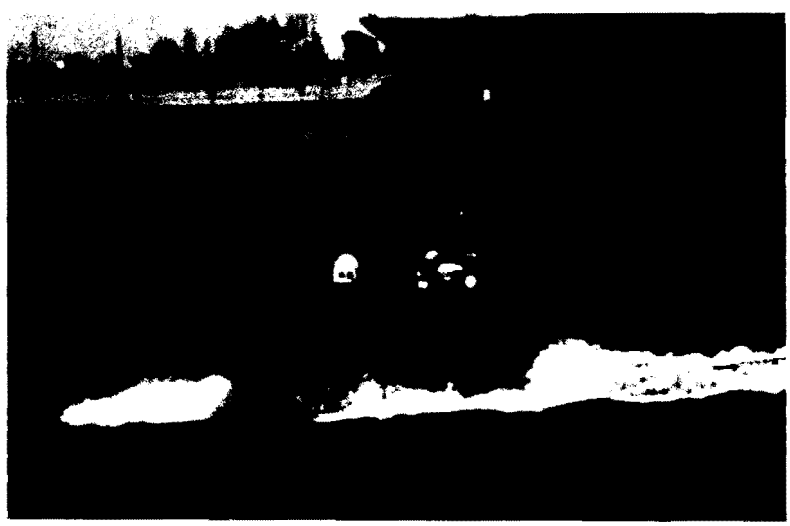

Figure 1: Navy USV Spartan Scout [6].

In order to ensure sure SAS materials will remain structurally sound during use, testing has to be executed to fully characterize the performance of the PU foam reinforced with fiberglass. As the Spartan Scout is at sea, the vessel will come in contact with moisture (humidity, salt water), extreme temperatures, UV light exposure, and combinations of each. Therefore, the importance to study SAS material under natural, environmental operating conditions is crucial.

1.2. SpaceAge Synthetic's Polyurethane Foam

The materials were supplied from SAS, located in Fargo, ND. The rigid PU foam product line offers several densities, compositions, and thickness options to suit various applications that require a water-resistant, lightweight, high strength core. The material exhibits exceptional specific strength and stiffness, while being tough, rot-resistant, and buoyant, all while maintaining excellent structural stability. The SAS composite can be used to replace plywood in many applications where it has superior properties. The product can be found in bus flooring, ice rinks, marine use, etc. [7]. Being able to reduce weight while maintaining excellent properties provides a huge advantage; making the material an excellent choice for new, advanced structures for use in marine applications.

Incorporating fiberglass into the rigid PU foam gives far superior mechanical performance compared with the neat foam. The idea is that the reinforcement carries much of the load, but because of the reinforcement's small cross-sectional diameter, the fibers cannot be loaded directly or transmit load from one to another. The addition of the matrix material allows the limitations to be overcome. The matrix binds the fibers together, transfers load between fibers, and protects against environmental conditions. The matrix also has a strong influence on some of the composite's mechanical properties including: transverse modulus and strength, shear properties, and compressive properties [8].

1.3. Composite Composition

The degradation of rigid PU foam composite material may transpire because of several factors: loss of strength of the fibers, loss of interfacial bond strength, chemical degradation of the matrix material, temperature effects on the modulus and strength of the matrix material, and accelerated degradation as a combination of more than one factor [8]. Factors that can also influence the strength and stiffness of composites are misorientation

of fibers, fibers of nonuniform strength, discontinuous fibers, interfacial conditions, and residual stresses [8].

Polymer matrix composites are more susceptible to high temperatures, prolonged exposure to UV light, and moisture than compared with metal matrix or ceramic matrix composites [3]. Composite properties can be influenced to a larger extent over the polymer matrix or reinforcement material alone since environmental conditions influence the fibers, matrix, and interface simultaneously. The degradation of the composite occurs as an interaction between the constituents along with each of the individual components [8]. In general, the polymer matrix is more vulnerable to degradation than the reinforcement. This leads to matrix-dominated properties (i.e. out-of-plane tensile strength) of the composite being more susceptible to environmental conditions than reinforcement dominated properties (i.e. in-plane tensile strength) [3].

Composite materials allow tailoring of properties for a particular design purpose. One can change the amount of reinforcement, reinforcement orientation, type of reinforcement, and processing technique. This versatility of controlling the anisotropy can be used to create a infinite number of unique designs and optimization for several constraints, such as weight, cost, and strength. Increasing the fiber content will increase the fiber-dominated properties until the matrix can no longer fully surround the fibers. As the fiber content increases, the matrix-dominated properties will slightly decrease as a result of less matrix content. However, additional reinforcement has a larger influence on the fiber-dominated properties than the matrix-dominated properties. One disadvantage of more reinforcement is the greater chance of processing difficulties. Another disadvantage of additional reinforcement is that the cost of the composite could increase which is not the case with SAS materials.

The fiber content will influence the amount of moisture uptake that can occur throughout a structure. Depending on the matrix and interfacial bond, the amount of fiber

content could increase or decrease the maximum saturation level and diffusion rate. As the fiber content increases, the maximum moisture saturation level will decrease, assuming a perfect bond and impermeable fibers. This emphasizes the matrix material being the driving factor for moisture diffusion. With less matrix material, there is less material to absorb the moisture, assuming the fibers are impermeable, which is not the case if natural fibers are used as the reinforcement. On the other hand, in some studies the water percentage has been found to increase slightly with fiber content [9]. The additional fibers allow for more "water wicking" along the interface of the fibers and matrix which will increase moisture absorption.

Most reinforcement fibers used in polymer matrix composites do not show dependence with temperature in normal operating temperature ranges. Therefore, the changes in the composite's mechanical properties with temperature are driven mainly by the changes within the polymer matrix material, which is much more sensitive to temperature variations [10]. However, temperature influence is not only limited to matrix-dominated properties. The composite can also experience significant changes in mechanical performance in fiber-dominated properties [10].

The mechanical response of composites not only depends on the fiber content, but also the architecture of the reinforcement. This reinforcement architecture can be found in many different forms from fibers (> 5 mm), whiskers (< 5 mm) , or particles (aspect ratio ~ 1) [11]. Each form has its own unique applications with fibers being the most common form and the most superior properties. Whiskers' mechanical properties are lower than that of the fibers due to the load not being fully transferred between whiskers and because of end effects [11]. Particles have the lowest mechanical properties and are generally used as a filler to reduce cost, reduce shrinkage, control viscosity, and improve stiffness [8]. Long fiber composites have attributed to many major innovations in the modern era. Fibers are materials that have a long length compared to the cross-section. This relationship between

length and cross-section is called the aspect ratio, which is the ratio of the length to the diameter of a fiber. Reinforcement property enhancement steadily increases with fiber length until a critical aspect ratio is reached and the fiber is considered "continuous" [11].

Besides the reinforcement architecture, the reinforcement material is also found in many different forms. Reinforcements are made from single filaments in a process called spinning. The filaments are than grouped together to form a tow, or "roving" when the reinforcement is fiberglass [11]. Rovings then are used to create a reinforcement fabric, which can be unidirectional, woven, or a non-woven fabric mat. A woven composite consists of interlaced rovings. Typical weave types are shown in Figure 2 and Figure 3.

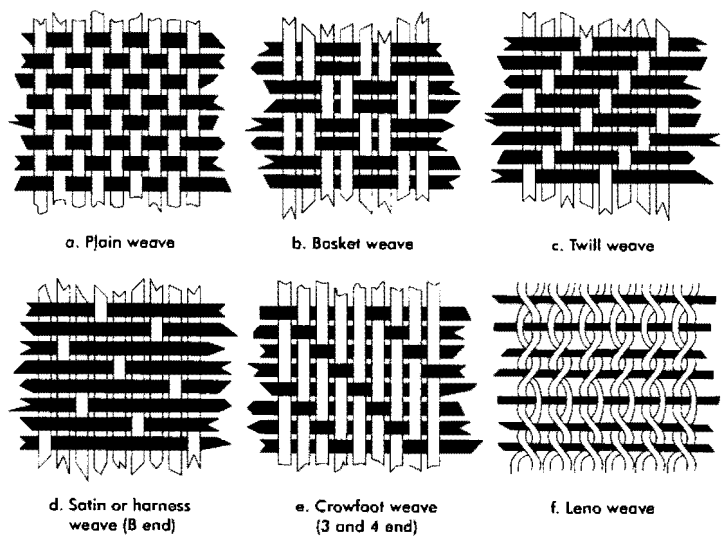

Figure 2: Schematics of woven composites fabrics [11].

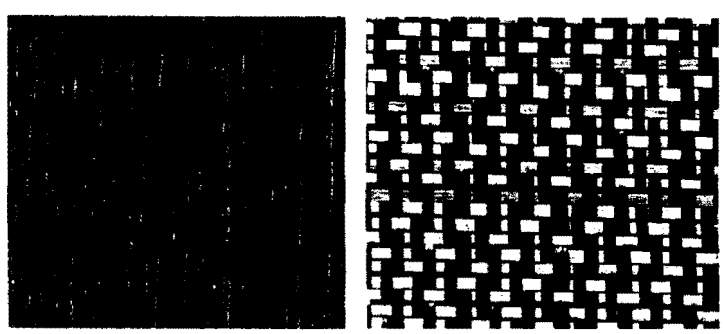

Figure 3: Mats of different weave architecture [12].

The effect of mechanical performance due to various environmental conditions can be related to the weave architecture within the reinforcement on polymer matrix composites. One study examined how the fiber architecture effects the diffusivity of moisture [12]. Both the neat resin and composite exhibited similar diffusion behavior, suggesting moisture diffusion is a matrix-dominated property [13]. The study also determined that the diffusivity is dependent on the fiber architecture but mainly the outer plies of the composite.

A different study showed that woven composites exhibited higher diffusion values versus a unidirectional composite with the same fiber volume fraction [12]. Irregular fiber distribution results in resin-rich regions (low fiber content) and resin-poor regions (high fiber content). The high cluster of fibers yields a very low localized diffusivity. It was also confirmed that flatter tow cross-section results in a lower diffusion rate [12]. This is a result of the weave pattern for flatter tows having smaller matrix pockets which results in a harder diffusion path. Different weave patterns will have a variation of openness, or space between the parallel fibers. The larger the openness will also result in a larger diffusion rate due to creating resin-rich areas.

As void content of the matrix increases, the mechanical performance of the composite will decrease due to less surface interaction. The void content is also directly related to the diffusivity rate and maximum saturation level [14]. As the number of voids increase, more free space for the diffusion of molecules is allowed to occur. The void content dependence is so strong that only 1% void content in a composite can more than double the amount of water absorbed [14]. In addition, the ratio of matrix resin/curing agent plays a role in the amount of moisture uptake. To a lesser degree, the fiber coating has also shown some influence that is related to the matrix/fiber interface [14].

1.4. Marine Grade Composites Previous Studies

The use of composite materials are steadily increasing in the marine industry with the advantages of ease of manufacture of complex forms, rot resistance, corrosion and chemical resistance, high specific strength and stiffness, and low maintenance [15]. Composites also provide the advantage of improved sonic characteristics [16], stealth, payload, range, and stability [17]. Structural sandwich composites have also received a great deal of attention within the marine industry but have been limited mostly to secondary structural applications due to very little research on interfacial fracture toughness under marine service environments [18].

Marine grade composites have been used extensively for structures including hulls, decks, bulkheads, sonar domes, and radomes. Composites are also being tailored and tested for critical components such as masts, submarine control surfaces, transmission shafts and propellers [1, 10] and can be found in life boats, racing yachts, coastal patrol boats, and naval mine-hunting ships [20]. Polyester resins reinforced with fiberglass are the most widely used composites in marine applications [16, 20]. Recently epoxies and vinyl esters are replacing many of the polyester resins due to ageing resistance [16], higher heat-distortion temperature, better water resistance, and better mechanical performance [20]. However, vinyl ester and epoxy are much more expensive, limiting the use to high end applications [16]. Many high performance structures including masts of racing yachts are using carbon fiber/epoxy facesheets in the use of sandwich composites [21].

Experimental testing has been done extensively for many polymer matrix composites. A few examples are: interfacial fracture toughness of PVC core sandwich composites with E-Glass/vinyl ester facesheeet [18], impact damage of fiberglass and Kevlar with a polyester matrix [15], interlaminar fracture toughness of fiber reinforced polymer matrix composites [16], mechanical performance due to post fire on glass reinforced polymer composites [20], delamination behavior of high modulus carbon/epoxy

[21]. There are many studies to determine how the structure can withstand the harsh marine conditions.

The intention of this study was to investigate marine grade materials for use within the Navy/SAS Spartan Scout project. Specifically to interpret how a vast range of environmental conditions impact the fiberglass-reinforced PU foam. In order to carry out the study, a test matrix was established to signify which materials to be tested in various environmental conditions. Once the materials were conditioned, they were tested to distinguish the effects versus a baseline material that was not conditioned.

CHAPTER 2. BACKGROUND/LITERATURE REVIEW

In this chapter, information is provided about the structure of rigid PU foam, along with previous studies showing effects after exposure to temperature, moisture, and UV light. First, the structure of PU foam is described. Next, various environmental conditions will be discussed that can affect the performance of rigid PU foam. Finally, information about a combination of environmental conditions is reviewed including UV radiation and moisture. Previous studies used a neat PU foam material, whereas this study investigated the performance with the PU foam material reinforced with fiberglass. The fiberglass constituent will have varying effects on the performance with different conditioning criteria.

2.1. The Structure of Rigid Polyurethane Foam

The basic chemistry for the formation of PU foam is a three-step process containing two essential components, isocyante and polyol. The variation of the two components is what leads to the vast family of PU polymers exhibiting widely different properties. Polyurethane foam is produced by reacting an isocyanate group ($-N = C = O$) with a polyol containing atow or more hydroxyl groups ($-OH$) [22]. If three or more reactive hydroxyl groups are present, crosslinks can be formed producing a thermoset PU [1].

In order to create the PU foam, the polymer must expand or is "blown" by a chemical reaction creating a gas which forms bubbles. The first step is the reaction of isocyanate with water creating carbamic acid, which is unstable and decomposes forming carbon dioxide gas and an amine. Further reaction of the amine with additional isocyanate gives a disubstituted urea. The polymerization process is an exothermic reaction giving off heat, which in turn, allows the diffusion of carbon dioxide gas to fill and expand the cellular polymer matrix, creating foam [22]. Figure 4 illustrates the polymerization process for PU foam.

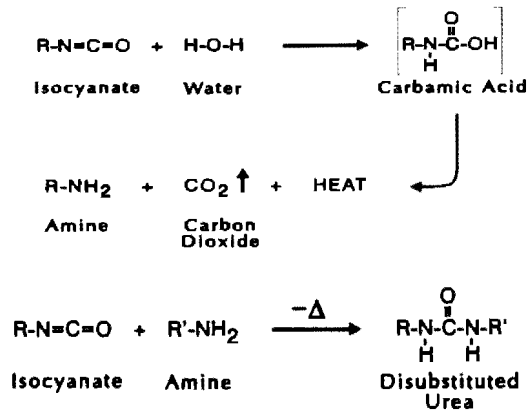

Figure 4: Polyurethane foam chemical reaction [22].

The physical and chemical character, structure, and molecular size of these compounds influence the polymerization reaction and final physical properties of the finished PU. In addition, additives such as catalysts, surfactants, blowing agents, crosslinkers, flame retardants, light stabilizers, and fillers are used to control and modify the reaction process and performance characteristics of the PU [1].

2.2. Temperature Impact

One of the most difficult challenges for composite designers is dealing with short- and long-term effects of temperature on polymer matrix composites [10]. Temperature can drastically change the instantaneous response of the composite, where mechanical, electrical and optical properties can undergo order of magnitude changes over a 100°C temperature change [10]. Strength and failure characteristics, especially interfacial and matrix-dominated properties will vary with temperature [2]. Polymerization processes are a function of the hygrothermal properties of the polymer matrix and the current hygrothermal state. A polymer composite tested today and after 10 years will have different properties and therefore mechanical and thermal responses (for all polymer matricies operated below the glass transition temperature with the exception of fully crystalline polymers) [10]. This

results from the re-arrangement of molecules due to molecular motion, which increases with increasing temperature [10].

2.2.1. Thermal Degradation

Organic materials generally are unstable at elevated temperatures and undergo a chemical breakdown. Generally, the polymer matrix is more susceptible to elevated temperatures than the fibers [8], especially in the case of PU foam and fiberglass. This is due to fiberglass having a higher degradation temperature of approximately 1800°C compared to the PU foam of approximately 290°C.

Polymer matrix composites are commonly exposed to excessive thermal gradients during service that become more detrimental over time. Thermal degradation may not create distinct defects, yet will degrade the matrix gradually, modifying its behavior significantly [23]. The failure of a ductile or brittle material is fundamentally different: brittle failure occurs fast. Material in the brittle state has a lower fracture toughness, low impact strength, and shows minimal signs of damage before failure, whereas ductile failure is more progressive.

The conditions influencing the ductile/brittle aspect of composites can be grouped into two categories. The first category is environmental parameters such as temperature, strain rate, and solvents. The second category influencing the behavior depends on parameters intrinsic to the material: the nature of the polymer matrix, fillers, and fibers [10].

Degradation of polymers is characterized by measuring the amount of volatiles given off by the material as a function of time and temperature or by measuring the loss in mass [3]. This degradation can be seen in Figure 5 of a glass-phenolic composite subjected to various temperatures over a period of time. It is shown that the weight loss increases with temperature and time. For this particular composite, the decomposition temperature is

slightly over 150°C (300°F). The decomposition rate is accelerated with increasing temperature.

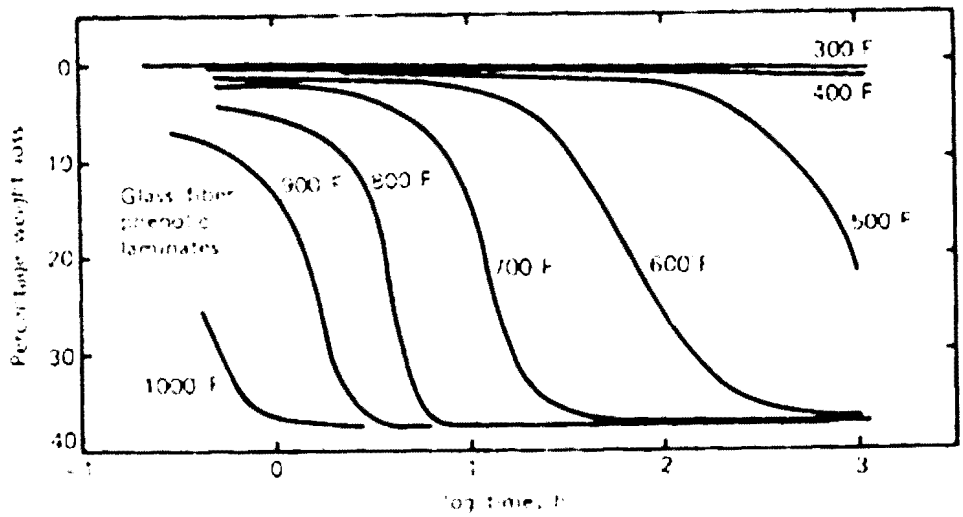

Figure 5: Thermal degradation of glass-phenolic system [8].

2.2.2. Stress-Strain Behavior

The hygrothermal state affects the stress-strain behavior of polymer matrix composites through the change in constituents due to temperature or moisture, and residual stresses due to processing. Temperature effects are most notable in matrix-dominated properties since the fibers are less sensitive than the matrix to extreme temperatures [2]. The effects of temperature on stress-strain behavior of common polymer matrix composites are illustrated in Figure 6 for a carbon/epoxy composite.

The figure shows three carbon/epoxy composites tested at different temperatures of 22, 60, and 128 °C. It is seen that the transverse modulus decreases steadily with an increase in temperature. This is resulted from the higher temperatures allowing more molecular motion within the polymer structure of the epoxy matrix, ultimately increasing the ductility of the carbon/epoxy composite. The trend of decreasing stiffness with an increase of temperature is expected to continue along with a performance decrease of other mechanical properties as well.

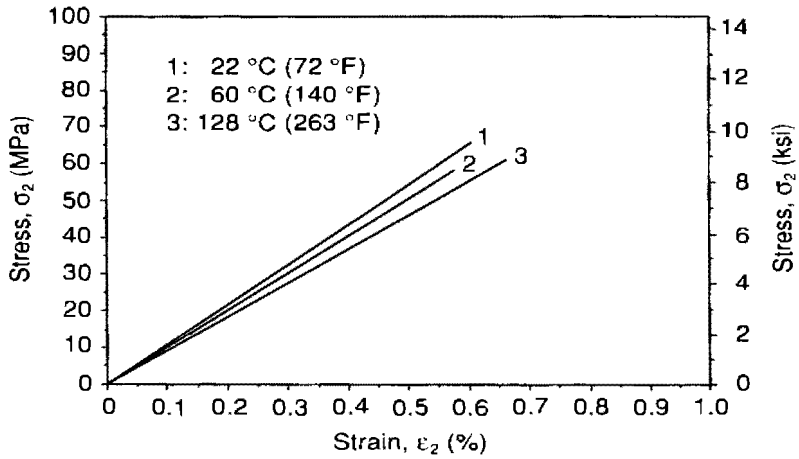

Figure 6: Transverse tensile stress-strain curve for carbon/epoxy composite at various temperatures [2].

Most polymer matrix composites exhibit a drop in tensile modulus with a increase in temperature. The drop can be attributed mainly to the changes in the matrix properties with temperature [2]. A polymer matrix subjected to elevated temperature shows changes in its mechanical properties instantaneously at the molecular level. This change could be large for the composite's transverse properties as stated earlier. However, the influence of temperature is not limited to matrix-dominated properties. Figure 7 shows the composite modulus as a function of temperature. The unidirectional carbon/vinyl ester composite experienced significant changes to the tensile modulus.

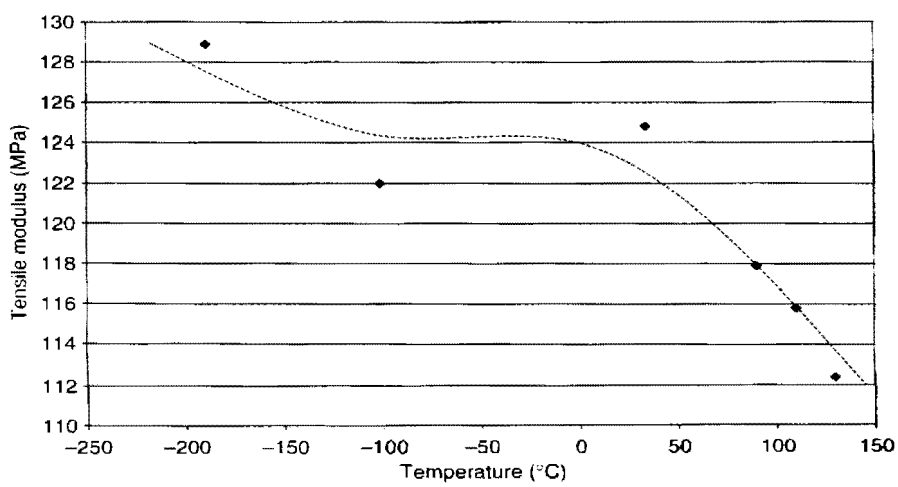

Figure 7: Unidirectional carbon/vinyl ester composite with polyurethane interface tested in longitudinal direction [10].

The modulus versus temperature curve can have different shapes, depending on the nature of the polymer. Figure 8 shows a modulus versus temperature curve for a typical polymer exhibiting a secondary relaxation. The figure is separated into four distinct regions: the glassy state (Region 1), the glass transition region (Region 2), the rubbery stage (Region 3), and the rubbery flow (Region 4).

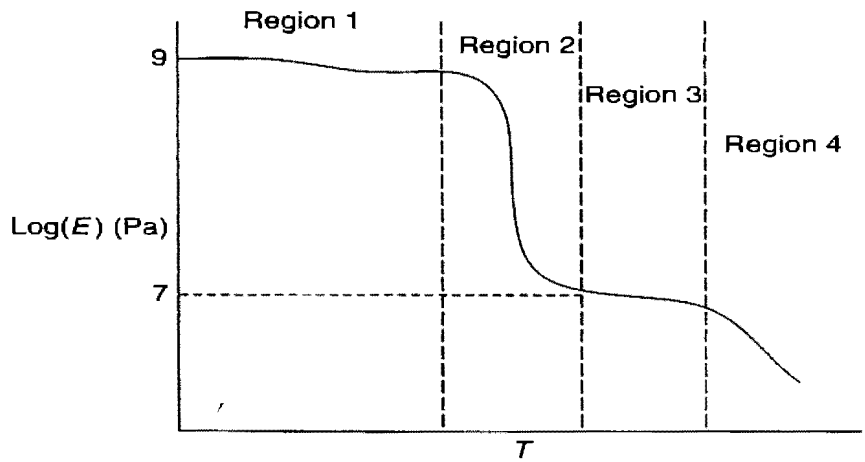

Figure 8: Modulus versus temperature for a typical polymer [10].

The first region of the modulus versus temperature curve is known as the glassy region. This region is characterized by a reasonably constant modulus. The glassy region has restricted molecular motion. The molecules act as if they are frozen and mainly display vibrational motions. The next region is called the glass transition temperature region. This is where the modulus of the material significantly decreases. A steep drop in the polymers instantaneous or storage modulus characterizes the glass transition region. Qualitatively, this region can be interpreted as the onset of long-range molecular motion. The temperature at which this transition temperature occurs depends on the material [10].

The third region is the rubbery stage. This region shows a moderately level modulus and corresponds to the long-range rubber elasticity. As the molecular weight of the polymer increases, the range of the third stage increases [10]. Fibers and fillers also

help hinder the molecular motion within the polymer chains, which increases the modulus and extends the rubbery plateau. A completely crosslinked polymer will extend the rubbery plateau up to the degradation temperature. Figure 9 shows the effect of cross-linking on the modulus as a function of temperature for polyisoprene. The final stage is known as the rubbery flow stage and is characterized by another drastic drop in modulus. If the temperature increases, the material exhibits the properties of a liquid. If the melting temperature for semi-crystalline materials was not reached, the crystalline clusters impart some rigidity to the material and impede the molecular flow along with the fibers [10].

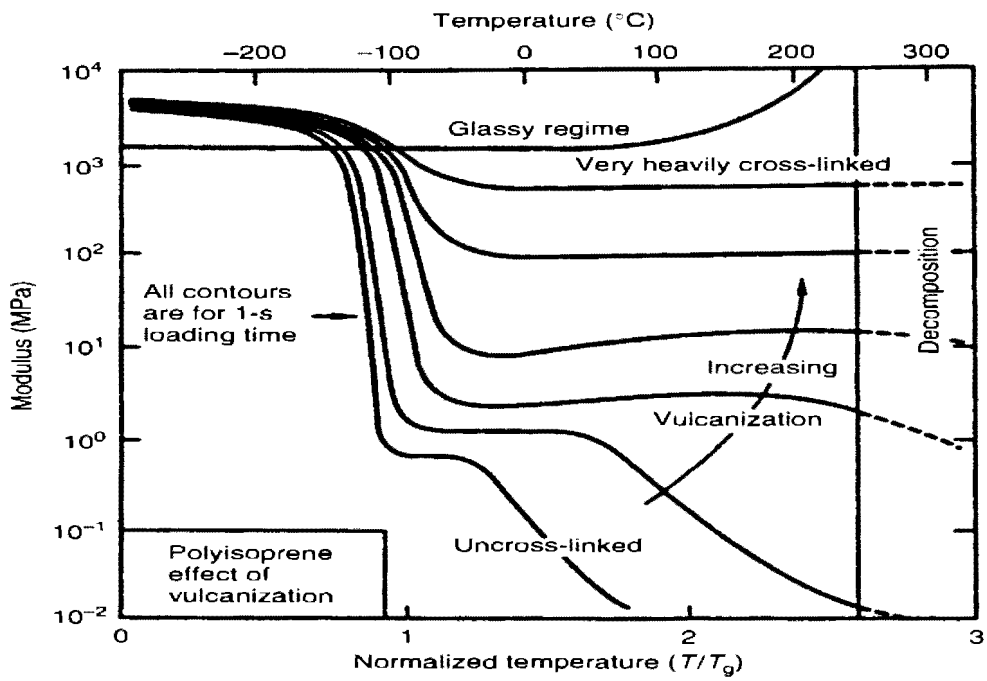

Figure 9: Influence of cross-linking on the modulus versus temperature curve [10].

2.3. Moisture Impact

A critical aspect when using fiber-reinforced polymer matrix composites in various applications is their performance in 'hot-wet' environments. Therefore, moisture absorption in composites is an ongoing research topic. All composites during the life cycle are exposed to moisture present in the ambient air and many composites will experience

contact with water at some point. Water absorption results from three processes: diffusion through the polymer matrix, water wicking of the fiber-matrix interface, and percolating flow [24]. The effect of moisture diffusion can vary the mechanical properties of polymer matrix composites as much as three orders of magnitude [10].

Due to the fact that moisture can cause plasticization of the polymer matrix, alter the stress state, and degrade the fiber/matrix interface [12], understanding of moisture absorption behavior is critical for predicting material and structural performance through the life of the composite. Plasticization is whenever a polymer swells or softens due to a solvent. This swelling permits increased chain movement which makes the plastic material softer and more flexible [1]. Also, as the material absorbs more moisture, the glass transition temperature decreases significantly [25] which relates back to the effects of plasticization.

2.3.1. Fickian Diffusion

Diffusion involves transportation of molecules from one part of the structure to another, or in the case of composites, matter is transferred into the matrix and sometimes into the fibers through random molecular motion [26]. In 1885 Adolf Fick realized the obvious analogy between heat transfer and moisture absorption as both are due to random molecular motions. Fick put the diffusion on a quantitative basis by adopting the mathematical equation of heat conduction derived by Fourier (1822). The theory of diffusion in an isotropic material is based on the hypothesis that the rate of transfer of diffusing substance through unit area is proportional to the concentration gradient measured normal to the section and is as follows:

$$F = -D\frac{\partial C}{\partial x} \qquad (1)$$

where F is the rate of transfer per unit area, C is the concentration of diffusing substance, x is the spatial coordinates measured normal to the section, and D is the diffusion coefficient. Equation 1 above was adapted as Fick's First Law. When considering a rectangular element

of volume, the fundamental differential equation of diffusion in an isotropic medium is derived from Equation 1 as follows:

$$\frac{\partial C}{\partial t} + \frac{\partial F_x}{\partial x} + \frac{\partial F_y}{\partial y} + \frac{\partial F_z}{\partial z} = 0 \qquad (2)$$

with x, y, and z being the coordinate axes, and t is time of exposure, and F is the rate of transfer in the given direction. Assuming a constant diffusion coefficient, F_x, F_y, F_z are given by Equation 1 and Equation 2 becomes Fick's Second Law of Diffusion:

$$\frac{\partial C}{\partial t} = D\frac{\partial^2 C}{\partial x^2} \qquad (3)$$

where x is the distance from one surface to the point of measurement. Fick's Second Law describes how the concentration field changes as a function of time. A concentration-dependent form of Fick's law with constant boundary conditions cannot describe the diffusion behavior of many polymers adequately. This is especially the case of extensive material swelling or with so-called "glassy" polymers, which exhibit "anomalous" or "non-Fickian" behavior. The essential distinction is that polymers in the rubbery state respond rapidly to changes. Anomalous effects can be directly related to the influence of the changing polymer structure on solubility and diffusional mobility. Deviations from Fickian behavior are associated with the finite rates at which the polymer structure changes in response to the sorption/desorption of penetrating molecules [26].

The second mechanism is known as "water wicking" which represents the water molecules flowing in between the fiber and matrix interface conveying water to the interior of the composites. This effect is larger if wetting of the fibers by the matrix is incomplete [24]. Figure 10 is a quarter section of a PU foam board exposed to water for different time durations, showing the distribution of water absorbed. It shows that water is absorbed through the exposed surface area and is transported to the center of the board over time until the material becomes fully saturated.

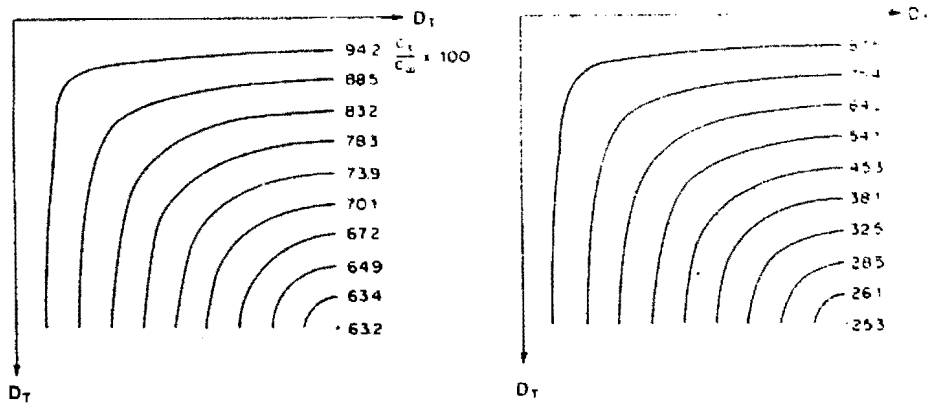

Figure 10: Water absorption profile through midplane of PU sheet
Left: after 100 min, Right: after 50 min [27].

Moisture absorption will affect material properties including tensile strength, shear strength, elastic modulus, fatigue, creep, impact, swelling, and electrical resistance. The strength and modulus will show more significant effects on matrix-dominated composites versus fiber-dominated composites [24]. This is a result of the polymer matrix materials being more sensitive to moisture and temperature than the polymer fibers.

2.3.2. Studying Moisture Absorption

There are different methods of measuring the water absorption of polymers. The water absorption of test specimens can be measured by first measuring the mass of the dry polymer and measuring the mass of the same polymer that has been fully submerged in water for a described immersion time using a mass balance. ASTM Standard D 570 describes this test procedure and can be used for all types of plastics. Another standard, ASTM D 2842, describes the test procedure for water absorption of rigid cellular plastics.

This test measures the buoyant force of the polymer while submerged under water. As more water is absorbed, the buoyant force will decrease and the resulting change in force is related to the mass of absorbed water. The difficulty of the test requires that the specimens be measured while still fully submerged in water but will mitigate the effects of adsorption, or the moisture on the surface of the specimen but not absorbed in the specimen.

A third test uses magnetic resonance spectroscopy and an MRI scanner to track water absorption in PU foam. This test is a non-destructive, three dimensional monitoring of water in PU foams [28]. Small amounts of water can be detected with high sensitivity but the monitoring equipment is very expensive and not accessible to most testing labs. Therefore, magnetic resonance spectroscopy is used very little since there are easier methods with much simpler test setups.

A fourth test (ASTM D 5229) is used to determine moisture absorption/desorption properties in the one, two, or three directions of a Fickian material. It is specified towards polymer matrix composites and is relatively simple to use. The test uses a mass balance to measure the mass before and after exposure to very good accuracy. The diffusivity coefficient of the material can be calculated using the full saturation mass of the material along with the mean moisture content as follows:

$$M(\%) = \frac{W_i - W_o}{W_o} \qquad (4)$$

where $M(\%)$ is the mean amount of absorbed moisture in a material, W_i is the conditioned specimen weight, and W_o is the initial specimen weight. The mean moisture content can be monitored over different time durations to generate absorption/desorption curves and in turn used to determine the material's diffusivity coefficient.

Moisture penetration is largely governed by diffusion followed by "water wicking" along the fiber-matrix interface of a composite. A representation of the interface between the fiber and matrix is shown in Figure 11. The diffusivity value in composites is related to: nature of the polymer, nature and geometry of the reinforcement, environment (concentrations, temperature, pressure, etc.) [10], substance exposed to, manufacturing voids [29], and the interface between the fibers and matrix. Polymers are characterized by the presence of free volume. This assumption is supported by the fact that diffusion in the amorphous phase occurs at a faster rate than in the crystalline phase of the material [10].

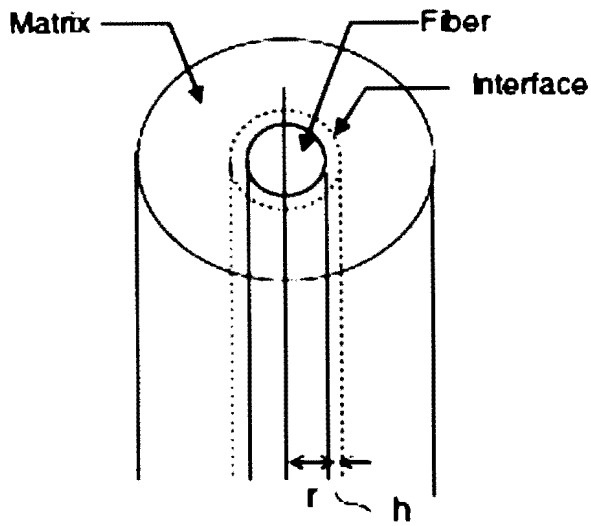

Figure 11: Representation of the interfacial free volume around an imperfectly bonded fiber in a composite [24].

One such study generated numerical models with good accuracy to determine water absorption in a rigid PU foam sheet [30]. The study derived models with a uni-, di-, and tri-dimensional kinetics of water transport through a PU sheet. The conditions consisted of 100% RH, or fully submerged in water, at room temperature. The models generated were variations of Fick's law. The derived theoretical models calculate the amount of water absorbed over an exposure to the moisture and were found by integrating Equation 3, Fick's Second Law, for the concentration of water with respect to volume.

The model is derived over a certain range of initial and boundary conditions that are determined prior to testing. The validity of the models were compared by testing the kinetics of absorption through experimentation with the theoretical values. Figure 12 shows kinetics of absorption of PU foam at 100°C with a one-dimensional transport comparing the calculated and experimental values. It can be seen from the figure that a very good correlation can be achieved from theoretical modeling to experimental test results. The diffusivity coefficient for the material would be calculated in the initial linear portion.

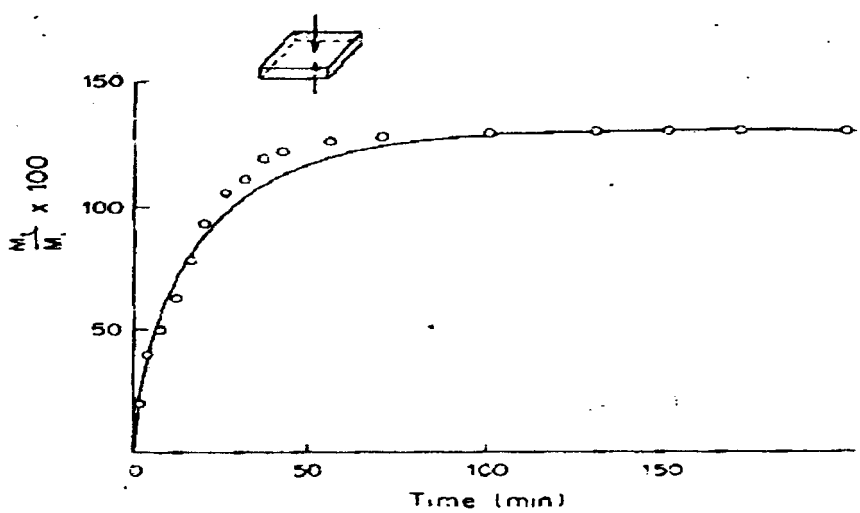

Figure 12: Validity of the kinetics of absorption of PU foam at 100°C with one-dimensional diffusion. —Theoretical, O Experimental [31].

Figure 13 is a plot of the moisture content of water absorbed over the square root of time for both longitudinal and transverse diffusivity. The longitudinal diffusivity corresponds with transportation through the face of the PU sheet where the transverse diffusivity is transportation through the thickness of the PU sheet. The longitudinal and transverse diffusivity values, D, where calculated from the absorption curve using a variation of Fick's Diffusivity equation [27]:

$$D = \pi \left(\frac{h}{4M_\infty}\right)^2 \left(\frac{M_t}{\sqrt{t}}\right)^2 \qquad (5)$$

where h is the thickness of the sheet considered for transport, M_∞ is the fully saturated water mass, and M_t is the mass at a specified time t. The longitudinal diffusivity represents a one dimensional diffusion, whereas the transverse diffusivity represents a two dimensional diffusion. It can be seen that the longitudinal diffusivity is greater than the transverse diffusivity but also contains a much larger surface area to absorb moisture. The affects from longitudinal and transverse diffusion are greatly affected my composite composition, including fiber volume content, fiber orientation, matrix, fiber/matrix interface, etc.

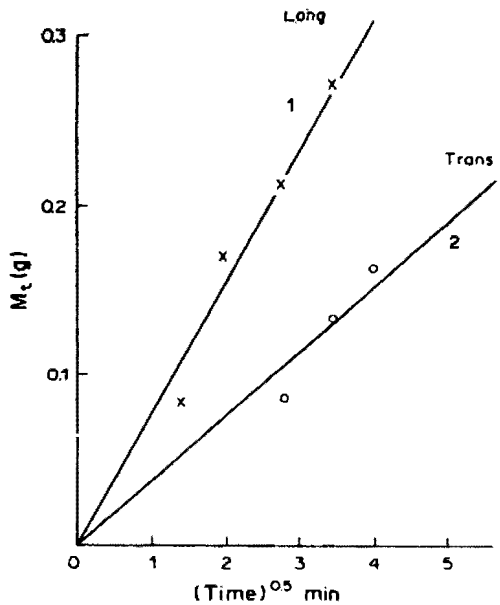

Figure 13: Square root of time dependence of the amount of water absorbed [27].

The given diffusivity coefficient equation needs to be noted that it is a general equation which does not include material parameters. The equation is solved from Fick's Law with given boundary conditions and merely is a basis. It was proven that the transverse diffusivity was approximately 16.7 times larger than the longitudinal diffusivity on an exposed surface area basis. As the composite is exposed to long durations of moisture, the interface tends to "relax" creating more free volume where moisture is able to be stored, increasing the maximum saturation level [24]. This goes to say that interfacial interaction between the fibers and matrix could be significant in the moisture absorption of the structure. Also, moisture absorption/desorption cycling or "fatigue", is a resulting factor in moisture uptake. The diffusion coefficient for each consecutive sorption cycle generally increases, along with the maximum saturation level [24]. The interfacial strength typically decreases due to each of the successive absorption/desorption cycles, allowing for a greater free volume and channels for moisture uptake.

2.4. Ultraviolet Exposure

Polymer matrix composites are widely used in industry due to their specific strength and stiffness, along with other properties. With the extensive use in industry, polymer composites can be subjected to harsh conditions like UV, combination of UV/thermal, and other natural weathering that could affect the mechanical performance of the composite. The natural weathering that could alter or degrade the mechanical properties is known as aging. Thermal aging denotes a change in physical and chemical properties with respect to a point at the end of the cure cycle. Aging does not always involve degradation of the mechanical properties [32], but it is known that PU undergoes significant structural changes on exposure to UV radiation, which causes degradation in their physical and mechanical properties [33-36]. There are physical changes that reflect molecular motion over time (reversible) and chemical changes (irreversible) that alter the structure of the macromolecular lattice (thermal oxidaztion, chain ruptures, post-cross-linking, etc.) [32].

2.4.1. Compositional Change Resulting from Ultraviolet Irradiation

The degradation amount is affected differently for each material due to the chemical structure of the polymer. In addition to thermomechanical stresses, the material is subjected to physical and chemical aging that may degrade the material and alter the residual performance of the structure [32]. The disadvantage to natural outdoor weathering is that it could take several years to obtain meaningful results.

There currently are varieties of accelerated weathering techniques that have been developed to utilize the process of natural weathering but in a reasonable time duration. These accelerated natural environment tests attempt to accelerate the natural environment with higher stress, higher intensity of UV radiation, elevated temperatures, and increased humidity without changing the failure mechanism [36].

2.4.2. *Discoloration Resulting from Ultraviolet Irradiation*

The main visible effects from UV degradation are usually chalky appearance (oxidation), color shift on the surface, and the material's surface becoming brittle which could induce cracks [37]. The effects are predominantly in the surface layer of the material and are unlikely to extend to depths greater than 0.5 mm into the surface. However, stress concentrations can form due to the highly brittle nature of some commodity plastics [37]. The majority of polymers undergo chain scission [1, 32, 33, 35] on exposure to radiation while cross-linking is found to occur in others [32], and a few polymers can undergo both chain scission and cross-linking [36, 38], including PU foam.

Transmission FTIR has been utilized to monitor the initial curing process of a polyurethane coating prior to being subjected to natural weathering. Figure 14 showed it took approximately nine days to cure. This is represented by the drastic reduction in the NCO peak at 2275 cm^{-1}. In addition, there is a slight increase of the band at 3387 cm^{-1} which is attributed to the formation of NH due to polyurethane and polyurea [36].

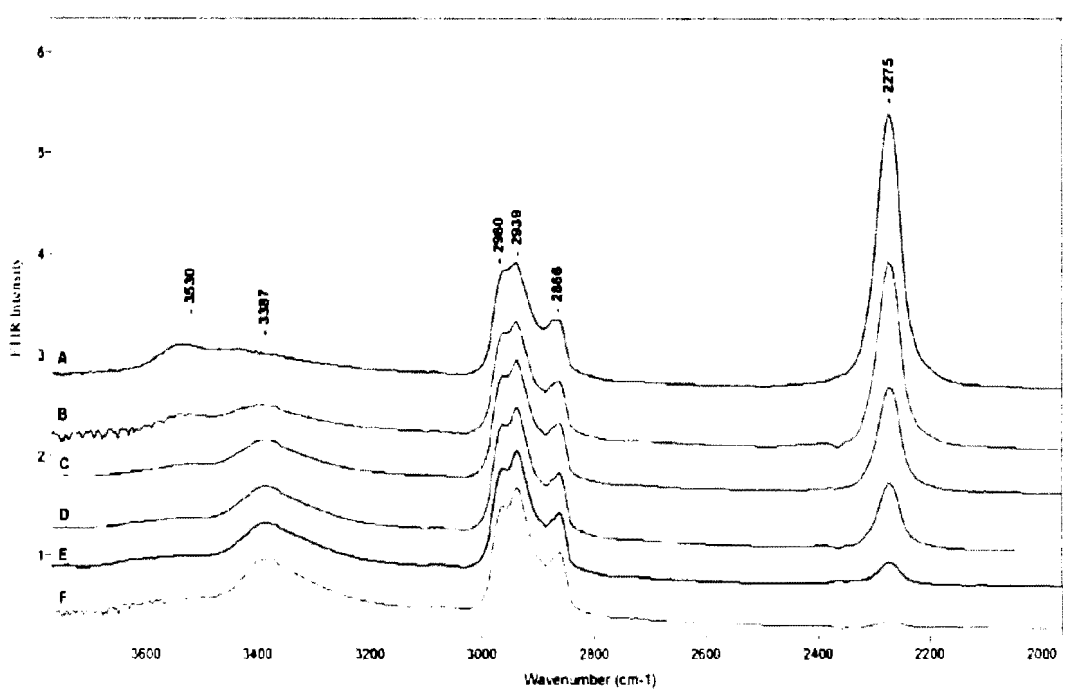

Figure 14: FTIR spectra of the reaction of NCO with polyol as a function of time: A=day 0; B=day 1; C=day 3; D=day 4; E=day 6; F=day 9 [36].

Figure 15 is shown to better illustrate the cure cycle for isocyanate residuals, 2275 cm^{-1} band, for polyurethane as a function of time. It can be seen that the FTIR intensity decayed to a minimal value at day 9 showing the system to have reached a cured state.

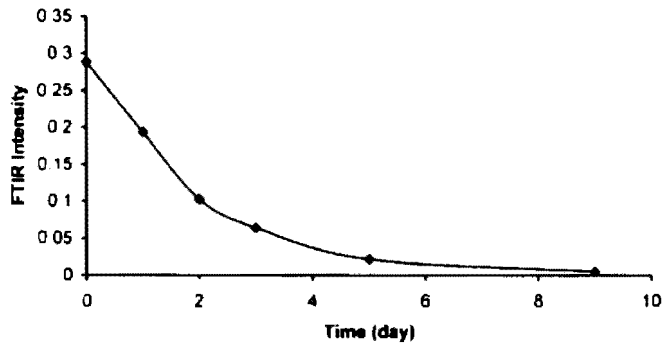

Figure 15: Cure rate of isocynate with polyol as a function of time. Taken at the NCO band at 2275 cm^{-1} [36].

Exposure to UV causes chain scission within the polyurethane structure. Followed by chain scission is the re-association that can lead to different conformational changes on the coating surface. A schematic of the UV degradation mechanism is shown in Figure 16.

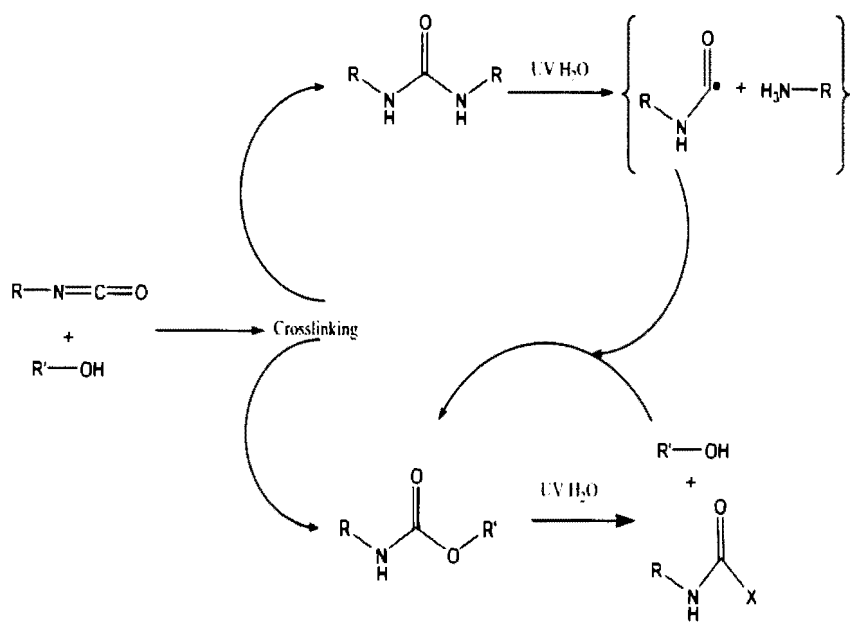

Figure 16: Scheme of UV degradation mechanism process [36].

Rigid polyurethane contains aromatic isocyanate in the structure, which will cause yellowing of the surface on exposure to UV light. The yellowing is a result of a oxidation reaction in the backbone of the polymer structure [33]. Photochemical degradation of the PU is associated with the chain scission of the urethane group and photooxidation of the CH_2 group between the aromatic rings. The UV irradiation modifies the chemical and physical characteristics of the PU surface, resulting in rapid color change and degradation.

The color change has been noted to occur as soon as four minutes after exposure to UV light [1]. Many studies have shown that the yellowing of PU is a very complex system involving a series of reactions producing quinonoid-type structures and photo-Fries type arrangement [33]. Quinones in PU foam are prepared by oxidation of the aromatic ring systems containing hydroxyl groups on one or both of the carbon atoms being converted to the carbonyl group and contain the yellowing pigments. Photo-Fries rearrangement involves a radical reaction mechanism and is also possible with deactivating substituents on the aromatic group.

Energy absorbed in the UV region produces changes in the electronic energy of the polymer molecule resulting from transitions of valence electrons. This excess energy may result in dissociation of the polymer or re-emitted as heat or light [15]. If the remitted light is in the visible region of the spectrum, discoloration in the polymer occurs. Polymers containing aromatic rings and oxygen in the form of ketonic or hydroxyl groups, like PU, are good photostabilizers reducing UV degradation [11].

As previously stated, PU foam and SAS composites are subjected to have discoloration occur when exposed to UV irradiation. The yellowness can be monitored with the use of a colorimeter. Yellowness is an optical property of a polymer that is a measure of the chromatic deviation from whiteness in wavelengths ranging from 570 through 580 nm. ASTM E 313 describes the procedure for calculating the yellowness index using Equation 6 as follows:

(6)

where X, Y, and Z are the CIE Tristimulus values and the coefficients depend on the illuminant of the measurement instrument. The color change is carried out by measuring the CIEL*a*b* values and can be converted to X, Y, and Z values. L*characterizes the grey value between 100 (white) and 0 (black), a* and b* are the chromaticity coordinates. The color change as a function of exposure can also be calculated by:

(7)

where the subscript 1 is the value before exposure to UV light and the subscript 2 is after being exposed. Figure 17 shows the total color difference for PU films being exposed with a fluorescent lamp UVA-351 type and a light intensity of 30mW cm^{-1}. Figure 18 shows the whiteness to darkness (L*) variation over exposure time. Both Figure 17 and 18 show that the majority of color change occurs within the initial 25 h and gradually plateaus with longer exposure durations.

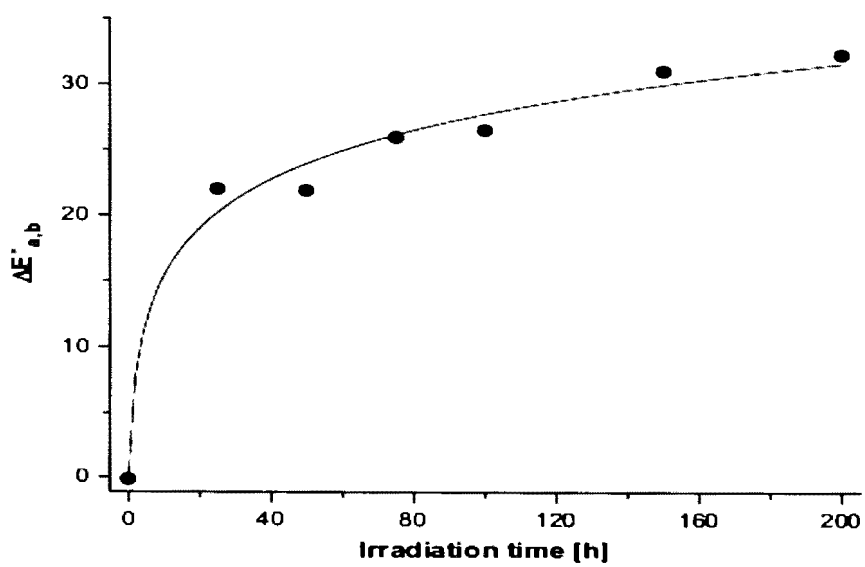

Figure 17: Color difference of $\Delta E^*_{a,b}$ versus UV exposure time [33].

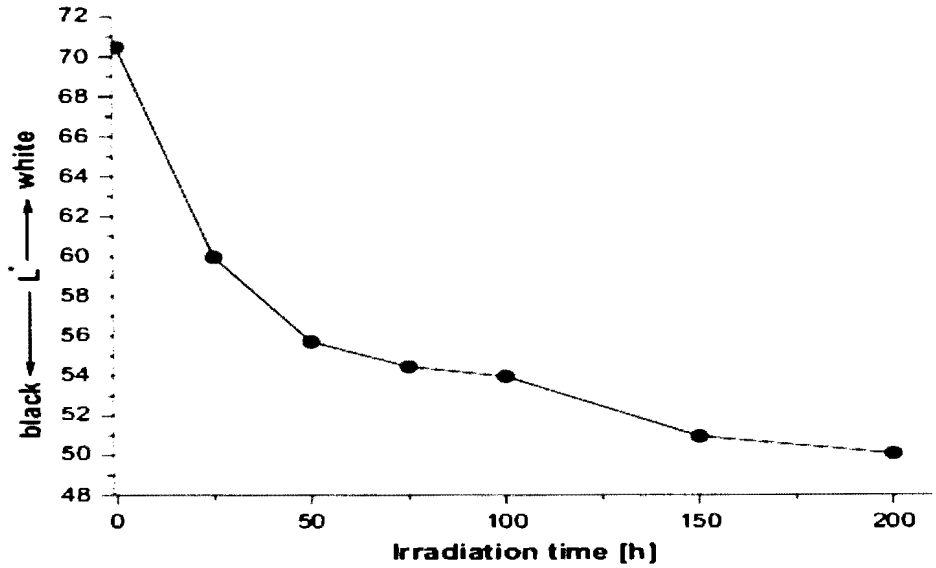

Figure 18: Variation of L^* versus UV exposure time [33].

As previously stated, polymers are known to both undergo chain scission and cross-linking when being exposed to UV radiation. Figure 19 shows a plot of polypropylenes rate of chain scission and cross-linking as a function of exposure time and depth of the sample. The figure shows that both chain scission and cross-linking rates increase near the surface (less than 0.15 mm) with exposure time and the rates decrease with depths greater than 0.15 mm.

More importantly, the chain scission rate occurs much faster than the cross-linking rate for the polypropylene samples. This is significant for that fact that chain scission is degradation occurring within the polymer structure and could have a considerable impact on the performance. The additional cross-linking will slightly show an increase in performance. The chain scission rate versus cross-linking rate is going to vary from one polymer to the next, but the concept of the chain scission rate occurring faster than the cross-linking lead to performance loss, which has been seen for PU foam.

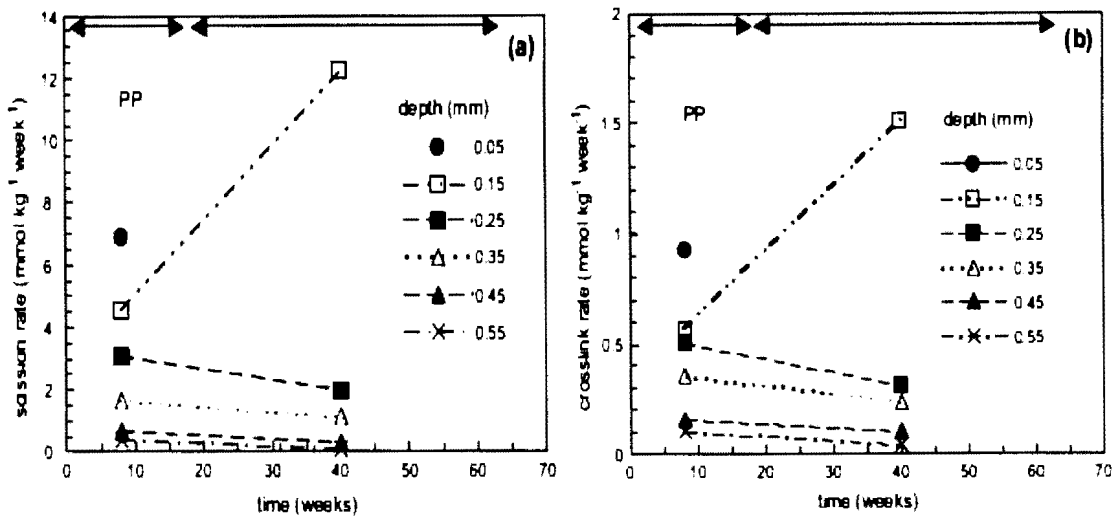

Figure 19: PP exposure to UV as a function of time
(a) chain scission rate; (b) crosslink rate [38].

2.4.3. Biocomposite Materials

The introduction of natural reinforcement within composites is steadily rising. The use of biocomposite materials combines the advantage of reducing the usage of synthetic petroleum products and replacing with a renewable natural resource while maintaining similar mechanical properties. Biocomposite materials also have a competitive price attribute due to its economical natural component. The addition of natural filler to polyurethane reinforced fiberglass foam is thus an opportunity to utilize the cellulosic part of the fiber for strength, and the lignin component for retardation of ultraviolet and thermal degradation. The natural filler will functionally act as a UV stabilizer, increasing the resistance to ultraviolet light while maintaining similar mechanical properties. This is the same idea that many of today's materials exhibit through the use of adding carbon black or titanium dioxide filler. Natural filler also allows the advantage of the composite the ability to be pigmented, whereas the carbon black gives the composite a grayish, black appearance.

CHAPTER 3. OBJECTIVE FOR THE RESEARCH

Polyurethane foam reinforced with fiberglass is suitable to be used in automotive, marine, and commercial applications due to its lightweight, rigid structure. In order for a material to be used in application, it needs to be characterized under the operating conditions it will be exposed to during the service life. The main scope of this work was to characterize SAS materials as affected by moisture, temperature, ultraviolet radiation, and combinations thereof.

The main objectives of this research were to:

- Generate mechanical property empirical models for SAS composites based on moisture uptake, temperature, and UV radiation.
- Compare the physical and mechanical performance of PU foam reinforced with fiberglass and various fillers after UV/moisture exposure.
- Evaluate effects of physical and mechanical performance of SAS composites for various UV exposure durations.

CHAPTER 4. EXPERIMENTAL PROCEDURES

This chapter outlines the overall experimental procedures, the materials used in this stud, details on sample preparation, and methods for replication of results are also explained. Finally, the various tests performed and the instruments used to measure the physical and mechanical properties of the specimens are summarized.

4.1. Materials

The fiberglass-reinforced PU foam composites were supplied from SAS located in Fargo, ND. The material consisted of a carbon black filled, closed cell, rigid polyurethane foam matrix with fiberglass reinforcement. The material sheets were processed using reaction injection molding (RIM) technology. In this process, two materials are mixed while injected into a closed mold [11]. The mixing of two materials cause a chemical reaction and initiates a foaming action. As the foaming process occurs, the materials expand and create a pressure within the mold. The generated pressure evenly distributes the foam throughout the reinforcement during the curing process.

The PU foam is a two-part system that consisted of an ester-type polyol with the addition of carbon black and a PMDI type isocyanate. The fiberglass is located closer to the edges to increase the stiffness of the material and is achieved by using a lightweight fiberglass filter material to maintain the correct loft between the two layers of additional reinforcement. The system consists of a proprietary polyurethane formula manufactured by BayOne Urethane Systems for SAS. The mixing ratio is 1.2:1 parts of isocyanate to polyol with densities ranging from 305 to 515 kg/m^3 and thickness variation from 9.5 to 25.4 mm.

Besides varying the density and thickness, the amount of reinforcement is also varied. This was achieved by the addition of two fiberglass woven rovings to the continuous fiber mats (CFM) and fiberglass filter material. The woven rovings are located near the top and bottom surface of the panel with a schematic shown in Figure 20. The

orientation from bottom to top is as follows: CFM, woven roving, filter, woven roving, and CFM. The non-woven roving series contains the two layers of CFM and the filter in between. The filter does not contribute much to strength and is just there to help loft the top layer up. The woven roving consists of a 5.4 kg bidirectional weave except the temperature test uses a 7.2 kg bidirectional weave and the CFM is a .3 kg mat.

The next variation consists of the natural surface texture as a result of processing versus the sanded surface. The natural texture is the surface that is left from the manufacturing process. This "natural" surface can also be sanded off. However, when the "natural" surface is sanded, some of the fiberglass reinforcement also is removed which reduces the mechanical properties. The amount of fiberglass reinforcement removed is related to the amount of fiberglass near the surface after processing.

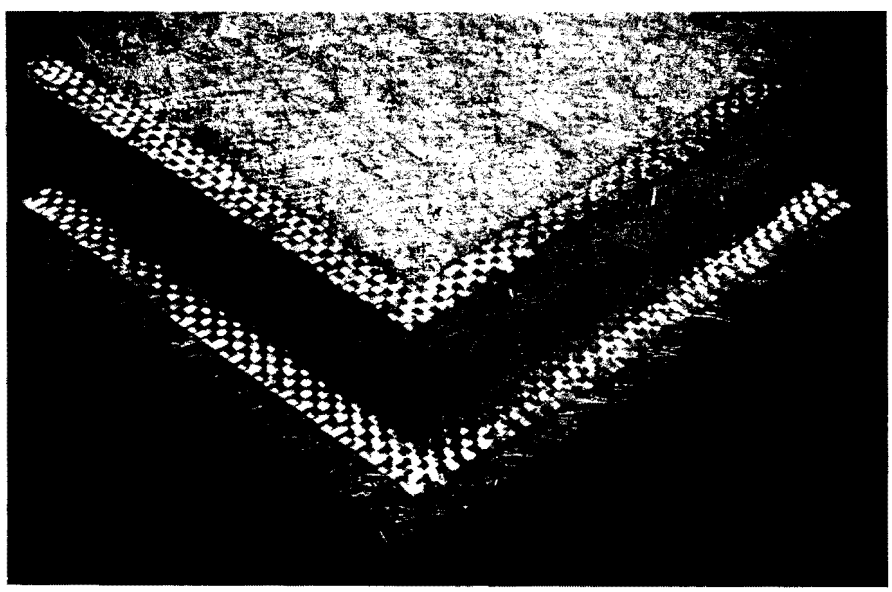

Figure 20: Fiberglass lay-up orientation.

In order to simplify the naming convention when describing the materials, the first three digits represent the global density in kilograms per cubic meter, followed by the thickness in millimeters. The woven roving was labeled with a "wr" and the non-woven roving did not contain any variable. The sanded surface did not contain any variable,

whereas the "natural" surface was labeled with a "n". For example, 415-25.4 represents a 415 kg/m^3 density with a thickness of 25.4 mm with no woven roving and is sanded. 415-25.4-wr-n is the same as the previous except with the addition of the two layers of woven roving and the natural (unsanded) surface. Table 1 shows the test matrix for the various tests performed along with some of the material properties that have a great importance on the performance of the SAS composites.

The microstructural properties of SAS polyurethane foam material have been studied in order to determine the degradation temperature, glass transition temperature, and mechanical properties for the material. The materials tested consists of the PU foam with no glass loading, as the fiberglass would alter the test results. SpaceAge Synthetics' most widely used foams are the 1.8 kg fast rise and 1.8 kg slow rise used in the two different reaction injection mold presses. This means the material will foam to 1.8 kg/m^3 density if there is no volume constriction applied. A 122-cm by 244-cm sheet of polyurethane foam was processed for each of the 1.8 kg fast rise and 1.8 kg slow foam and had an approximate density of 5.0 kg/m^3.

ASTM standards were followed as closely as possible, but with slight variances. This is a result of ensuring the material to respond in a normal behavior under the specified conditions. This complexity of behavioral response is a result of the PU foam and the addition of fiberglass. The standards depict on composite laminate, pure foam cores, sandwich composites, or pure polymers whereas SAS material is not a definite resemblance of any of the preceding examples. Many factors influence the material behavior, which was the determining factor on choosing standards and the slight differences within them in order to achieve normal behavior. Thorough testing was done to achieve the correct material behavior's response to different environmental and mechanical conditions.

Table 1: Material test matrix

Sample ID	Thickness (mm)	Global Density (kg/m^3)	Foam Density (kg/m^3)	Fiber Volume Fraction	Resin Volume Fraction	Void Volume Fraction
Temperature						
385-12.7	12.7	385	335	2.58%	27.84%	69.58%
450-12.7-wr	12.7	450	335	7.61%	22.24%	70.15%
Moisture Absorption						
350-9.5	9.5	350	290	2.98%	24.16%	72.86%
515-9.5	9.5	515	450	2.98%	38.15%	58.87%
515-9.5-wr	9.5	515	385	8.47%	25.92%	65.61%
415-12.7	12.7	415	320	2.58%	30.63%	66.79%
415-12.7-wr	12.7	415	320	8.47%	17.52%	74.01%
415-25.4	25.4	415	370	2.23%	31.41%	66.36%
415-25.4-wr-n	25.4	415	370	3.18%	29.31%	67.51%
415-25.4-wr	25.4	415	370	3.18%	29.31%	67.51%
515-25.4	25.4	515	465	2.23%	39.81%	57.96%
515-25.4-wr-n	25.4	515	465	3.18%	37.71%	59.11%
515-25.4-wr	25.4	515	465	3.18%	37.71%	59.11%
UV Radiation						
515-9.5	9.5	515	450	2.98%	38.15%	58.87%
515-9.5-wr	9.5	515	385	8.47%	25.92%	65.61%
UV/Condensation						
350-12.7-neat	12.7	350	305	2.58%	25.04%	72.38%
305-12.7-CB	12.7	305	255	2.58%	20.84%	76.58%
345-12.7-SF	12.7	345	300	2.58%	24.48%	72.94%

4.2. Performance Characterization

Due to the structure of the SAS composite, there is a certain degree of variance within the material. This variance is attributed to processing (i.e. temperature, humidity, cure rate, poly/iso ratio, etc.). It is the nature of a foam material to have a variation within each panel and also panel-to-panel. This variation comes into consideration when determining the mechanical performance along with other material properties.

After the specimens were conditioned for the appropriate exposure duration, tensile specimens were tested for mechanical properties. The tensile tests were executed using an MTS test frame with 250 kN load cell and hydraulic wedge grips. The test frame is located at NDSU within the Mechanical Engineering Department and can be seen in Figure 21.

Figure 21: MTS load frame.

The tests were performed in accordance with ASTM D 1037 with a crosshead rate of 5 mm/min. To achieve an acceptable failure mode, the tensile test specimens had a 25 mm gauge section width compared to the 37.5 mm called out in the standard and can be

seen in Figure 22. In order for the tensile test to be valid, the specimen had to have a correct fracture, or a fracture that occurred within the gauge section. Figure 22 shows the correct fracture mechanism of the specimen where the break occurred within the gauge section.

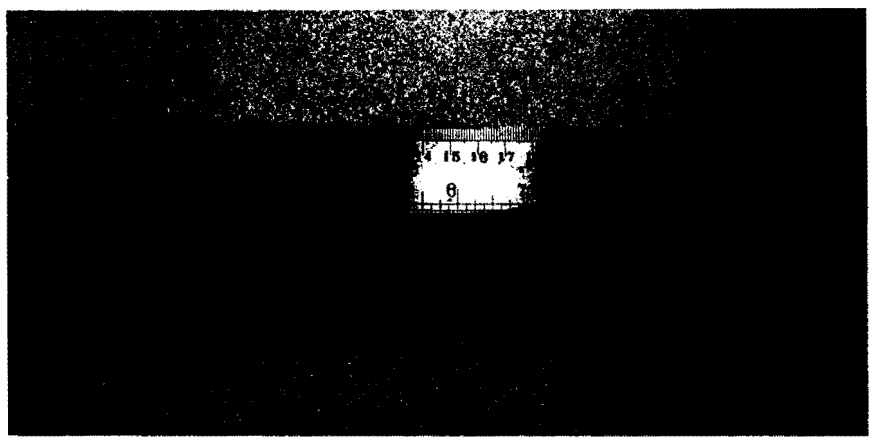

Figure 22: Tensile specimen.

An MTS extensometer (model number: 632.25B-20) was placed on the gauge length of the specimen to measure the change in length during the tensile test. This length change is used to calculate the strain using simple stain equation. The length change is monitored in the material during loading and the load cell measures the applied load as a function of time. Strain is the ratio of the extended length to the original length, whereas stress is the ratio of the applied load to the cross-sectional area measured in the gauge length.

Using the stress and strain measurements from the tensile test, the ultimate strength and Young's modulus of the sample can be calculated. These mechanical properties were used to compare the qualitative effects due to the impact environmental conditioning has on the tensile performance. The extensometer is shown during a test in Figure 23 and is the black equipment attached to the gauge length of the specimen. This extensometer is removed prior to failure where the strain only needed to be measured in the elastic region.

Figure 23: Tensile test with extensometer.

4.3. Temperature

The tensile performance of 385-12.7 and 450-12.7-wr series materials were characterized to determine the effects of temperature change on the material properties. Tensile specimens of the reinforced PU foam were exposed to a range of temperatures including: -40, -18, 28 (ambient), 66, 93, and 121°C. The specimens were conditioned for 30 min at the specified temperature in the chamber prior to being tested to allow for the specimens to reach equilibrium. The specimens were characterized through the use of tensile tests, where the mechanical properties were likewise determined to characterize the changes in performance. A comparison between the 385-12.7 and 450-12.7-wr series was selected to determine the effects the woven roving has on temperature effect.

Temperature testing was executed in accordance to ASTM D 1037 standard for tensile specimens. Testing was performed with a 250 kN MTS load frame and MTS environmental chamber (Figure 24). Four tensile specimens were exposed to each of the temperatures described above and the results included a mean with standard deviation.

Figure 24: MTS load frame with environmental chamber.

4.3.1. Verification of Specimen Geometry

In order to be used with the MTS environmental chamber, the specimens needed to be altered. A 203.2-mm length was added to one end of the standard grip section to allow the specimen to be clamped in the grips (Figure 25).

Figure 25: Extended tensile specimen.

This extension was needed to keep the test section (specifically the gauge length) in the environmental chamber while one end of the grip length was outside of the chamber in order to reach the top grip fixture. Figure 26 shows the specimen with the extensometer gripped in the fixtures while the specimen was being cooled. One can also see how the additional 203.2 mm grip length is used since the chamber does not allow for the top fixture to be located within the chamber.

Figure 26: MTS environmental chamber.

4.4. Moisture Absorption

In order to fully understand the mechanism and extent of moisture uptake through the material, they were compared with varying density, thickness, and reinforcement loading. Each of the tests consisted of measuring the moisture uptake with suitable time durations and the mechanical performance after being conditioned.

4.4.1. ASTM Standards

Since there is not one ASTM standard that covers the water absorption of a reinforced, closed-cell PU foam; two different standards were used to fully capture the

material properties once submerged in water. ASTM D 570 describes the procedure for determining the relative rate of absorption of water by plastics when fully immersed. The standard calls for measuring the properties at 2 h, 24 h, and a long-term immersion to determine the total water absorbed at full saturation. Also, the standards calls for 2 h boil immersion test which is used to represent a worst case scenario. At the specified time duration, the specimens are removed from the distilled water and the surface adsorption moisture is removed with a dry cloth from any moisture that was accumulated on the surface but not yet absorbed in the specimen. The specimens are weighed to the nearest 0.001 g immediately, and then placed back into the water. ASTM D 5229 describes the procedure for calculating the mean moisture content by Equation 4 stated earlier. The standard also calls for calculating the material diffusivity previously stated in Equation 5.

4.4.2. Specimen Preparation and Characterization

The specimens were cut to 76.2 mm long by 25.4 mm wide by the thickness of the material in accordance to ASTM D 570. Each sample set consisted of five samples and a mean with standard deviation was used to represent the material results. After the specimens were cut to size, a stainless steel foil tape (ASTM 5229) was applied to mitigate moisture diffusion through the edges to obtain a one-dimensional Fickian diffusion. The samples were conditioned in a VWR convection oven at 50°C for 24 h following ASTM 570 to remove any moisture present from atmospheric conditions. The specimens were cooled and and the mass was measured using a Mettler Toledo mass balance to 0.1 mg accuracy.

Once the samples were prepared, they were fully submerged in distilled water. The samples were removed at the specified time durations and the surface was dried to remove any adsorption moisture, or the moisture that is on the surface but not absorbed in the material. Once the samples reached full saturation, the samples were removed from the water bath and the desorption curve was measured by recording the mass over time in

ambient lab conditions . Next, the stainless steel foil tape was removed and measured to account for the accurate sample mass.

4.4.3. Tensile Test

Tensile tests were performed for each of the sample sets at exposure durations of: 2, 24, 72, and 2 h boil. Each sample set consisted of four specimens and a mean value with standard deviation was calculated to represent the material properties. An unconditioned sample set was also tested for baseline comparative purposes. The tensile specimen geometry was the same as previously stated and a test rate of 5 mm/min was used.

4.5. Ultraviolet Irradiation Test Procedure

A Q-Lab QUV accelerated weathering test chamber was used to condtion the 515.95 and 515-9.5-wr specimens. The test conditions used ASTM G 154 cycle 2 (UVA-340, 8 h of UV at 1.55 W/m^2 at 70 ± 3 °C black panel temperature with an approximate wavelength of 350 nm) as a guideline excluding the condensation cycle. The only difference is cycle 2 calls for 8 h UV at 70 ± 3 °C black panel temperature followed by 4 h condensation at 50 ± 3 °C black panel temperature. The panels were exposed for 240 h of UV per side with no condensation.

Prior to being conditioned to the QUV accelerated weathering chamber, the specimens were tested using a bench-top colorimeter (Macbeth ColorEye Model # 7000). The colorimeter instrument was used to monitor the color change (increase in yellowness) due to being conditioned to UV radiation. A CIE L*a*b* scale was used to measure the specimen color, which was then converted to an XYZ scale for calculating the yellowness index (YI) according to ASTM E 313 and Equation 6 previously stated.

The specimens were exposed for 240 h per side with a second 515-9.5-wr specimen exposed for 480 h per side. After being exposed, the samples were again measured using the ColorEye to determine the YI change due to the weathering. After the color was

measured, the specimens were prepared into tensile specimens and tested using the MTS load frame. Each sample set consisted of five specimens.

4.6. Ultraviolet/Condensation Test Procedure

A small scale press with a mold was used to process the samples for the UV/condensation test using SAS materials. This procedure was to incorporate different filler materials within the SAS product line on a trial basis.

Furthermore, this study involved the comparison of conditioned and unconditioned materials subjected to common environmental conditions. Specifically, this investigation focused on analyzing the performance of natural fiber-reinforced rigid PU foam versus the same PU foam filled with carbon black, and neat PU foam for baseline comparison.

The PU foam material had a free-rise density of 96.1 kg/m^3. The polyurethane foam with the addition of carbon black had a free-rise density of 64.1 kg/m^3. Sunflower hulls with 44 wt. % cellulose and 22.5 wt. % lignin was used for filler material. Each of the polyurethane foam panels contained a 42.5 g fiberglass CFM with an additional layer of filter material placed in between the CFM, creating a fiberglass-reinforced composite.

Two panels for each of the three samples were processed allowing one set to act as the baseline properties and the other set to be conditioned: natural PU foam, natural PU foam with 20% by weight ground sunflower hull filler, and natural PU foam with carbon black filler. The six panels were processed using reaction injection molding with a 31.75-cm by 31.75-cm aluminum mold and a 1.25-cm thickness. A density of approximately 320.3 kg/m^3 was the target density when processing each panel.

One set of the panels was conditioned in a Q-Lab QUV chamber following ASTM D 4587 cycle 2: UVA-340, 4 h of UV at 0.89 W/m^2 and 60 ±3 °C black panel density followed by 4 h of dark condensation at 50 ±3 °C black panel density. The panels were exposed for 252 h of UV and 252 h of condensation per side. The second set was unconditioned and used for baseline comparison properties. Figure 27 shows the three

different panels and the unconditioned color variance between them. The top panel is filled with carbon black, the bottom left panel is filled with sunflower hull, and the bottom right panel is the neat PU.

Figure 27: Set of the unconditioned processed panels;
Top: carbon black filled, Bottom Left: sunflower filled, Bottom Right: neat PU.

After the panels were processed and one set was conditioned in the QUV chamber, the panels were cut using a table saw to 30.5 cm by 25.4 cm and the density was calculated. Next, the panels were cut into 5.1-cm by 25.4-cm strips, followed by being routered into tensile specimens using an aluminum tensile specimen jig. Figure 28 shows the finished tensile specimens for the unconditioned, baseline sets for the three panels.

Figure 28: Set of tensile specimens.

After the all the tensile specimens were cut to the appropriate geometry, the cross-sectional area was measured within the gauge length of each specimen. Prior to testing, the specimens were placed in an oven for 8 h at 50°C to remove any moisture that could affect the mechanical performance during testing. Each processed panel allowed for five tensile specimens to be tested, and a mean value and standard deviation of the five specimens was taken for the mechanical properties.

4.7. Fourier Transform Infrared Spectroscopy

Fourier transform infrared spectroscopy (FTIR) spectra were obtained with the unconditioned and the conditioned UV/condensation samples of the surface, 0.25 mm, 0.5 mm, and 2 mm depths. FTIR was used to measure compositional changes within the specimen caused by the environmental conditioning. FTIR passes IR radiation through a sample (transmitted), where some of the infrared radiation passes through the sample and some is absorbed by the sample.

A spectrum is generated to represent the molecular absorption/transmission, creating molecular fingerprints. These molecular structures or "fingerprints," are unique in which there are no two alike. These fingerprints can be used to determine the compositional change, quality or consistency, and amount of components in a mixture. A FTIR Nicolet 6700 spectrometer was used in the attenuated total reflectance (ATR) mode on a Zn-Se crystal with a resolution of 4.0/cm and 32 scans were taken for each specimen between a wavelength of 4000 and 650 cm^{-1}.

4.8. Differential Scanning Calorimetry

The glass transition temperature will vary dependently with the amount of cure achieved through the polymerization process. The objective was to observe the change in the glass transition temperature with the amount of post cure for the material. Polyurethane foam was processed on two different presses and were tested for comparison

as a function of cure temperature. Differential scanning calorimetry (DSC) measures temperature and heat flow associated with thermal transitions within the material. These thermal transitions allow the determination of the glass transition temperature of the PU foam which results in a distinct change in heat capacity. TA Instruments Q1000 DSC was used on neat PU foam that was post-cured at 100, 125, 150, and 175 °C for 4 h in a convection oven. The PU foam was tested within different locations throughout the panel. The DSC testing performs three cycles (heat, cool, heat) and a general curve is shown in Figure 29. The DSC samples were executed from -50 °C to 175 °C at 20 °C/min, followed by a cool cycle to -50 °C as fast as possible, and finally heated to 175 °C at 20 °C/min.

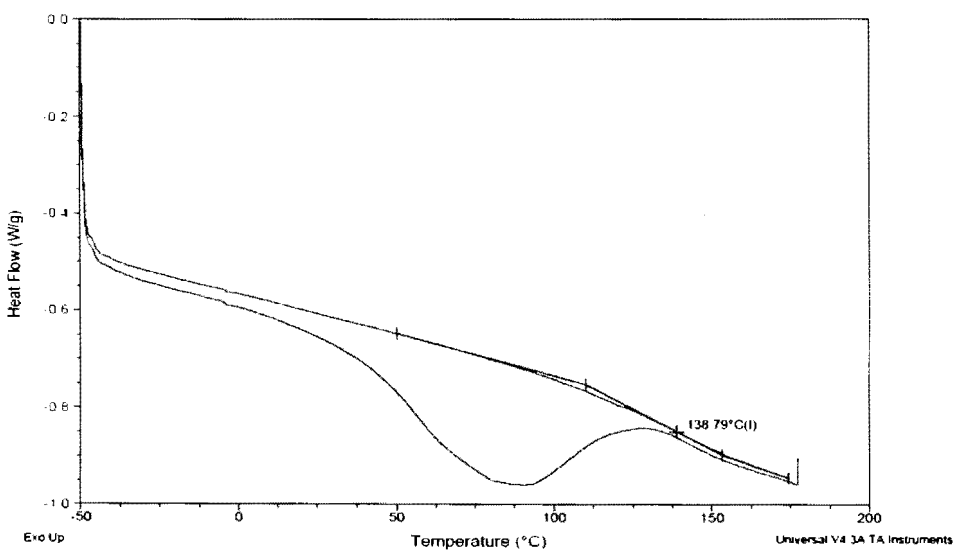

Figure 29: Typical DSC curve.

4.9. Thermogravimetric Analysis

The decomposition temperature of the SAS composite was determined using thermogravimetric analysis (TGA) which progressively heats the material while finite weight change is recorded as a function of temperature. The weight changes were associated with the volatilization or decomposition of components within the samples. Many materials initially have a slight amount of moisture present due to humidity in

atmosphere. This initial moisture when dried will be present on the TGA curve with a slight decrease in weight at the first portion of the curve. The results of the TGA test were plots of weight change versus temperature.

A TA Q500 TGA instrument was used to test the PU foam as received from SAS in order to determine the two decomposition temperatures of the material. The materials consisted of a non-post cured samples from the two different presses used and was tested in an inert nitrogen atmosphere. The material mass was recorded as the specimens were heated until almost all the mass was decomposed. The general TGA curve is shown in Figure 30. The large weight percentage decreases represent the first and second decomposition temperature for the PU foam. The TGA samples were heated to 800 °C at a rate of 10 °C/min followed by air cooled for 20 minutes.

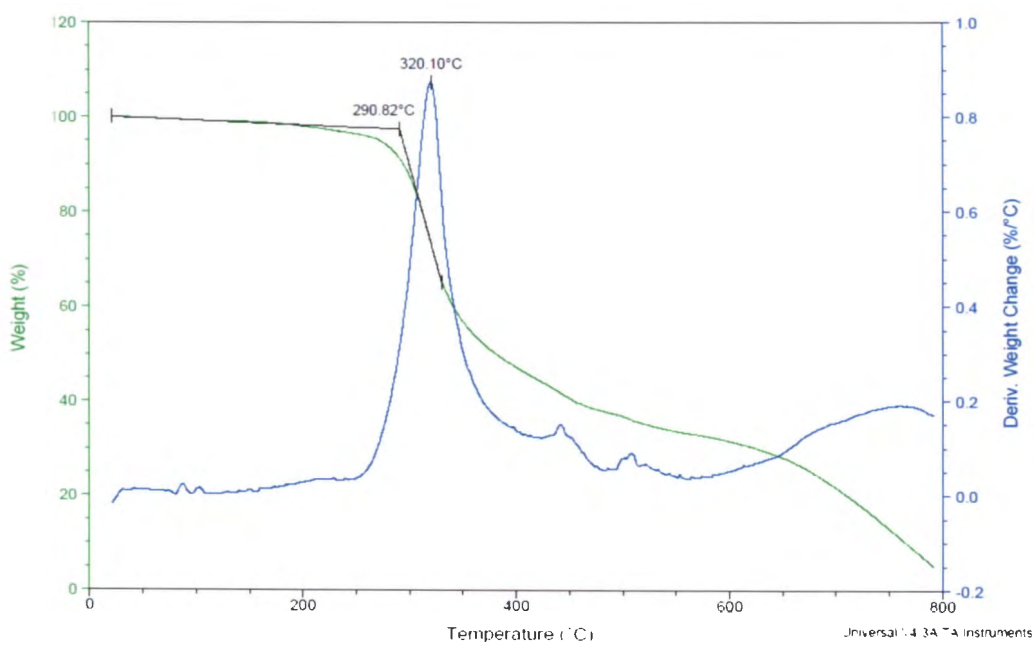

Figure 30: Typical TGA curve.

The following chapters present and interpret the results obtained throughout this study of environmental conditions impact. The focus of this work was to investigate the effects of different environmental conditions on PU foam reinforced with fiberglass in order to evaluate the mechanical and physical properties.

CHAPTER 5. RESULTS AND DISCUSSIONS

5.1. Temperature Test Results

The first environmental condition investigated was temperature and the influence on the strength and modulus of SAS composites. The standard specimen geometry was evaluated against the extended specimen geometry under ambient conditions to verify that the design of the extended specimen provided equivalent results. With the given mean and standard deviation, both specimens performed similarly, proving the extended specimens were suitable to use for the temperature testing. After the extended specimen geometry was confirmed to be equivalent to the standard specimen dimensions, testing was performed for the temperature range from -40 °C to 121 °C.

5.1.1. 385-12.7 Series

Table 2 shows the mechanical performance for the 385-12.7 series as a function of temperature. It was apparent that the strength and Young's modulus decrease as the temperature increases. This occurs because the PU foam matrix material becomes more ductile with increasing temperature. As the matrix becomes more ductile, more molecular movement is achieved within the polymer chains, which ultimately reduces the strength and modulus. As the temperature decreases, the molecular motion is hindered, which requires a higher amount of energy to move the molecular chains. This hindered motion increases the strength and modulus.

Table 2: Tensile Properties of 385-12.7 Series at Various Temperatures

Temperature	-40 °C	-18 °C	Ambient Standard (28 °C)	Ambient (28 °C)	66 °C	93 °C	121 °C
σ (MPa)	14 ± 1.9	16 ± 1.6	12 ± 0.8	12 ± 2.0	10 ± 1.5	9 ± 0.7	7 ±1.1
E (MPa)	860 ± 45	769 ± 72	630 ± 25	638 ± 110	606 ± 125	578 ± 7	438 ± 60

Figure 31 shows the linear portion of the stress-strain curve for the 385-12.7 series tested at various temperatures. It was evident that the modulus decreases with an increase in temperature, where the most dramatic effect was seen between -40 °C and -18 °C, where the material behaves in a much more brittle manner. It was also shown that the 66 °C and 28 °C exhibit very similar moduli. The curves shown were generated using one sample per set that demonstrated similar properties with mean properties of the set.

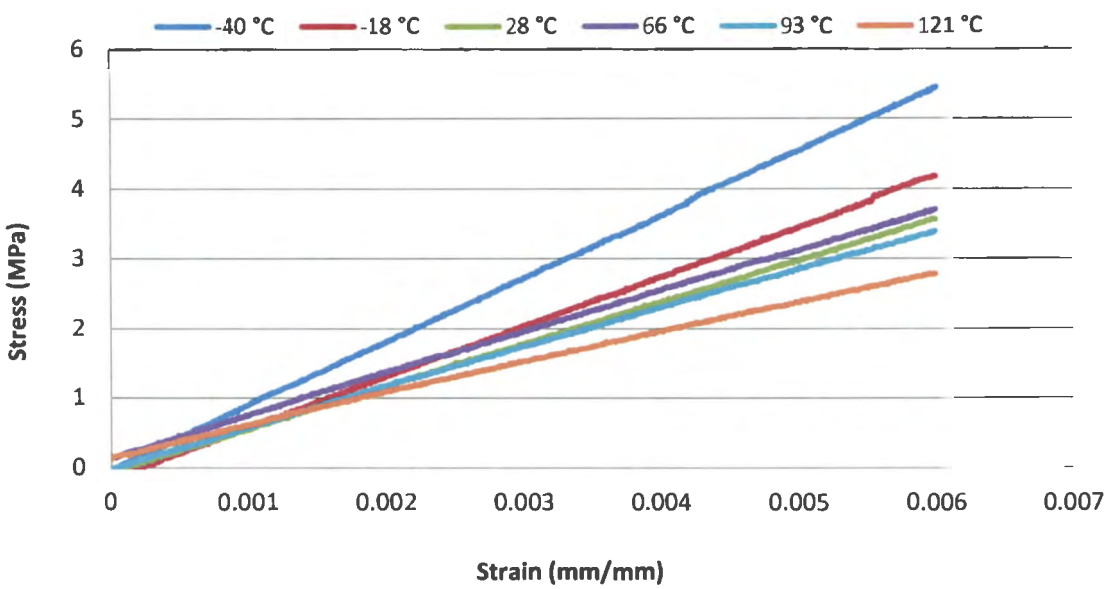

Figure 31: 385-12.7 Stress-Strain curves at various temperatures.

The mechanical property versus temperature trend is better illustrated in Figure 32. The figure shows that there is a relatively linear relationship between tensile strength and temperature. From this figure, an empirical expression is created using the trend given for the material property as a function of temperature. It is important to understand that the empirical expressions developed are valid within the temperate range tested. It quantifies how the strength decreases as the temperature increases, as expected. The tensile strength had a 21% drop between -40 °C and the ambient temperature. The material also exhibited a 52% decrease in strength over the entire temperature range of -40 °C to 121 °C. The

relationship between tensile strength and temperature was demonstrated by the following empirical expression:

$$\sigma = -0.0507 * T + 13.419 \qquad (8)$$

where σ is the tensile strength in MPa and T is the °C temperature. The empirical expression had a coefficient of determination (R^2) of 0.9375 against the test date. This correlation showed a good correlation between the fitted expression and the test data, where a perfect fit has a coefficient of determination of 1.0. The coefficient of determination is a statistical measurement to show how well the regression line approximates the test data.

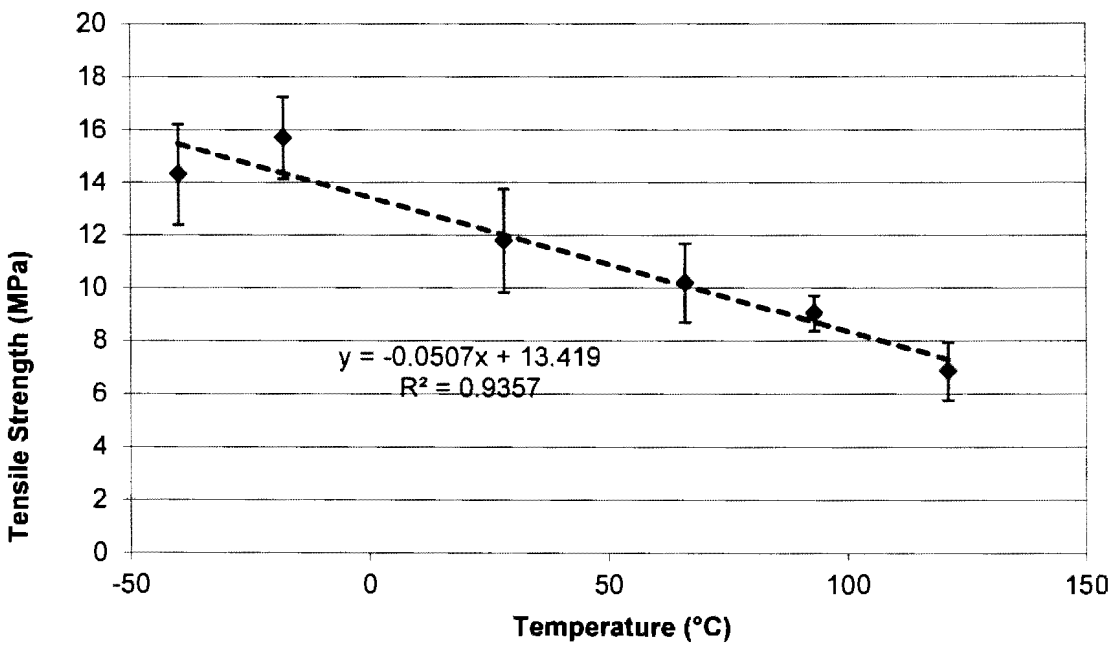

Figure 32: Tensile strength vs. temperature for 385-12.7 material.

Figure 33 shows the linear relationship between the tensile modulus and temperature for the non-woven roving series. Similar to Figure 31 and the expected trend, the Young's modulus decreases with increasing temperature. The relationship of stiffness as a function of temperature had an empirical expression as follows:

$$E = -2.2928 * T + 743.84 \qquad (9)$$

where E is the Young's modulus in MPa and T is the temperature in °C. The regression line had a R^2 value of 0.948 exemplifying a very close fit with the recorded test data. This correlation coefficient showed a slightly better fit than the tensile strength for the 385-12.7 series

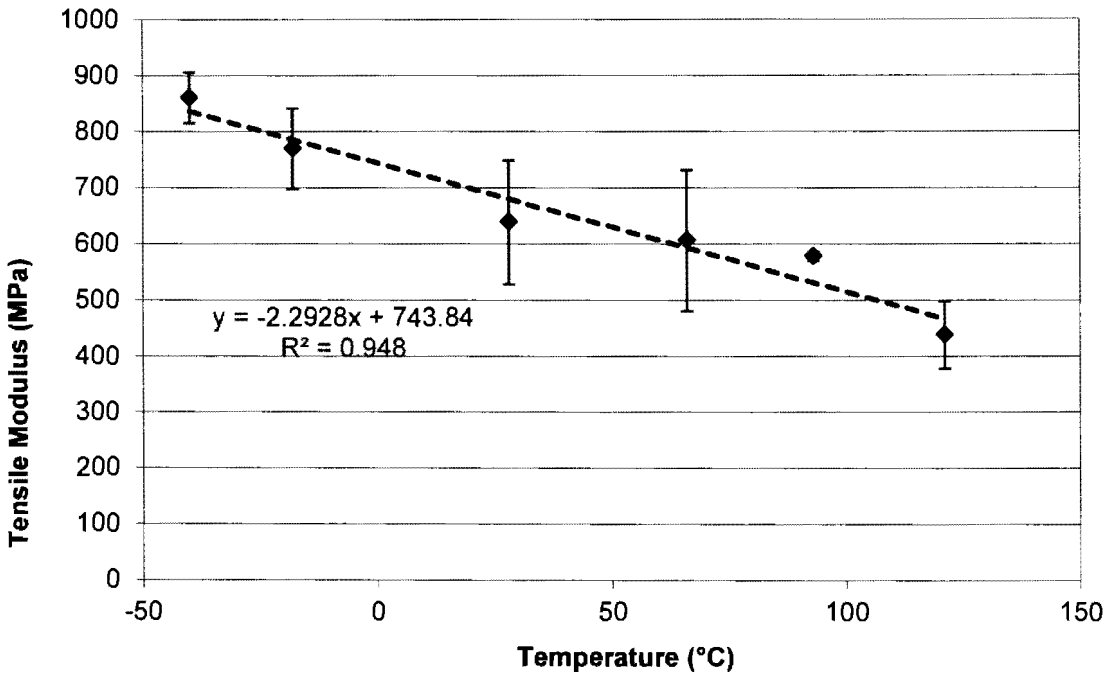

Figure 33: Tensile modulus vs. temperature for 385-12.7 material.

Both the tensile strength and modulus increase with decreasing temperature due to the restriction of the long-range molecular motion within the polymer structure of the PU foam matrix. However, due to the increase of strength and modulus, the strain to failure will significantly decrease, which is characteristic of a brittle structure. Both the strength and stiffness empirical expressions had a good fit with the "fitted" curve shown from the coefficient of determination.

5.1.2. 450-12.7-wr Series

The next set of temperature tests consisted of comparing the performance for the 450-12.7-wr (i.e. woven roving) series. The tensile strength and tensile modulus means

with standard deviations are recorded in Table 3 for the six various temperatures along with the results for the normal tensile geometry tested at ambient atmospheric conditions.

Table 3: Tensile Properties of 450-12.7-wr Series at Various Temperatures.

Temperature	-40 °C	-18 °C	Ambient Standard (28 °C)	Ambient (28 °C)	66 °C	93 °C	121 °C
σ (MPa)	61 ±1.0	54 ±1.3	12 ±0.8	39 ±2.5	36 ±4.3	34 ±1.8	32 ±3.1
E (MPa)	2503 ± 58	2242 ± 62	2006 ± 71	1980 ± 189	2013 ± 100	1852 ± 178	1504 ± 167

Figure 34 shows a stress-strain curve of the 450-12.7-wr series tested at various temperatures. It is clearly shown that the modulus decreases with the increase in temperatures as in the case of the non-woven series. The curves are generated using one sample per set that demonstrated the most similar properties to the mean tensile strength and modulus for that individual set.

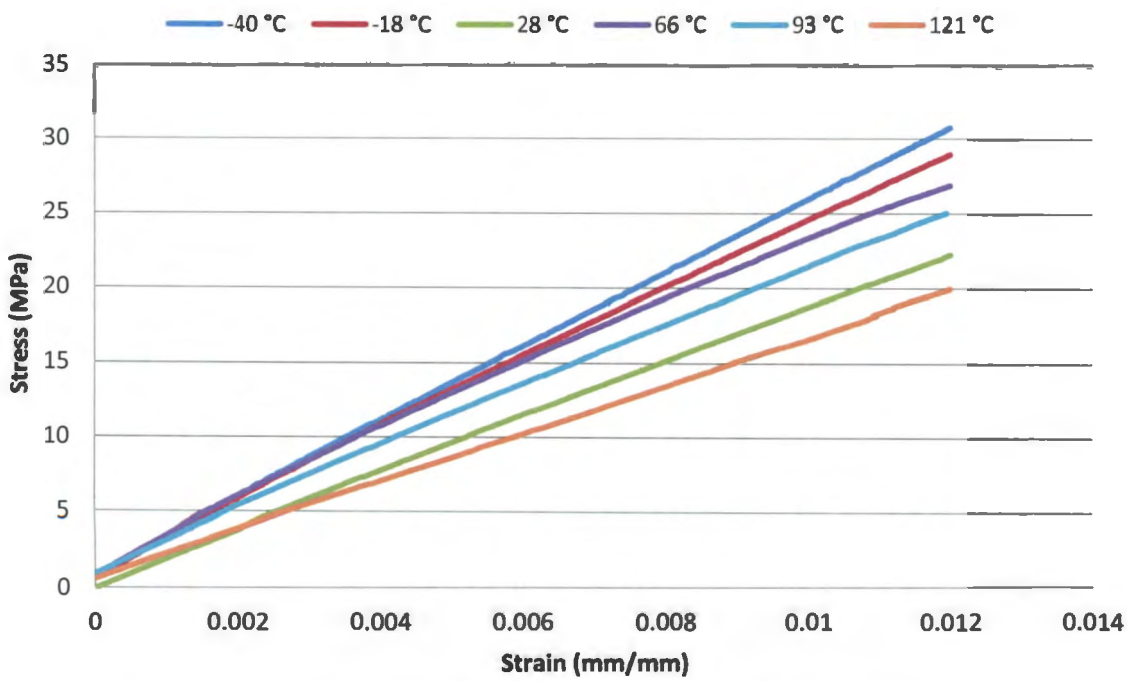

Figure 34: 450-12.7-wr Stress-Strain curves at various temperatures.

The 450-12.7-wr series trend of the tensile strength versus temperature is shown in Figure 35. Each data range contains a mean of four samples with standard deviation. The fiberglass-reinforced rigid PU foam exhibited a tensile strength of 32 ± 3.1 MPa at 121 °C and a tensile strength of 61 ± 1.0 MPa at -40 °C, thus resulting in a 48% decrease in strength over the entire temperature spread. The tensile strength is represented with the following empirical equation:

$$\sigma = 0.0013 * T^2 - 0.2779 * T + 47.745 \qquad (10)$$

where σ is the tensile strength in MPa and T is the °C temperature. The "fitted" curve showed very good correlation with the test data having a R^2 value of 0.9884 which is much better than the 385-12.7 series.

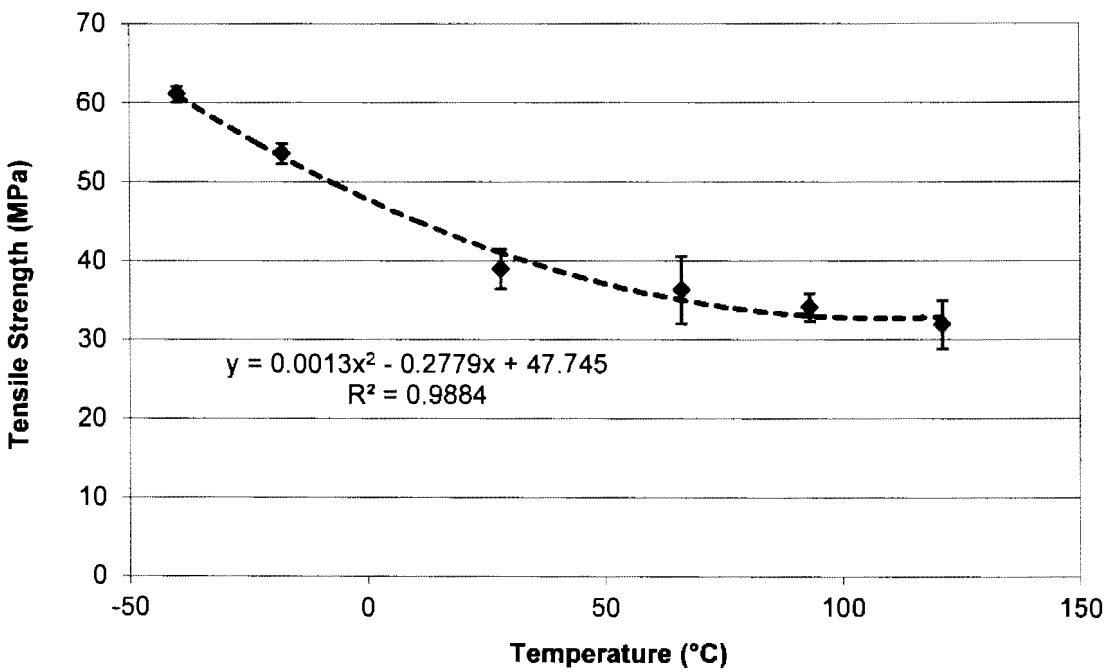

Figure 35: Tensile strength vs. temperature for 450-12.7-wr material.

Figure 36 illustrates the linear trend for tensile modulus versus temperature. The modulus at -40 °C was 860 ± 45 MPa compared to 438 ± 60 MPa at 121 °C resulting in a 49% decrease in Young's modulus over the temperature range examined. The modulus at

room temperature was 638 ± 110 MPa resulting in a 35% increase when compared with the modulus at 121 °C. The tensile modulus is represented by the following equation:

$$E = -0.0046 * T^2 - 4.7492 * T + 2236.6 \qquad (11)$$

where E is the Young's modulus in MPa and T is the temperature. The "fitted" curve had a correlation value of 0.9009 showing an acceptable fit between the empirical equation and the test data.

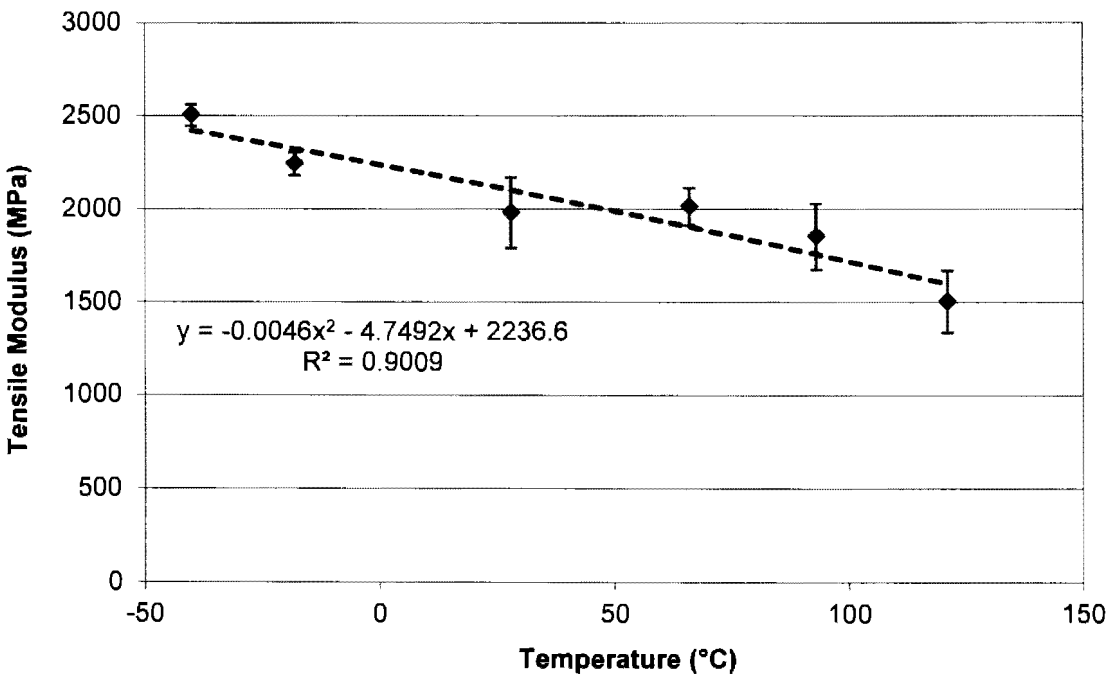

Figure 36: Tensile modulus vs. temperature for 450-12.7-wr material.

It was shown that the fiberglass-reinforced PU foam material is immensely susceptible to extreme temperatures. It was found that the strength and modulus decrease with increasing temperature for both the 385-12.7 and 450-12.7-wr series. However, the woven roving series has a more drastic decrease when comparing the slopes of the trend lines previously stated. The slope for the strength was approximately 3.5 times higher for the woven roving series and approximately 2.2 times higher for the modulus over the temperature range. This shows that the strength and modulus decreased at a faster rate with increasing temperature for the woven roving series.

As the temperature decreases, the foam becomes more brittle resulting in an increase in strength and modulus. As a result of the foam being more brittle, the strain-to-failure also reduces. The fiberglass was suspected to have minimal effect from the temperature and maintain the material properties until the matrix can no longer bind the fibers together or the PU foam decomposes. It was also suspected that the woven roving series would have had less of an impact from temperature due to the fiberglass have less of an effect.

The 385-12.7 series had R^2 values of 0.9357 and 0.9480 for the strength and stiffness, respectively, showing very good correlation between the test data and the "fitted" empirical expression. The 450-12.7-wr series had an R^2 value of 0.9884 for the strength fitted empirical expression showing a very good correlation and the stiffness empirical expression had an R^2 value of 0.9009 showing an acceptable correlation.

5.2. Moisture Test Results

Every material is inevitably subjected to moisture during use, even if it is as minute as moisture present in the atmosphere. Many underlying factors determine the amount of moisture uptake a material will exhibit. This section studied the major influential factors that determine the moisture properties in SAS composites.

The quantitative objectives for the moisture absorption section of the study were to show how the moisture uptake is related to material parameters (i.e. thickness, density, void content, fiberglass content). The moisture content was determined at specified intervals in terms of the percentage mass change from absorption/desorption. Five samples were tested for each set and Table 4 and 5 show a one-dimensional diffusion of mean moisture content with standard deviation. Stainless steel foil tape was applied to the edges to mitigate moisture uptake from edge effects. The samples were also dried prior to measuring to remove any adsorption. Table 4 shows the results for the moisture absorption/desorption content of the 9.5-12.7 mm samples, whereas Table 5 shows the

results for the 25.4 mm samples. The following results consist of samples that were fully submerged in distilled water at room temperature, except the specimens labeled "boil" which were fully submerged in boiling distilled water. The specimens were dried under ambient "lab" conditions and the fiberglass is assumed impermeable.

Table 4: Moisture Absorption/Desorption Content of 9.5-12.7 mm Samples

	Series:	415-12.7	415-12.7-wr	350-9.5	515-9.5	515-9.5-wr
2 hr						
	Mean	0.71	1.01	1.39	0.49	0.75
	STDV	0.11	0.08	0.18	0.06	0.10
24 hr						
	Mean	2.61	2.58	3.85	2.21	3.02
	STDV	0.33	0.21	0.45	0.19	0.29
72 hr						
	Mean	5.59	4.98	6.23	5.00	5.41
	STDV	0.62	0.74	0.58	0.31	0.73
144 hr						
	Mean	7.05	5.84	8.04	6.08	6.60
	STDV	0.86	1.06	0.75	0.74	1.18
2 hr Dry						
	Mean	9.03	6.98	7.86	4.97	5.60
	STDV	0.55	1.49	2.66	0.61	1.29
24 hr Dry						
	Mean	4.10	2.86	3.05	2.46	2.92
	STDV	0.65	1.00	0.60	0.49	0.54
72 hr Dry						
	Mean	2.42	1.55	1.80	1.54	1.96
	STDV	0.30	0.33	0.13	0.23	0.24
2 hr Boil						
	Mean	8.76	11.90	9.72	6.15	6.11
	STDV	1.26	0.37	0.83	0.51	0.52

Table 5: Moisture Absorption/Desorption Content of 25.4 mm Samples

	Series:	415-25.4	415-25.4-wr-n	415-25.4-wr	515-25.4	515-25.4-wr-n	515-25.4-wr
2 hr							
	Mean	0.62	0.84	0.47	0.63	0.60	0.76
	STDV	0.12	0.10	0.11	0.06	0.17	0.10
24 hr							
	Mean	1.47	1.56	0.91	1.46	1.37	1.79
	STDV	0.18	0.17	0.03	0.20	0.15	0.15
72 hr							
	Mean	2.50	2.70	1.65	2.96	2.28	2.87
	STDV	0.23	0.29	0.18	0.49	0.23	0.20
144 hr							
	Mean	3.74	3.54	1.90	3.25	2.66	3.45
	STDV	0.32	0.40	0.12	0.34	0.24	0.16
2 hr Dry							
	Mean	9.82	8.73	4.90	6.16	4.86	6.11
	STDV	1.04	0.55	0.33	0.39	0.45	0.14
24 hr Dry							
	Mean	5.58	5.02	2.50	3.74	2.62	3.67
	STDV	0.58	0.21	0.14	0.07	0.09	0.06
72 hr Dry							
	Mean	3.73	3.32	1.61	2.68	1.53	2.47
	STDV	0.51	0.14	0.08	0.07	0.05	0.03
2 hr Boil							
	Mean	10.73	8.14	6.04	5.17	3.73	5.07
	STDV	0.98	0.53	0.52	1.08	0.39	1.40

5.2.1. Absorption/Desorption Curves

Once the specimens reached maximum saturation, they were removed and allowed to dry in ambient conditions. Thereafter, the moisture absorption/desorption data was plotted as a function of the square root of time to be able to compare diffusivity coefficients (slope of the initial portion of the curve). Figure 37 and Figure 38 show the absorption/desorption curves for the test specimens. The linear portion at the onset of the test is used to calculate the diffusivity, or rate of moisture transfer. The moisture curves increase until they reach a saturation level.

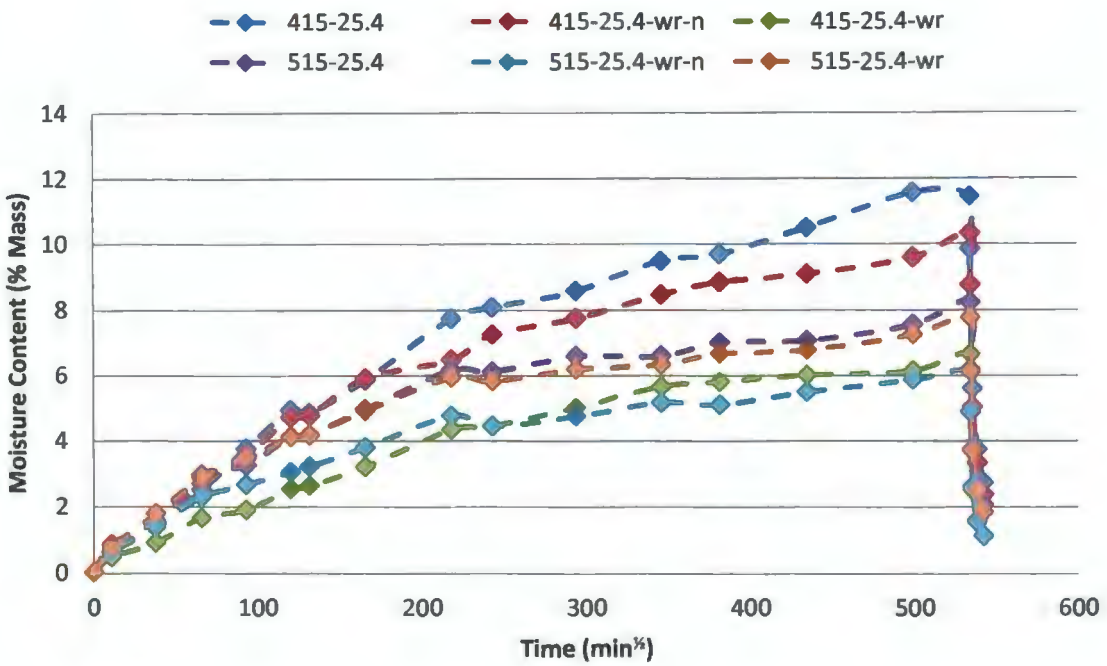

Figure 37: Moisture absorption/desorption curves for 25.4 mm thickness tested at room temperature with 100% RH.

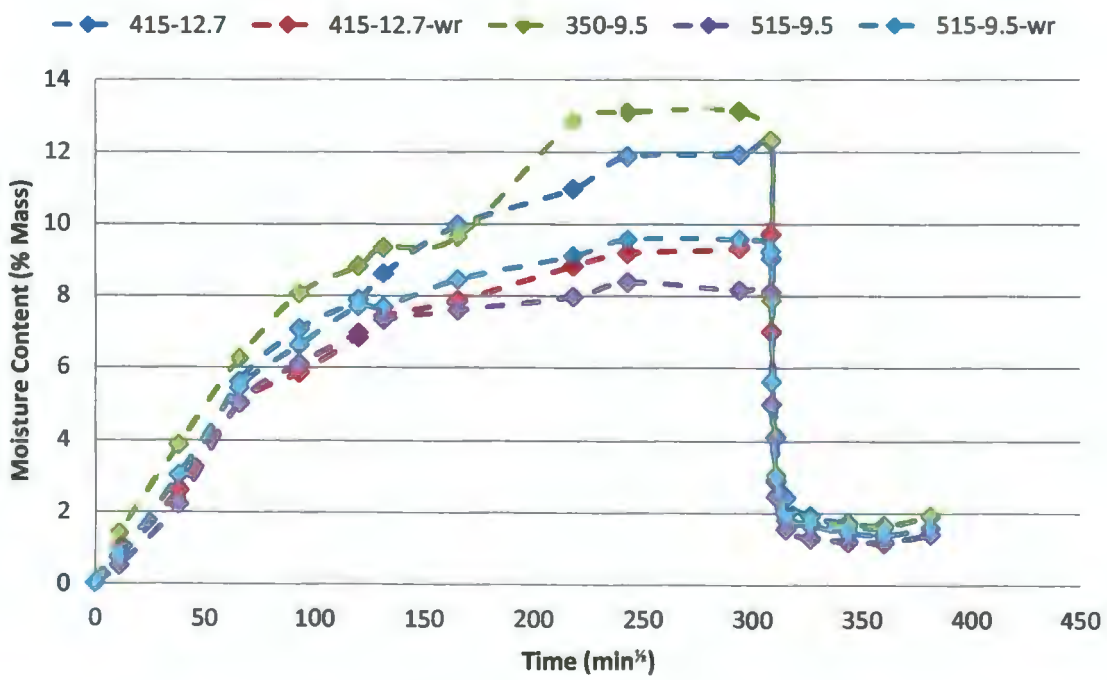

Figure 38: Moisture absorption/desorption curves for 9.5-12.5 mm thickness tested at room temperature with 100% RH.

Figure 38 shows the absorption/desorption curve for the 9.5 and 12.5 mm samples fully submerged in room temperature distilled water. The moisture content of the samples was plotted as a function of the square root of time. It is noted that the time variable is less than that of the time in Figure 37. This is due to the thinner sample thickness reaching the maximum saturation level in a shorter duration. Again, the linear portion of the curve was used to determine the diffusivity coefficient for the samples.

5.2.2. Diffusivity Coefficient

After the absorption/desorption curves were plotted, the diffusivity coefficient was calculated. The diffusivity coefficient was determined at the initial linear portion of the curves. In general, the diffusivity coefficient should increase with temperature, void content, material density, along with other conditions and material parameters. Table 6 lists the diffusivity coefficients in mm^2/s for each of the tested materials and was calculated after 24 h exposure duration. The 24 h exposure duration was chosen since it showed the best fit with the absorption curves. The diffusivity coefficient was calculated using Equation 5.

Table 6: Diffusivity Coefficient for SAS Composite at Ambient Temperature at 100% RH

Series	Diffusivity Coefficient (mm^2/s)	Thickness (mm)	$M_{t\ @\ 24\ hr}$ (% mass)	M_∞ (% mass)
415-25.4	2.35E-5 ± 6.96E-6	25	1.47	11.56
415-25.4-wr-n	3.25E-5 ± 5.19E-6	25	1.56	10.31
415-25.4-wr	2.67E-5 ± 3.46E-6	25	0.91	6.63
515-25.4	4.46E-5 ± 6.08E-6	25	1.46	8.21
515-25.4-wr-n	6.82E-5 ± 1.09E-5	25	1.37	6.11
515-25.4-wr	7.09E-5 ± 6.08E-6	25	1.79	7.75
415-12.7	1.67E-5 ± 3.80E-6	12.7	2.61	12.29
415-12.7-wr	3.08E-5 ± 6.75E-6	12.7	2.58	9.70
350-9.5	1.89E-5 ± 7.12E-6	9.5	3.85	13.12
515-9.5	1.28E-5 ± 1.95E-6	9.5	2.21	8.37
515-9.5-wr	2.52E-5 ± 4.43E-6	9.5	3.02	9.56

From the table of the diffusivity coefficients, it was shown that the 515-25.4-wr series had the fastest absorption rate of 7.09E-5 ± 6.08E-6 mm^2/s and the 515-9.5 series had the slowest rate of 1.28E-5 ± 1.95E-6 mm^2/s, resulting in a difference of approximate a factor of 5.5. The variance within the diffusivity coefficient was resulted from the thickness difference between the two series. The 515-25.4, 515-25.4-wr, and 515-25.4-wr-n series all have high diffusion rates compared to the rest. This was due to a large absorption rate initially, predominately near the surface and then the diffusion rate drastically reduced, resulting in a low maximum saturation level. This is shown from the difference of 415-25.4 and 515-25.4 series having a similar moisture uptake content of approximately 1.46 after 24 h and the 415-25.4 having a saturation content of 11.56 versus 8.21 for the 515-25.4 series. Due to the nature of the high initial moisture absorption and low saturation level, results in the fast diffusivity coefficients.

Figure 39 shows a side-by-side comparison of the diffusivity coefficients for the 25.4 mm thick samples. The figure compares similar layup orientations but with different material densities to show the impact of material density on the diffusivity coefficient. It can be seen for all three orientations that the diffusivity is greatly affected by the material density. The figure showed that the diffusivity coefficient increased with increasing density. As the PU foam density increased the diffusion rate increased and will be discussed in further detail later as there are more than just material density that affects the diffusivity coefficient. The diffusivity coefficient showed a 90% increase for the 515-25.4 versus the 415-25.4 series. The woven roving series exhibited the largest increase of 166% with 7.09E-5 mm^2 diffusivity coefficient for the 515-25.4-wr series from 2.67E-5 mm^2 for the 415-25.4-wr series, followed by the woven roving and no sanded surface with 110% increase.

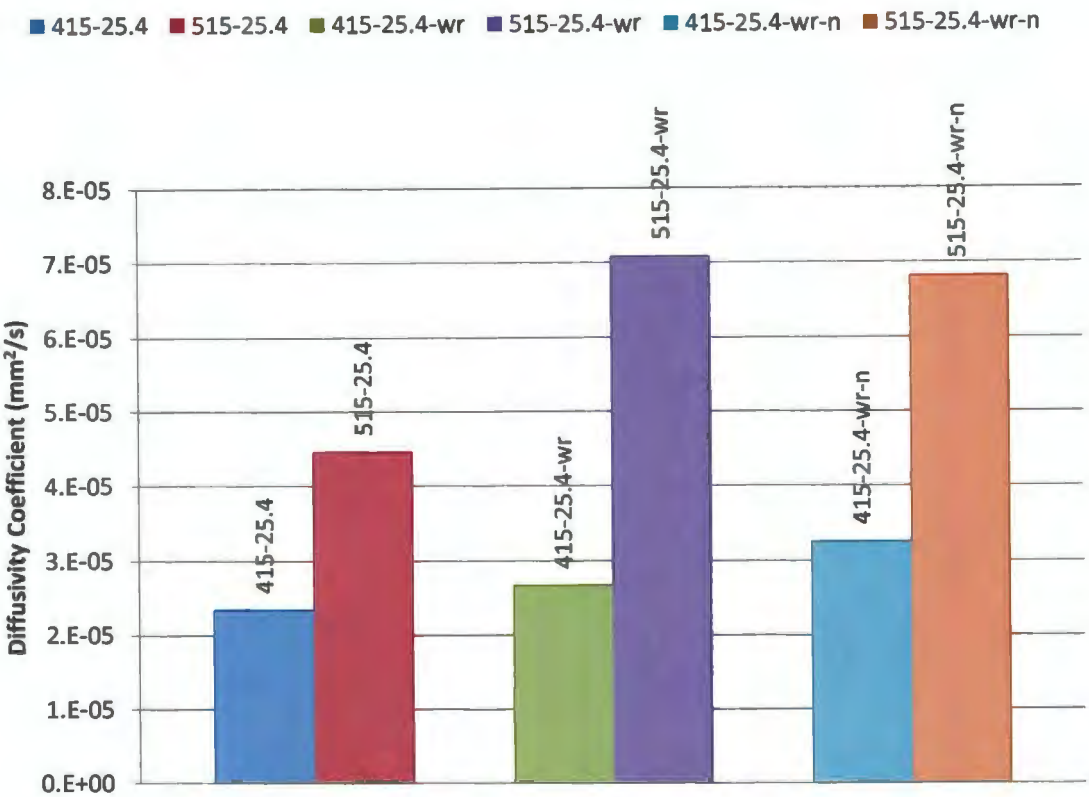

Figure 39: Diffusivity coefficients for 25.4 mm thickness samples.

Figure 40 shows a "radar" plot containing the moisture absorption properties and material parameters for the different moisture test samples. Since there are multiple material parameters that have a combination effect within the material, it is essential to plot all the parameters together in order to visualize how the material responds from the interaction of material parameters. The parameters consist of foam density, fiber content, void content, moisture saturation content, diffusivity coefficient, and thickness. In order to plot all parameters at once, each category had to be normalized by dividing by the largest value within its own category. Zero represents the lowest value and one represents the largest value. The woven roving series is represented with a dashed line where the non-woven roving series is represented by a solid line.

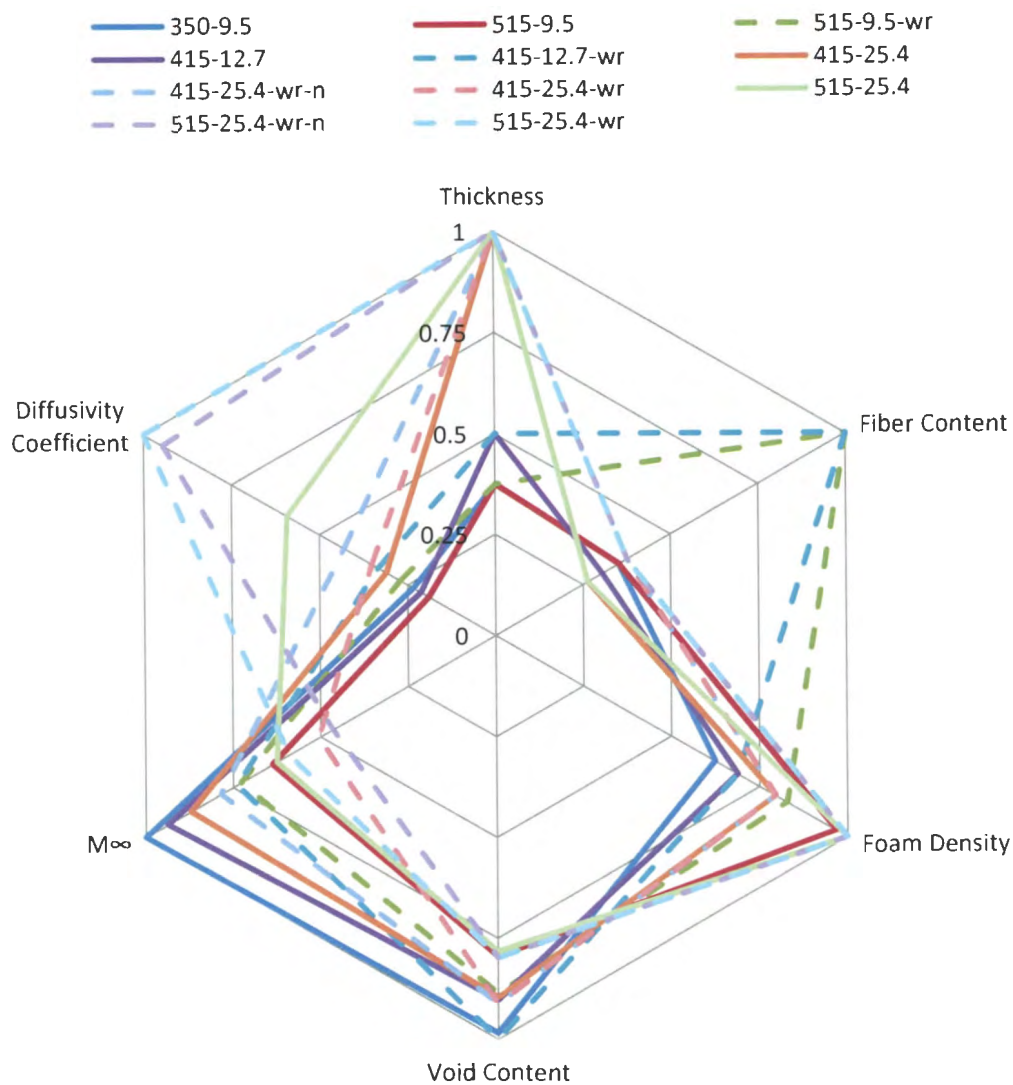

Figure 40: Radar plot of material parameters and moisture absorption properties.

The tensile strength and stiffness are affected by moisture absorption but were not included on the previous plot due to one set of samples not being tested. However, the strength and stiffness are functions of the foam density, fiber content, and void content. As the foam density and fiber content increase, the strength and stiffness are expected to increase, and as the void content increases, the strength and stiffness are expected to decrease.

One of the most influential parameters on the moisture saturation level is the material's void content. As the void content increases, the moisture content increases. This is a result of more "free" volume within the material allowing additional space for the moisture molecules. The void content typically decreases as the foam density increases due to the higher density foam creating thicker cell walls during processing. These thicker walls result in generating smaller voids, and less void content, ultimately resulting in less "free" volume. In addition, the void content also decreases as the fiber content increases due to layup orientation prior to being reaction injection molded. The fiber content is related to the thickness of the material. As the thickness increases, the fiber content tends to decrease. This is due to the layup orientation prior to processing.

The diffusivity coefficient is a complex material property and is a function of multiple parameters. The diffusivity tends to increase with increasing thickness and foam density, and decreasing void content. It is suspected that initially voids are filled with CO_2 which have to diffuse out of the material in order for the moisture molecules to diffuse in the material. The higher density foam puts a larger pressure within the structure and upon contact with moisture, the material plasticizes (softens) allowing faster diffusion of CO_2 out of the structure and moisture in via a capillary affect.

As another verification, an SAS conducted study was conducted consisting of testing full scale production panels fully submerged in room temperature water with the addition of applying a pressure on the material. Once pressure was applied, bubbles from the material rose to the surface which likely was the trapped CO_2 gas exiting. As pressure increased, a larger amount of gas left the material and a higher amount of moisture was absorbed. The addition of exceptionally high pressure caused the material to approximately double in weight in a very short duration. This additional pressure can confirm how the higher foam density applies a larger pressure within the material, resulting in a higher

diffusivity coefficient. However, this additional pressure due to material density could be so slight that the impact on maximum moisture uptake is insignificant.

The next step of the moisture absorption test was to determine how the experimental results follow theoretical results using the following equation [13]:

$$M = M_{\infty}\left\{1 - exp\left[-7.3\left(\frac{Dt}{h^2}\right)^{0.75}\right]\right\} \qquad (12)$$

where M is the moisture content at time t, D is the diffusivity coefficient, h is the sample thickness, and M_{∞} is the saturation moisture content. The equation was derived for Fickian diffusion, assuming a one-dimensional flow field. The above equation is a basis of Fickian diffusion and does not include material parameters, but a mere representation of general one-dimensional diffusion for a set of given boundary conditions. Figure 41 shows the results for the theoretical and experimental data for the 25.4 mm samples. The experimental data was marked with the diamond points and the theoretical data is noted with the dashed lines. A best curve was fitted using the experimental data to determine the diffusivity and moisture saturation content.

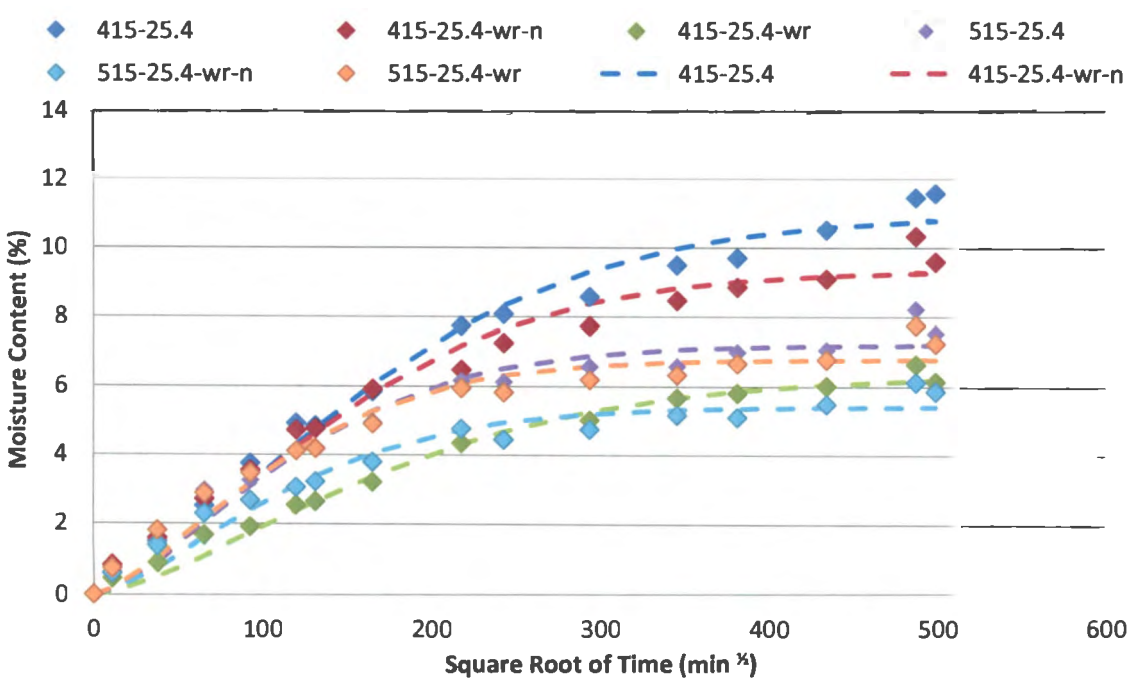

Figure 41: Experimental vs. theoretical modeling for moisture absorption for 25.4 mm thick samples: ♦ (Experimental) -- (Theoretical).

Shown from Figure 41, the theoretical data underestimates the moisture content for the initial portion and maximum saturation content compared to experimental results. Table 7 shows the results comparing the data fit for the experimental versus theoretical for the 25.4 mm samples. The diffusivity for the theoretical model was not determined at a specified time, rather a range of data, whereas the experimental diffusivity was calculated at 24 h of moisture exposure. The theoretical diffusivity is shown to be lower than the experimental resulted from underestimation of moisture content in the initial portion of the test. The 515-25.4 series exhibited the lowest percentage of error of 9.7% and the 515-25.4-wr-n exhibited the highest percentage of error of 39.9%. Table 7 also shows the saturation level displays relatively lower percentages of error for the theoretical results.

Table 7: Single Stage Model of Moisture Absorption Properties for 25.4 mm Series

Series:	415-25.4	415-25.4-wr-n	415-25.4-wr	515-25.4	515-25.4-wr-n	515-25.4-wr
Theoretical Diff (mm^2/s)	2.08E-05	2.67E-05	1.93E-05	4.03E-05	4.28E-05	4.78E-05
Experimental Diff (mm^2/s)	2.34E-05	3.24E-05	2.65E-05	4.46E-05	7.12E-05	7.53E-05
% Error	10.8%	17.7%	27.0%	9.7%	39.9%	36.6%
Theoretical m_∞ (% mass)	10.92	9.31	6.30	7.20	5.41	6.77
Experimental m_∞ (% mass)	11.44	10.31	6.63	8.21	6.11	7.75
% Error	4.5%	9.7%	5.0%	12.3%	11.5%	12.6%

Figure 42 displays the experimental and theoretical moisture absorption results for the 9.5-12.7 mm samples. Again, the experimental results are noted with the diamond points, and the theoretical curves are noted with the dashed lines. The theoretical curves were applied in order to determine the diffusivity coefficient and saturation content. It can be seen that the data fits very well for the 515-9.5 series, but not very well for the 350-9.5 series. This can be attributed to the variance throughout the SAS material due to processing.

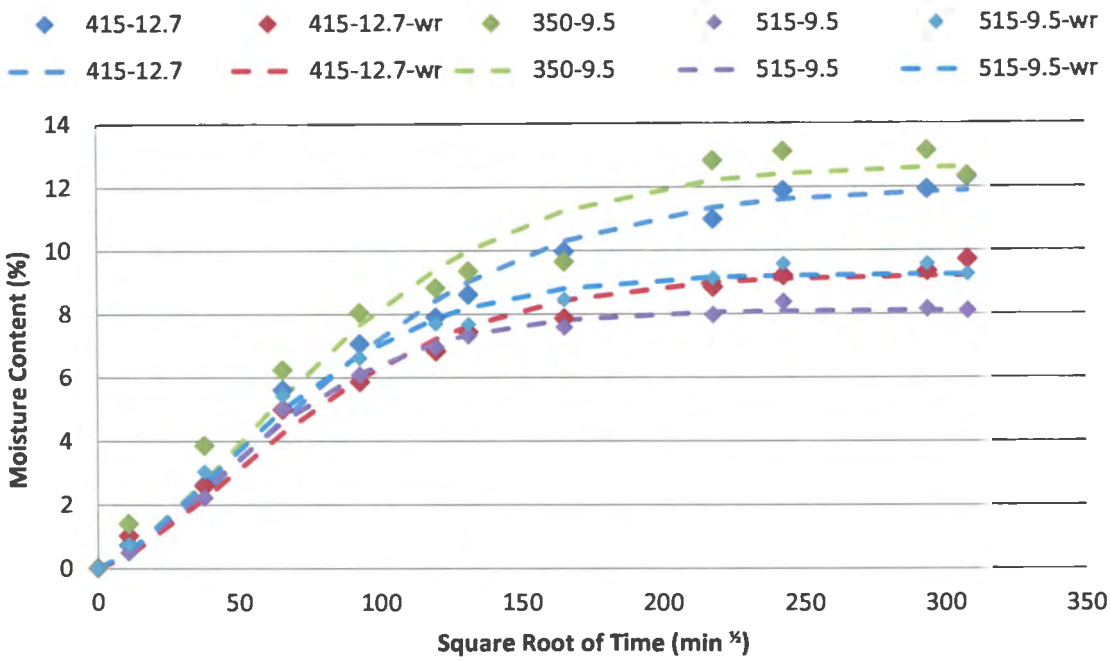

Figure 42: Experimental vs. theoretical modeling for moisture absorption for 9.5-12.5 mm thick samples: ♦ (Experimental) -- (Theoretical).

Table 8 shows the tabulated results for the experimental and theoretical data with the percentage of error difference. It can be seen that the 515-9.5 series showed a 4.3% error in diffusivity coefficient and a 10.8% error in the moisture saturation level, showing a good fit. However, the 350-95 series did not display a good fit with a 57.5% error in diffusivity and a 17.6% error in moisture saturation. Some of this error from the modeling can be accounted for the mathematical model not factoring in material parameters that affect the moisture results (i.e. void content, density, reinforcement content, temperature).

Table 8: Single Stage Model of Moisture Absorption Properties for 9.5-12.7 mm Series

Series:	415-12.7	415-12.7-wr	350-9.5	515-9.5	515-9.5-wr
Theoretical Diff (mm^2/s)	1.73E-05	2.32E-05	1.11E-05	1.95E-05	1.75E-05
Experimental Diff (mm2/s)	2.03E-05	3.02E-05	2.62E-05	1.87E-05	2.58E-05
% Error	15.0%	23.0%	57.5%	4.3%	31.9%
Theoretical m_∞ (% mass)	11.95	9.20	12.67	8.10	9.23
Experimental m_∞ (% mass)	10.91	8.84	10.77	7.31	8.51
% Error	9.5%	4.0%	17.6%	10.8%	8.4%

5.2.3. *Mechanical Tensile Performance*

Figure 43 and Figure 44 show the tensile performance of the 8 series tested after being conditioned at room temperature with 100% RH. When comparing both figures, it can be seen that the strength and modulus follow the same trend for each individual series, or when the strength increases, the modulus also increased. The anticipated trend was thought to show a decrease in tensile strength and modulus as the exposure time increased because of the plasticizing of the samples that occurs.

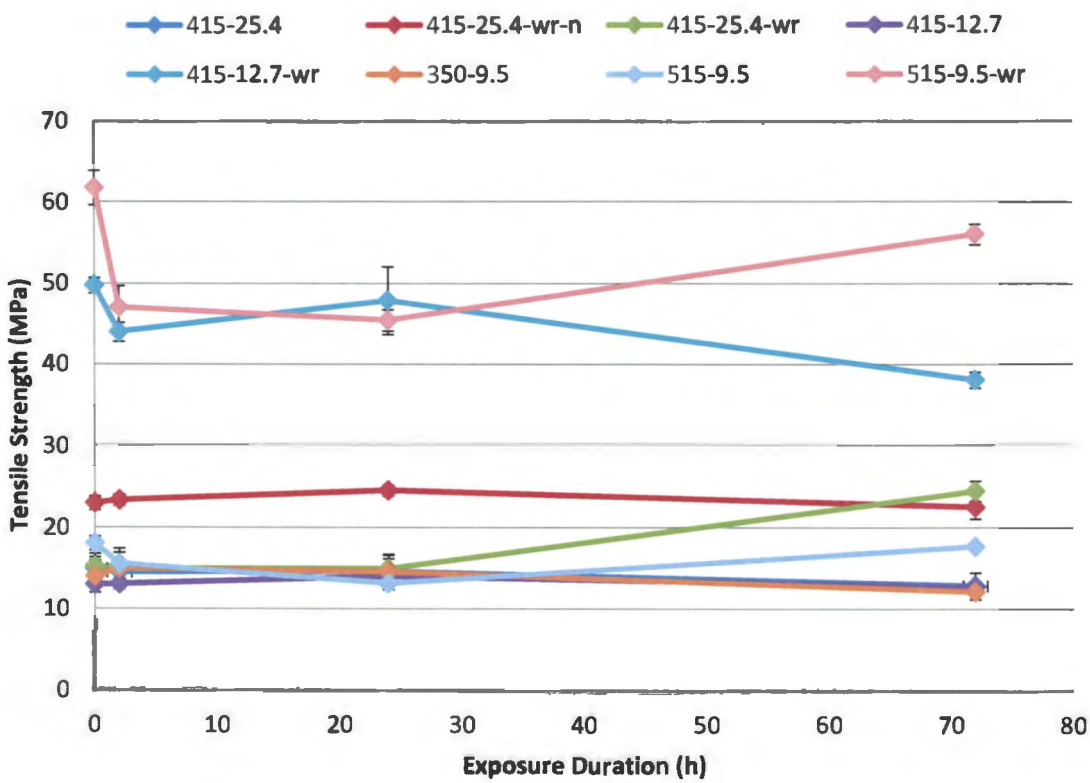

Figure 43: Tensile strength as a function of exposure to 100% RH at ambient temperature.

However, it can be seen that this is not always the case, especially for the 515-9.5-wr series, which shows an exceptionally large increase in performance at 72 h of exposure for both strength and stiffness alike. The 415-12.7-wr series decreased in performance after only 2 h but then increased at 24 h, and again decreased after 72 h of exposure. This inconsistent trend can be concluded to variance from one panel to the next.

The difference between each of the test durations is minimal to where it shows that there is not real evidence that moisture is causing a performance loss after 72 h of exposure.

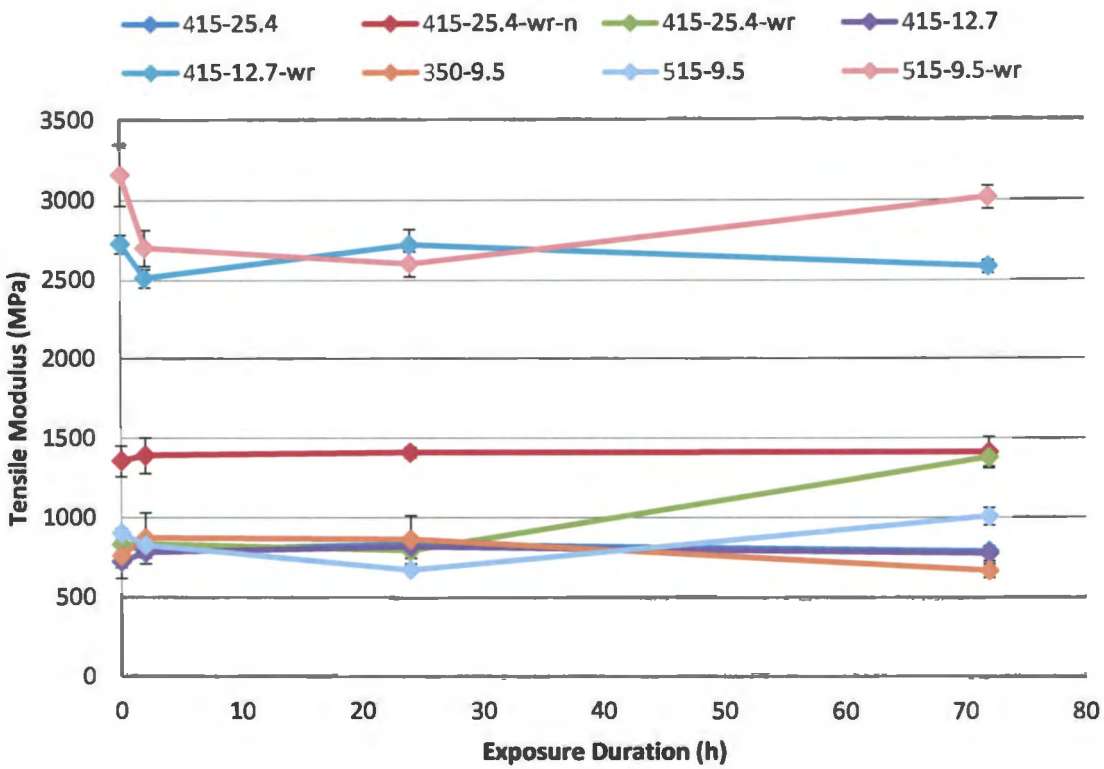

Figure 44: Tensile modulus as a function of exposure to 100% RH in ambient temperature.

Table 9 shows the results for the tensile tests for the non-woven roving series after being subjected to moisture with 100% RH. The table includes a control sample along with samples tested at 2, 24, 72 h, and 2 h boil. It can be concluded that the 2 h boil tensile test did result in the lowest tensile performance for all four of the series which was expected as it was to represent a worst case scenario The table also showed that the 72 h of 100% RH at ambient conditions had no statistical affect on the tensile strength and stiffness. This could be resulted to the moisture being predominately near the surface and hasn't reached the bulk of the material.

Table 9: Tensile Performance After Subjected to 100% RH for Non-woven Roving Series

		350-9.5		515-9.5		415-12.7		415-25.4	
Control		σ_{ult} (MPa)	E (MPa)	σ_{ult} (MPa)	E (MPa)	σ_{ult} (MPa)	E (MPa)	σ_{ult} (MPa)	E (MPa)
	Mean	14	760	18	901	13	722	15	830
	STDV	2.0	139	0.9	30	0.4	34	1.4	56
2 hr		σ_{ult} (MPa)	E (MPa)	σ_{ult} (MPa)	E (MPa)	σ_{ult} (MPa)	E (MPa)	σ_{ult} (MPa)	E (MPa)
	Mean	15	871	16	825	13	780	15	793
	STDV	2.5	160	0.4	29	0.6	31	1.1	46
24 hr		σ_{ult} (MPa)	E (MPa)	σ_{ult} (MPa)	E (MPa)	σ_{ult} (MPa)	E (MPa)	σ_{ult} (MPa)	E (MPa)
	Mean	15	863	13	672	14	816	15	834
	STDV	2.2	150	0.4	14	0.3	29	2.0	53
72 hr		σ_{ult} (MPa)	E (MPa)	σ_{ult} (MPa)	E (MPa)	σ_{ult} (MPa)	E (MPa)	σ_{ult} (MPa)	E (MPa)
	Mean	12	667	18	1007	13	775	13	787
	STDV	0.9	43	0.3	55	0.7	47	1.6	51
2 hr boil		σ_{ult} (MPa)	E (MPa)	σ_{ult} (MPa)	E (MPa)	σ_{ult} (MPa)	E (MPa)	σ_{ult} (MPa)	E (MPa)
	Mean	13	753	13	785	12	697	10	645
	STDV	1.5	107	0.6	35	0.3	24	1.1	92

Table 10 shows the results for the same tensile testing as the previous table except it includes the woven roving series results. Similarly, the performance was expected to decrease with exposure except the 2 h boil, which should result in the lowest performance due to the increased temperature. However, not all series followed this hypothetical trend. The 415-12.7 series resulted in an increase in performance after 2 h and even higher performance after 24 h of exposure, then the 72 h decreased and the 2 h boil showed the worst performance. Conversely, the 415-12.7-wr series followed the expected trend except at 24 h, where the performance was better than at 2 h of exposure. Again, the unexpected tensile performance trends can be attributed to processing variances and unexpected moisture absorption within individual samples.

Table 10: Tensile Performance After Subjected to 100% RH for Woven Roving Series

		515-9.5-wr		415-12.7-wr		415-25.4-wr-n		415-25.4-wr	
Control		σ_{ult} (MPa)	E (MPa)	σ_{ult} (MPa)	E (MPa)	σ_{ult} (MPa)	E (MPa)	σ_{ult} (MPa)	E (MPa)
	Mean	62	3156	50	2726	23	1353	15	830
	STDV	2.1	191	0.9	57	0.8	95	1.5	56
2 hr		σ_{ult} (MPa)	E (MPa)	σ_{ult} (MPa)	E (MPa)	σ_{ult} (MPa)	E (MPa)	σ_{ult} (MPa)	E (MPa)
	Mean	47	2701	44	2510	23	1388	15	834
	STDV	2.7	113	1.2	58	0.7	111	2.0	53
24 hr		σ_{ult} (MPa)	E (MPa)	σ_{ult} (MPa)	E (MPa)	σ_{ult} (MPa)	E (MPa)	σ_{ult} (MPa)	E (MPa)
	Mean	45	2600	48	2721	24	1406	15	793
	STDV	1.3	78	4.2	98	0.6	32	1.2	46
72 hr		σ_{ult} (MPa)	E (MPa)	σ_{ult} (MPa)	E (MPa)	σ_{ult} (MPa)	E (MPa)	σ_{ult} (MPa)	E (MPa)
	Mean	56	3016	38	2582	22	1408	24	1376
	STDV	1.3	72	1.0	41	1.4	98	1.2	56
2 hr boil		σ_{ult} (MPa)	E (MPa)	σ_{ult} (MPa)	E (MPa)	σ_{ult} (MPa)	E (MPa)	σ_{ult} (MPa)	E (MPa)
	Mean	41	2460	36	2214	21	1345	10	645
	STDV	3.1	119	2.1	68	1.8	75	0.9	92

The fiberglass-reinforced PU foam was processed into 1.2-m by 2.4-m sheets. Within the large sheets, there are going to be inconsistencies. These inconsistencies are results of processing large volume sheets where the local density can vary from the global density during the curing process. In addition, the amount of cure, void content, fiber content, etc., can vary locally within a sheet. It is these processing variances that attribute to the tensile performance, where there are slight differences from one sample set to the next. These processing inconsistencies not only had an effect on the tensile performance, but also for the moisture uptake. When you combine the effect on both the tensile performance and moisture uptake, the results could lead to the unexpected results.

From the previous test data, it was unclear on that trend of mechanical performance due to being exposed moisture. In order to show the results are valid, a confidence level with 95% confidence was determined for the strength and stiffness for 6 of the tested sample sets. The results are shown in Table 11 with the mean value and a 95% confidence level.

Table 11: Tensile Performance Showing 95% Confidence Level

		415-12.7		415-25.4		515-9.5	
		σ_{ult} (MPa)	E (MPa)	σ_{ult} (MPa)	E (MPa)	σ_{ult} (MPa)	E (MPa)
Non-Woven Roving	Control	13 ± 0.6	722 ± 53	15 ± 2.3	830 ± 90	18 ± 1.5	901 ± 46
	2 h	14 ± 0.5	816 ± 46	15 ± 3.2	834 ± 84	13 ± 0.7	672 ± 22
	24 h	13 ± 1.0	780 ± 49	15 ± 1.8	793 ± 73	16 ± 0.7	825 ± 47
	72 h	13 ± 1.1	775 ± 74	13 ± 2.6	787 ± 81	18 ± 0.5	1007 ± 88
	2 h boil	12 ± 0.4	697 ± 37	10 ± 1.7	645 ± 146	13 ± 1.0	785 ± 55
		415-12.7-wr		415-25.4-wr		515-9.5-wr	
		σ_{ult} (MPa)	E (MPa)	σ_{ult} (MPa)	E (MPa)	σ_{ult} (MPa)	E (MPa)
Woven Roving	Control	50 ± 1.5	2726 ± 91	15 ± 2.5	830 ± 90	62 ± 3.8	3156 ± 311
	2 h	48 ± 6.6	2721 ± 157	15 ± 3.2	834 ± 84	45 ± 2.1	2600 ±124
	24 h	44 ± 1.9	2510 ±92	15 ± 1.9	793 ± 73	47 ± 4.3	2701 ± 180
	72 h	38 ± 1.5	2582 ±65	24 ± 2.0	1376 ±88	56 ± 2.0	3016 ± 114
	2 h boil	36 ± 3.3	2214 ± 107	10 ± 1.5	645 ± 146	41 ± 4.9	2460 ± 190

From the previous table, it is apparent that the previous tensile test results are valid. This is confirmed with a 95% confidence level showing very good correlation to the standard deviation from the test data. This confirmation shows that moisture uptake had a minimal effect on the tensile performance for exposure in ambient conditions, whereas a decrease in performance was noted when subjected to the boiling water which represents a worst case scenario. This shows that the material can withstand up to the moisture in the environment, making the material suitable to be used within the Navy.

5.3. Ultraviolet Irradiation Results

The next evaluation consisted of testing the reinforced PU foam in a 100% UVA test environment. Previous studies have shown that yellowing does occur [1, 33, 37], thus the objective of the study was to take it one-step further and determine how the mechanical performance is affected by UV irradiation. UVA can cause a photochemical effect within the polymer structure, which could be beneficial or lead to degradation of the material [37].

Table 11 lists the mechanical performance for the 515-9.5 series subjected to 240 h of UVA exposure in a QUV environmental chamber. The first observation was the large discoloration on the surface of the conditioned panels as shown in Figure 45. UV exposure can also lead to a rapid loss in mechanical performance [32-36]. This loss is caused by random chain scission of bonds within the polymer chain resulting in the formation of free radicals [36]. UV irradiation modifies both physical and chemical characteristics of the PU foam surface. The UV exposure can induce photooxidation and thermal oxidation on the surface of the material [32, 33, 37].

5.3.1. Discoloration Shift

The synthesized aromatic PU undergoes photodegradation with gradual change of color. The photochemical degradation of the PU is specifically associated with the scission of the urethane group and photoxidation of the central CH_2 group between the aromatic rings in the backbone of the polymer structure [33]. This chain scission of the aromatic rings will also reduce rigidity. The photooxidation takes place in the aromatic ester structure of the urethanes via a quinonoid route. The urethane bridge oxidizes to a quinine-imide structure. This structure is a strong chromophore, which results in the yellowing of urethanes. Therefore, the mechanism of PU photodegradation is very complex.

Figure 45: Discoloration as a result of UVA exposure.

In this study, the discoloration was characterized using colorimetry. Figure 46 shows the YI as a function of the exposure to UV. It can be seen that the yellowness increased drastically within the first 240 h for both the woven roving and non-woven roving series. The woven roving series was extended to 480 h of exposure and continued to increase from the 240 h exposure. The non-woven roving series exhibited a 418% increase in YI after 240 h of exposure. The woven roving series displayed less of an increase compared to the non-woven roving series of 265% after 240 h and 339% after 480 h. The non-woven roving series exhibited a much larger color shift due to the exposure of UVA irradiation. This is attributed to the woven roving series having the additional fiberglass near the surface. This reinforcement acts as a blocker against UV irradiation, resulting in the lesser color change.

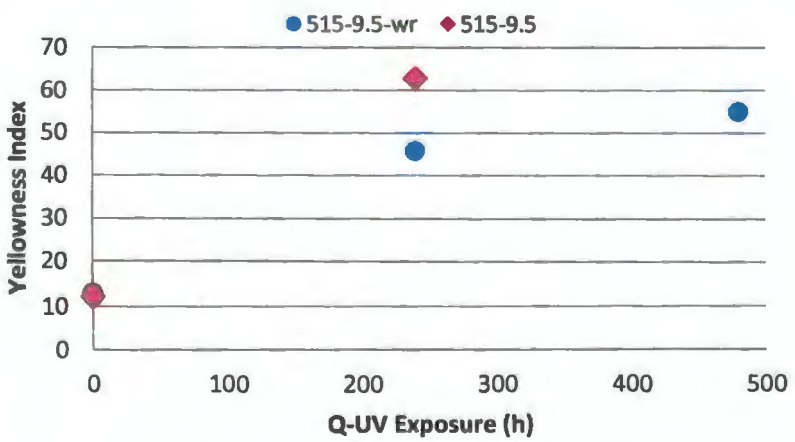

Figure 46: Yellowness Index as a function of UVA exposure.

5.3.2. *Mechanical Tensile Performance*

The second observation was the slight increase in brittleness on the surface. The brittleness is a product of the UV promoting additional cross-linking. This additional cross-linking can be directly related to the extent of cure [1]. For that reason, the UV has a post cure affect on the surface of the PU foam matrix material. Table 12 shows the tensile test results for the 515-9.5 series. A 95% confidence level (95% CL) was determined for the given range of data and shows very good correlation with the standard deviation from the sample set, showing that the test results were valid. The strength showed a 11.7% decrease from 18 ± 0.9 MPa to 16 ± 2.0 MPa after exposure.

Similar to the tensile strength, the modulus decreased from 901 ± 30 MPa to 815 ± 120 MPa from being exposed resulting in a 9.6% decrease in strength. In addition, the standard deviation showed a significant increase after being exposed to UV irradiation, especially within the Young's modulus. This increase in standard deviation was because of the UV irradiation causing chemical changes on the surface. However, these changes do not occur consist enough across the entire surface, which resulted in the increase in standard deviation throughout the SAS composite. This is significant because the standard deviation is anticipated to increase as the exposure to UV irradiation increases.

Table 12: 515-9.5 UVA Exposure, 1.55 W/m^2 @ 60 °C

	Control		240 h Exposure	
	σ_{ult} (MPa)	E (MPa)	σ_{ult} (MPa)	E (MPa)
Mean	18	901	16	815
STDV	0.9	30	2.0	120
95% CL	1.1	37	2.5	148

Figure 47 and 48 show bar charts of the unconditioned and conditioned 515-9.5 series tensile strength and tensile modulus respectively. The mean tensile strength shows a slight decrease in mechanical properties. This loss in performance can be attributed to the chain scission that is occurring through the polymer backbone within the structure. The

performance loss is expected to continue with prolonged exposure as a result of degradation continuing to occur.

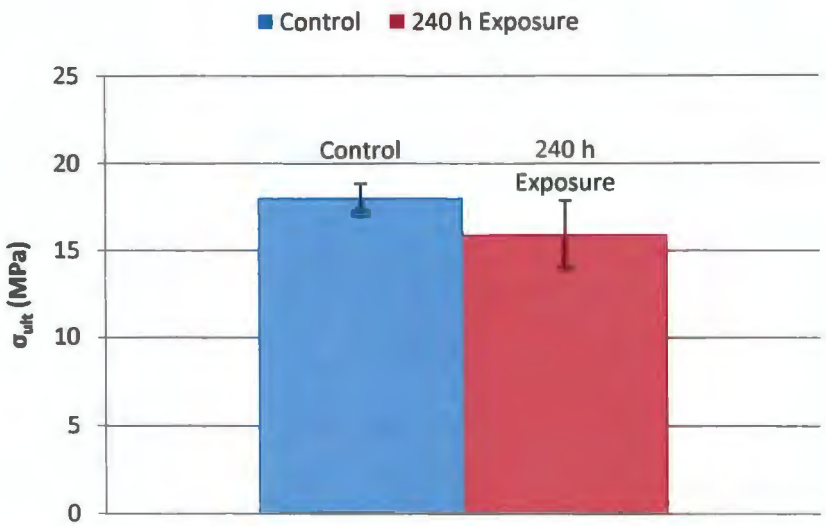

Figure 47: 515-9.5 Ultimate tensile strength comparison.

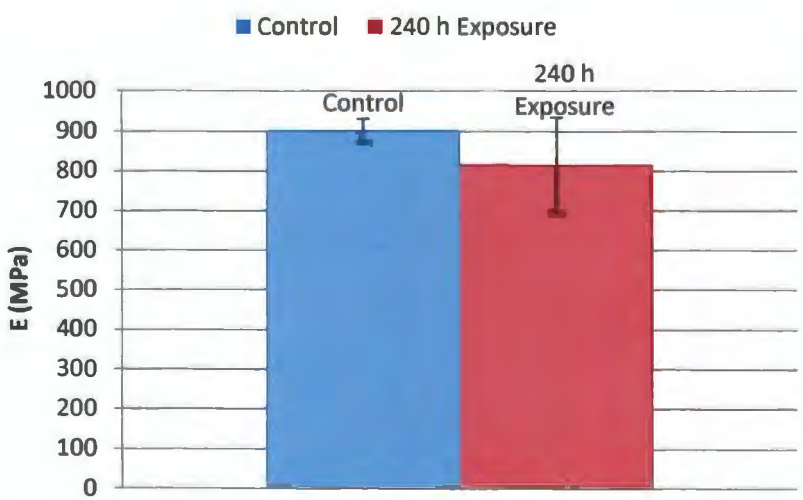

Figure 48: 515-9.5 tensile modulus comparison.

The next aspect of the UV test was to determine the influence the additional woven roving had on the mechanical performance of the reinforced PU foam compared to with the non-woven roving series. Similar to 515-9.5 series, the 515-9.5-wr series exhibited yellowing upon exposure to UVA irradiation. This is expected as the discoloration occurs

only on the surface of the panel, whereas the woven rovings are located below the surface. After exposure for 240 and 480 h, the panels were tensile tested. The results of the tensile test are shown in Table 13 with a mean of five specimens and standard deviation for both tensile strength and modulus. The table also displays a confidence level of 95% (95% CL) to validate the test data. The given confidence level shows that the test data has very good correlation to the given standard deviation for the sample sets.

Table 13: 515-9.5-wr UVA Exposure, 1.55 W/m^2 @ 60 °C

	Control		240 h Exposure		480 h Exposure	
	σ_{ult} (MPa)	E (MPa)	σ_{ult} (MPa)	E (MPa)	σ_{ult} (MPa)	E (MPa)
Mean	44	2577	45	2676	44	2495
STDV	1.7	133	3.6	117	3.4	85
95% CL	1.7	132	2.5	148	4.2	106

The tensile strength and modulus was shown in Figure 49 and 50, respectively. The same trend is seen for both where after 240 h of exposure the properties slightly increase and then decrease. This can be attributed to the initiation of additional cure (cross-linking) up to 240 h after which, chain scission is occurring upon further exposure.

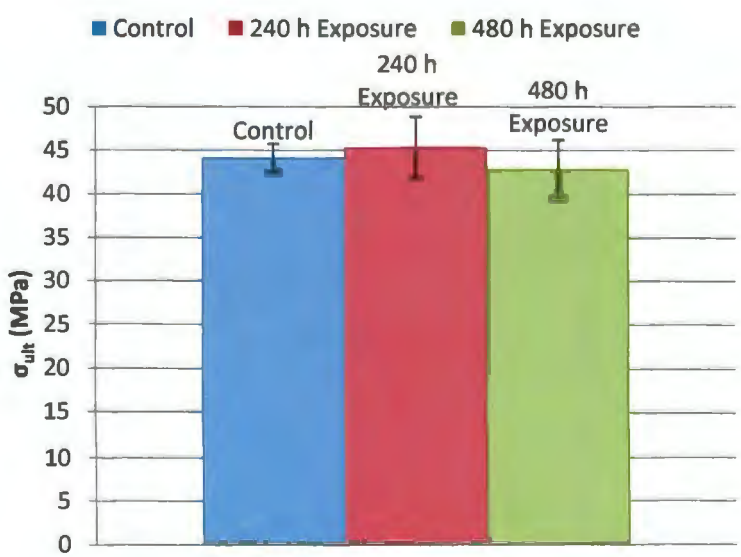

Figure 49: 515-9.5-wr tensile strength comparison.

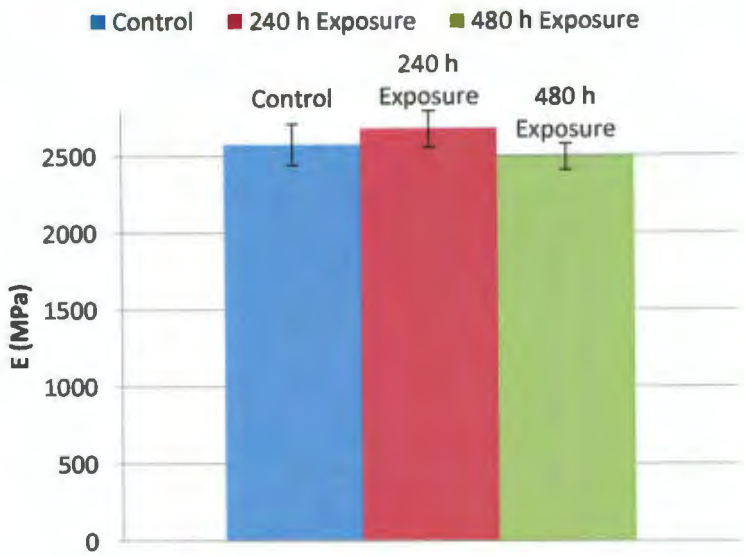

Figure 50: 515-9.5-wr tensile modulus comparison.

The cross-linking was suspected to slightly increase but the effect of chain scission was thought to be the cause of degradation through the polymer structure. The chain scission had a much larger impact than cross-linking, which ultimately is the driving factor for the reduction in strength and modulus. Further testing is needed to better exhibit the rate of cross-linking versus chain scission, and in turn, would better illustrate the mechanical performance effect as a result of UV exposure. Therefore empirical expressions of tensile property change as a function of UV exposure could not be established in this study.

After 240 h of UV exposure, the non-woven roving series showed a slight decrease in properties where the woven roving series showed a slight increase. This shows that the woven roving acts as a UV "stabilizer", inhibiting the UV penetration. The woven roving series did show a decrease in performance after 480 h of exposure, likely where chain scission was impacting the mechanical performance to a greater extent than the additional cross-linking.

5.4. Ultraviolet/Condensation Results

The idea of combining UV and condensation was to incorporate multiple degradation mechanisms within the same conditioning to imitate a real situation. Previous testing showed both UV and moisture to have an effect on the reinforced PU foam. The quantitative objectives for this study were to evaluate PU foam composites and develop a biocomposite material that exhibits simultaneous enhancement in the following quantities:

- Produce a quality panel with the use of 20% by weight sunflower hull filler.
- Show similar baseline properties when comparing the neat PU, the neat PU with sunflower filler, and the carbon black filled PU.
- Maintain similar tensile strength and modulus after UV/moisture exposure for the panel with sunflower filler.
- Prove that biocomposites can be used to increase performance.

5.4.1. Discoloration Shift

One of the characteristics from being conditioned to UV exposure is the color change. This can be seen in Figure 51 for all three of the conditioned panels. The panel with the addition of 20% by weight sunflower was a challenge to process, where it can be noted in Figure 51a with the disparity of color change throughout the panel.

(a) (b) (c)

Figure 51: Set of UV exposed panels for 252 h of UVA @ 0.89 W/m^2 and 60 °C and 252 h condensation @ 50 °C (a) carbon black, (b) neat, (c) neat with 20% SF filler.

5.4.2. Processing Quality

One visualization that was noted for the panels processed with the 20% sunflower hull filler was the uneven distribution of the filler throughout the panel. As the panels were being processed, the sunflower filler generated a very thick consistency when mixed with the polyurethane foam. This thick mixture along with the fiberglass filter hindered the distribution of sunflower filler during the foaming process throughout the panel. This variance can be seen in Figure 52 by the color variance throughout the cross-section of the panel where the filler settled to the bottom. This uneven distribution is going to create variation throughout the panel locally and have an impact on the mechanical properties which could be significant.

Figure 52: 20% by weight sunflower filler distribution.

The unconditioned and conditioned panels were machined into tensile specimens and the color shift as a result of being conditioned can be compared in Figure 53. The color change is a result of the oxidation occurring on the surface due to the presence of oxygen in the atmosphere. As previously stated, the color shift is due to photooxidation taking place in the aromatic ester structure of the urethanes via a quinonoid route. This structure is a strong chromophore, which results in the yellowing of urethanes.

(a) (b)

Figure 53: Set of tensile specimens: (a) unconditioned, (b) conditioned; Top: sunflower filled, Center: carbon black filled, Bottom: neat PU.

In order to quantify the discoloration of the reinforced PU foam, colorimetry was performed on the unconditioned and conditioned specimens and a YI was calculated using Equation 6. Figure 54 shows the YI for the three materials with the data points starting with the unconditioned specimens' YI and ending at the conditioned specimens' YI of 252 h. All three samples did show a significant increase in YI due to exposure with the carbon black filled increasing the largest percentage of 375% followed by the sunflower filled and then the neat PU with 186% and 120% respectively in YI. The variation of the color shift is also largest on the sunflower filled panel which can be seen from Figure 53. This was resulted from the inconsistent distribution of the sunflower filler during processing.

However, the carbon black PU has the lowest YI prior and subsequent to exposure, which is from the addition of carbon black as a filler material. This color shift could be significant when the material is exposed to sunlight during its use. Over time the yellowness will continue to increase along with properties breaking down on the surface. The material may require additional fillers or UV "stabilizers" to mitigate the color shift occurring on the surface of the SAS composites.

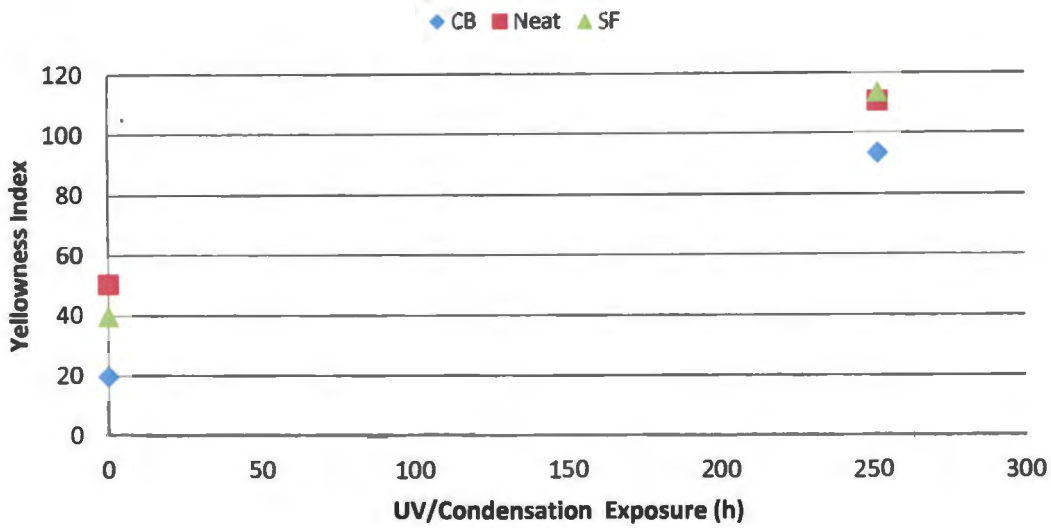

Figure 54: Yellowness Index for the conditioned samples according to ASTM E 313.

5.4.3. Mechanical Tensile Performance

After the specimens were tested, the mechanical properties were calculated and analyzed. Table 13 shows a comparison of the mechanical performance for each of the 6 panels. The ultimate tensile strength is represented by σ_{ult} and the tensile modulus is represented by E. The percentage error shows the difference in density between the baseline, or unconditioned, panel versus the conditioned panel and the percentage drop illustrates the mechanical performance decrease between the baseline panel and the exposed panel. Each value represents a mean of 5 samples with standard deviation for the sample set. The mechanical property values were normalized by density to show the specific strength and specific stiffness for the six reinforced PU foam panels.

The data was normalized by dividing properties measured by the panel density in order to more accurately compare properties as the panel density is a driving factor for material performance. The panels showed slight deviations within the density due to processing capabilities. Table 14 shows the specific mechanical properties for each of the 6 panels. The carbon black-filled is noted "CB" where the exposed set is labeled "Exposed". Likewise, the Neat PU is unfilled, and the sunflower-filled is represented by "SF".

Table 14: Specific Mechanical Property Comparison for UV/Condensation Exposure

Sample	Density (kg/m3)	% Difference	σult (MPa/g/cm3)	STDV	% Drop	E (GPa/g/cm3)	STDV	% Drop
CB	304.3	-	63	4.4	-	3.5	0.2	-
CB Exposed	304.3	0.0	54	2.4	13.7	2.9	0.2	17.6
Neat PU	314.0	-	69	4.6	-	4.0	0.3	-
Neat PU Exposed	352.4	12.2	59	5.4	14.2	3.1	0.3	23.0
SF	355.6	-	46	2.7	-	2.7	0.2	-
SF Exposed	346.0	2.7	39	2.6	14.7	2.6	0.1	6.8

As shown from Table 14, the ultimate tensile strength percent drop was all very similar with the carbon black panel having the least amount of degradation due to exposure. The modulus of elasticity had a larger discrepancy between performance loss after being exposed to the weathering conditions. The sunflower filler exhibited a 6.8% drop in stiffness, whereas the carbon black and neat PU panels demonstrated a much larger decrease of 17.6% and 23.0% respectively. Figure 55 and 56 shows side-by-side comparisons of the specific tensile strength and tensile modulus for each of the six panels, demonstrating the mechanical property loss due to exposure.

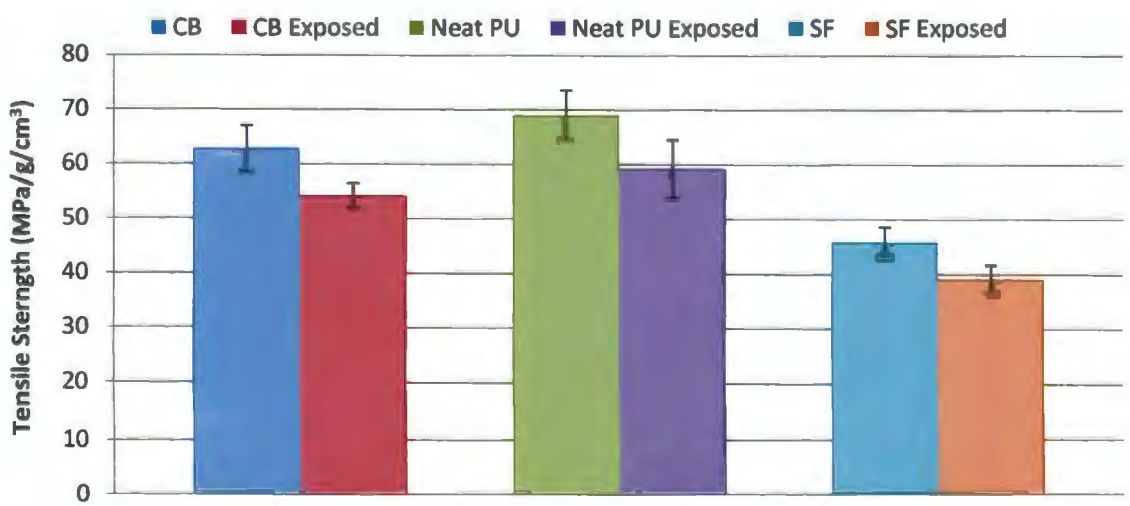

Figure 55: Specific ultimate tensile strength comparison.
Exposed 252 h @ 0.89 W/m^2 @ 60°C and 252 h condensation @ 50°C.

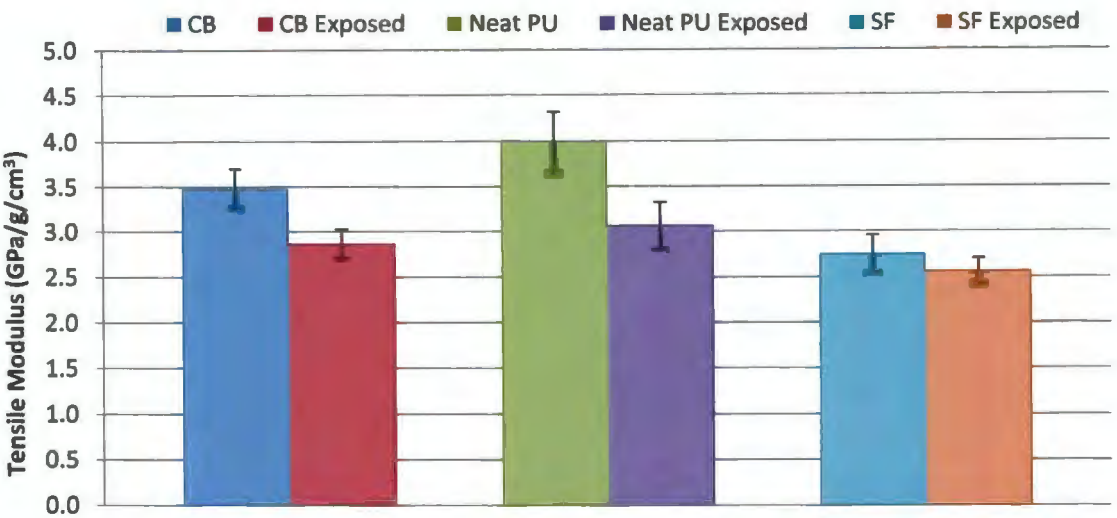

Figure 56: Specific tensile modulus comparison.
Exposed 252 h @ 0.89 W/m^2 @ 60°C and 252 h condensation @ 50°C.

In order to validate the test data, a 95% confidence level was determined for both strength and stiffness for each of the six tested sample sets. The neat PU series displayed a tensile strength of 21 ± 2.4 MPa and tensile modulus of 1080 ± 114 MPa after being exposed to UV/condensation. This shows a very good correlation with the standard deviation of 1.9 and 92 MPa for strength and stiffness, respectively. Given this correlation, it allows one to confidently say the test results are valid. The CB-filled series had a 95% confidence level of ± 1.1 MPa for tensile strength and ± 80 MPa for the tensile modulus after being exposed. Similarly, the SF-filled series showed a tensile strength of 16.3 ± 1.2 MPa and a tensile modulus of 976 ± 94 MPa with 95% confidence prior to exposure. The SF-filled series had a tensile strength of 14 ± 1.1 MPa and a tensile modulus of 885 ± 61 MPa with 95% confidence subsequent to exposure.

As the three panels were exposed to a combination of UV light, moisture, and temperature, it is apparent that the material has undergone a change in properties. First, a shift in color was noticed for each of the exposed panels. Next, a drop in both ultimate tensile strength and tensile modulus was noted. This drop could be a result of any or a

combination of the three conditions the panels were subjected to. Prior testing showed PU foam did in fact absorb moisture, which ultimately reduced the mechanical performance. However, the specimens were dried to try and mitigate the damage moisture has on the material (i.e. remove the reversible plasticization effect of moisture absorption). In addition to the moisture affects, prolonged exposure to the elevated temperature could also affect the mechanical performance (i.e. induced cross-linking or variation of the strength/stiffness) however, the temperature remained well below the materials degradation temperature during the environmental conditioning.

The introduction of ground sunflower hull was to act as a stabilizer to resist the damage done from UV exposure while also maintaining similar baseline properties compared to the same material with no filler. The mechanical testing results did show a performance loss from the addition of sunflower filler. This could be attributed to poor distribution of filler throughout the panel during processing along with inconsistency between panels. The poor distribution causes a separation of the secondary bond interaction which will hinder cross-linking. This secondary bond obstruction allowed the materials ductility to increase. The sunflower filler was shown to exhibit similar properties compared to the carbon black filler. Nevertheless, the properties for the carbon black filler did surpass that of the sunflower filler with the exception of the tensile modulus being higher for that of the sunflower filler after being conditioned to the UV/moisture test.

The discrepancy in mechanical performance can be attributed to processing inconsistencies and the two different PU foams having slight variance in properties. The neat PU foam reinforced with fiberglass showed the best performance among all the panels for the baseline and conditioned properties. After the tensile strength was normalized, the percentage of performance loss for each of the three panels was very similar. The addition of neat sunflower filler did exhibit the least amount of performance loss for the tensile modulus of the material.

5.4.4. *Fourier Transform Infrared Spectroscopy*

Fourier transform infrared spectroscopy (FTIR) spectra were obtained with the unconditioned and the conditioned UV/condensation samples of the surface, 0.25 mm, 0.5 mm, and 2 mm depths. FTIR was used to generate a spectrum to represent the molecular structures absorption/transmission of the infrared radiation. These molecular structures or "fingerprints" are unique.

These fingerprints were used to determine the compositional changes within the specimen caused by the environmental conditioning. Figure 57, 58, and 59 show the FTIR spectra for the neat PU, carbon black filled PU, and PU with 20% by weight sunflower filler. Each of the three figures have a spectrum for a control panel, the surface of the exposed panel, and 0.25, 0.5, and 2 mm depths in the surface of the exposed panel. Each spectrum had a baseline fit in order to bring each curves' peaks and valleys on the zero absorbance or "baseline". Also, each curve was normalized using the C=H band at 2866 cm^{-1} to the make the comparison absorbance/transmission of individual peaks of interest.

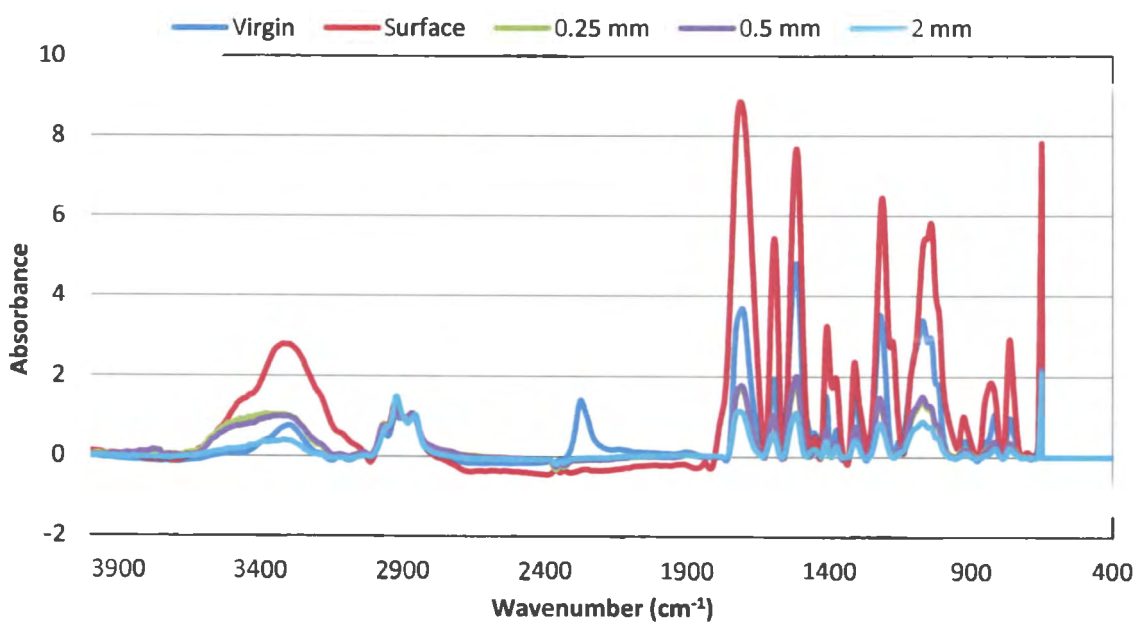

Figure 57: FTIR spectra of neat PU foam.

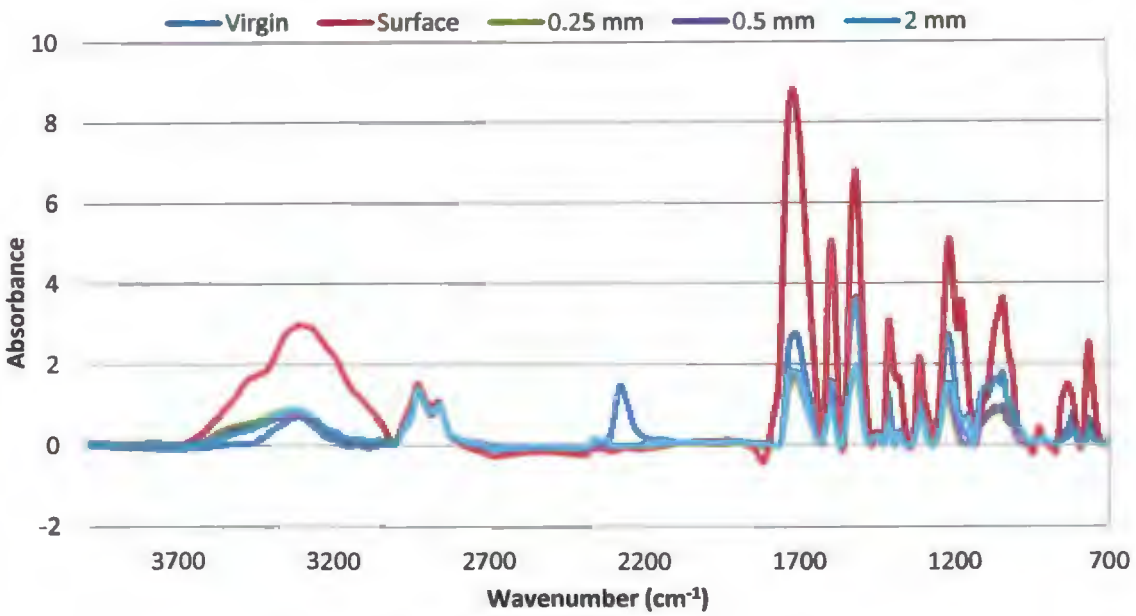

Figure 58: FTIR spectra of CB-filled PU foam.

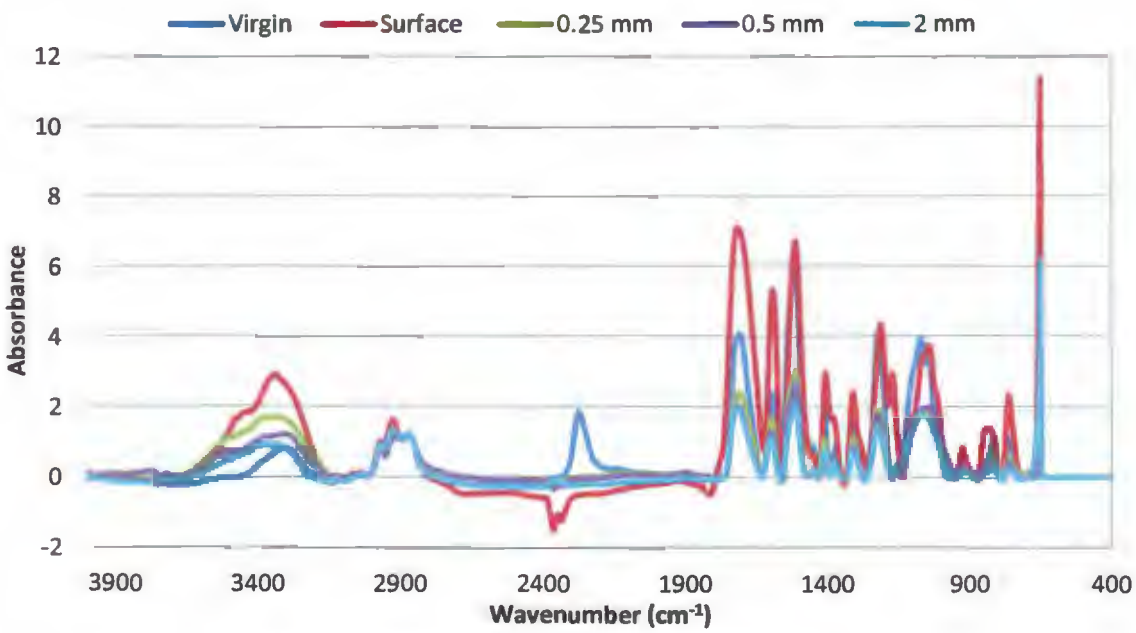

Figure 59: FTIR spectra of SF-filled PU foam.

After the full spectra were plotted, additional spectra plots were plotted to better show the significant "fingerprints" where the reinforced, rigid PU foam was affected by the UV radiation. The three key areas were at 3300, 2260, and 1700 cm^{-1}. The 3300 cm^{-1} peak represents a N-H band, the 2260 cm^{-1} band represents the NCO peak, and the 1700 cm^{-1}

represents the C=O peak. Figures 60, 61, and 62 shows the spectra at the 3300 cm^{-1} peak for the neat PU foam, carbon black filled, and sunflower filled respectively. Thus, in the 3600-3000 cm^{-1} region the signal at the 3300 cm^{-1} peak is characteristic of the stretching vibration of the N-H group. The decrease of the band intensity corresponding to the N-H group indicates a decomposition of urethane structures as a result of UV irradiation [33].

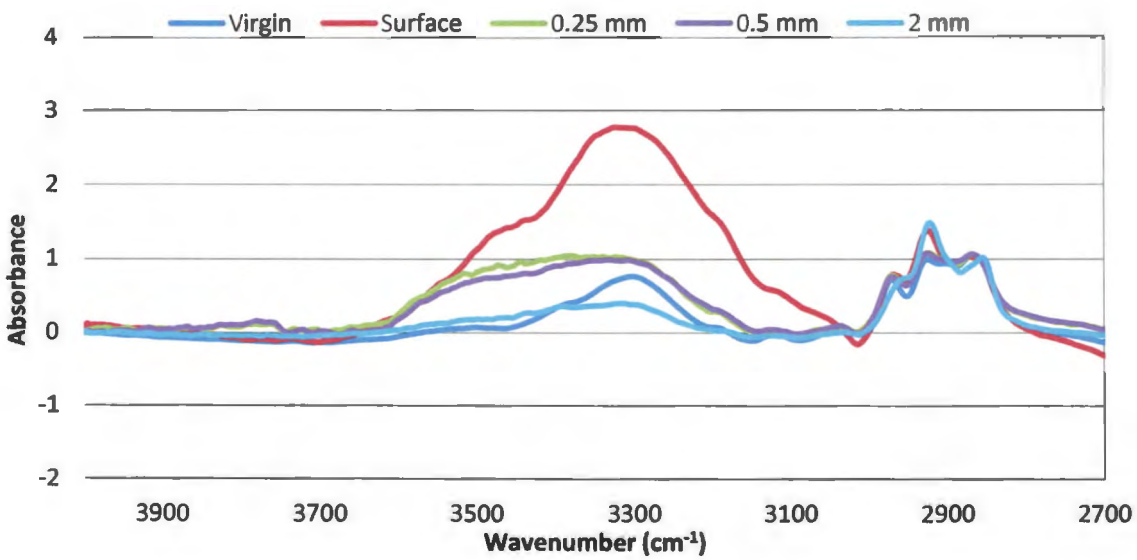

Figure 60: FTIR spectra of neat PU foam at 3300 cm^{-1}.

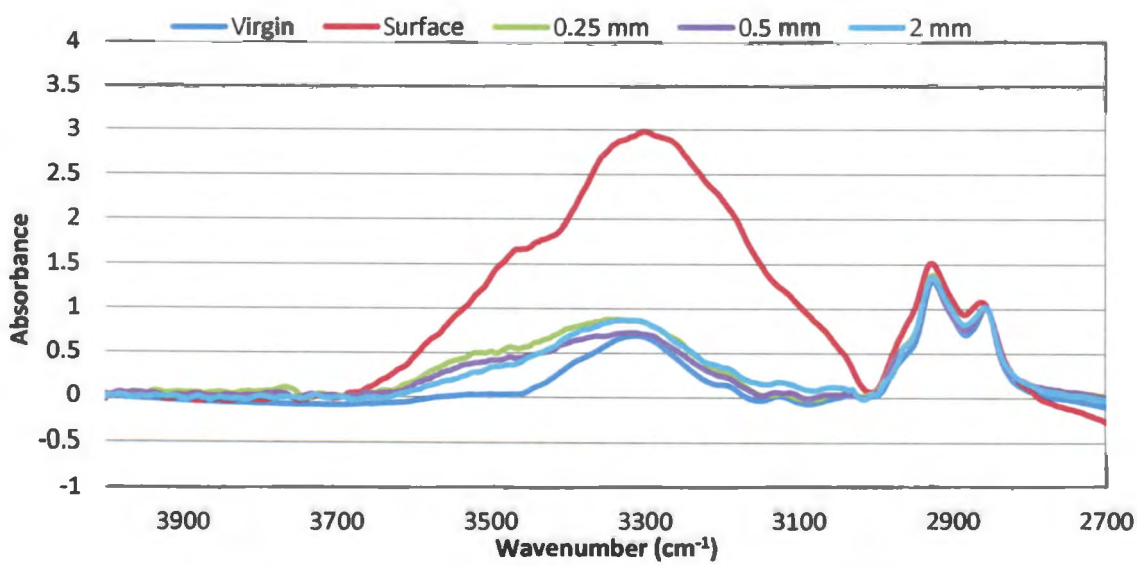

Figure 61: FTIR spectra of CB-filled PU foam at 3300 cm^{-1}.

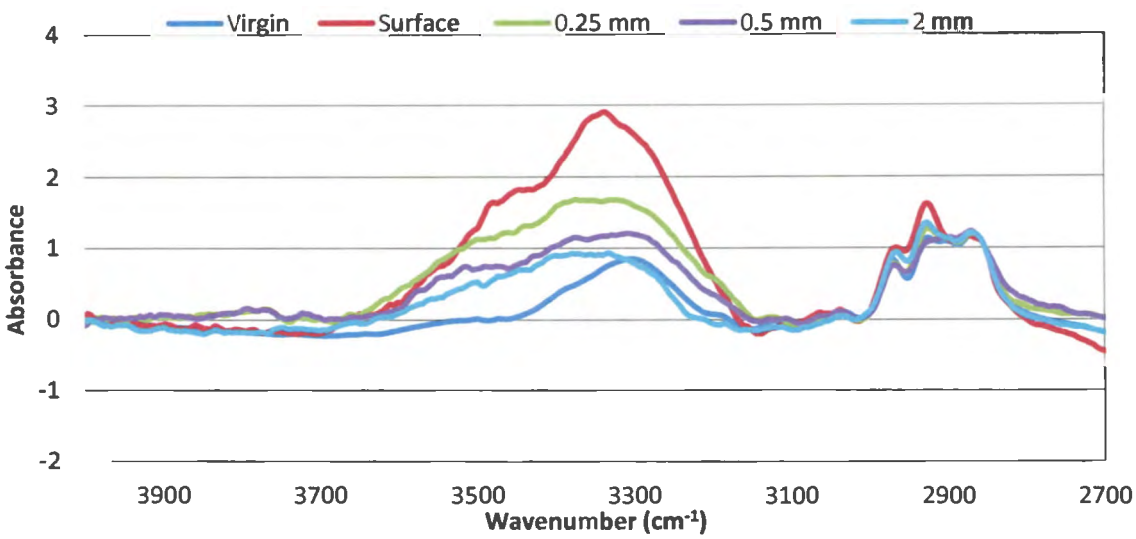

Figure 62: FTIR spectra of SF-filled PU foam at 3300 cm^{-1}.

Figures 63, 64, and 65 shows the spectra at the 2260 cm^{-1} peak for the neat PU foam, carbon black filled, and sunflower filled respectively. The band at the 2260 cm^{-1} peak is characteristic of the NCO group. It can be seen for all three of the following figures that there is a drastic reduction in intensity when compared with the control sample. This drastic reduction is evidence that UV exposure can be attributed to the additional cure. The NCO stretching is a due to the isocyanate curing during exposure to UV irradiation [36].

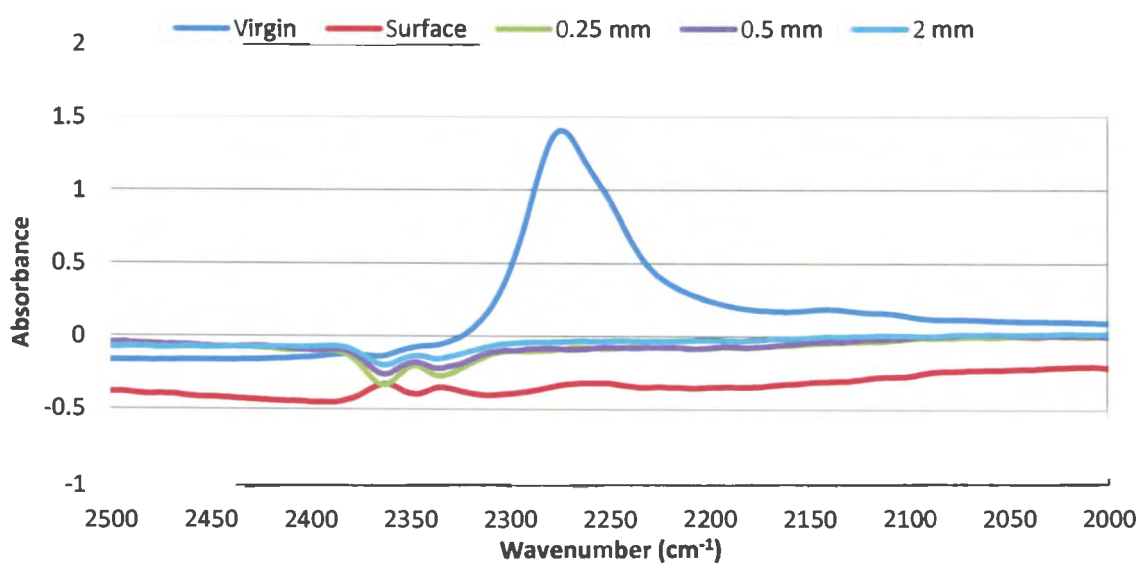

Figure 63: FTIR spectra of neat PU foam at 2260 cm^{-1}.

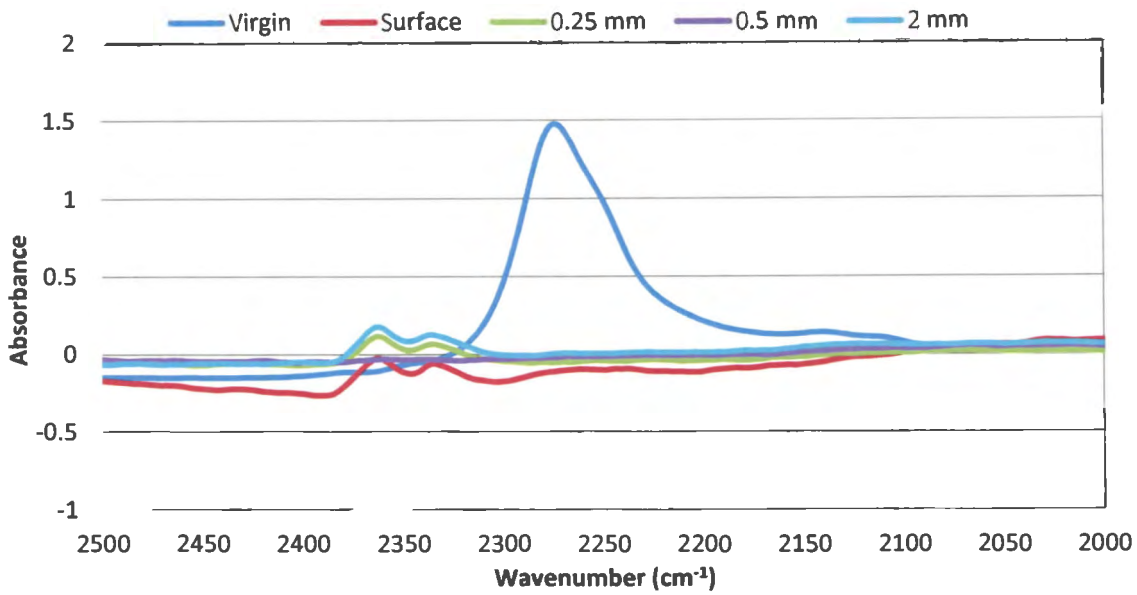

Figure 64: FTIR spectra of CB-filled PU foam at 2260 cm^{-1}.

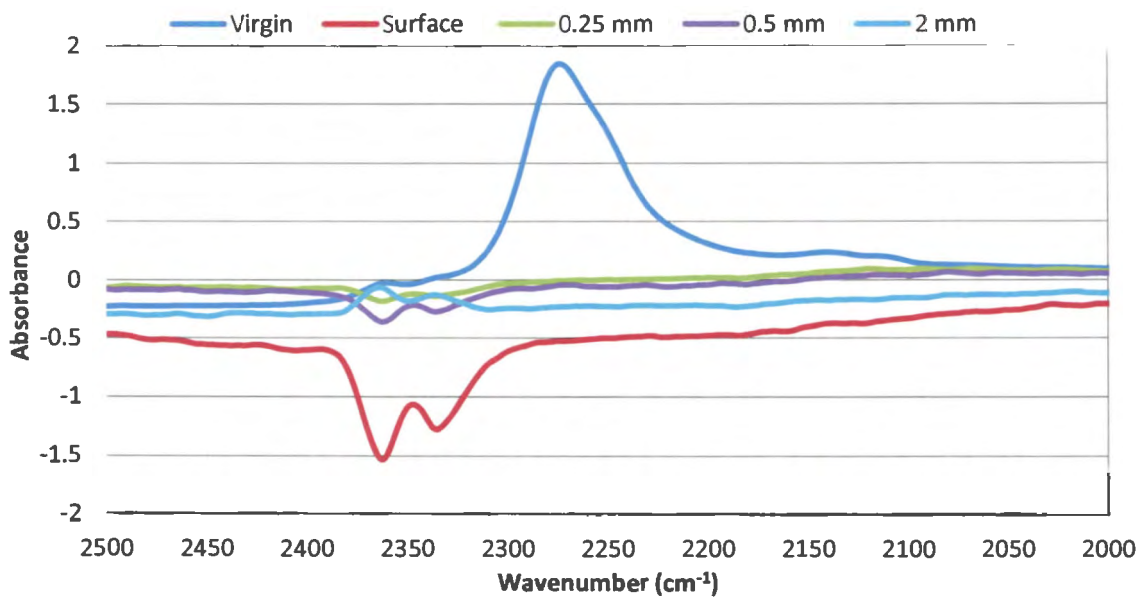

Figure 65: FTIR spectra of SF-filled PU foam at 2260 cm^{-1}.

Figures 66, 67, and 68 shows the carbonyl stretching region (1800-1600 cm^{-1}) focusing primarily on the 1700 cm^{-1} peak for the neat PU foam, carbon black filled, and sunflower filled respectively. The bands in this region can be assigned both to the hydrogen bonded carbonyl vibration, NH-(C=O)-NH of polyurea, and to the free carbonyl stretching

[35]. The band at the 1700 cm^{-1} peak is the C=O group stretching. It can be seen for all three of the following figures that the UV exposed surface has the largest intensity, followed by the unexposed sample. It can also be seen that the 0.25, 0.5 and 2 mm depths all have relatively similar absorbance intensity. The carbonyl stretching vibration appears to be a complex absorption band and shows that the reinforced PU foam does undergo molecular changes indicated by the increase on the surface of the exposed sample.

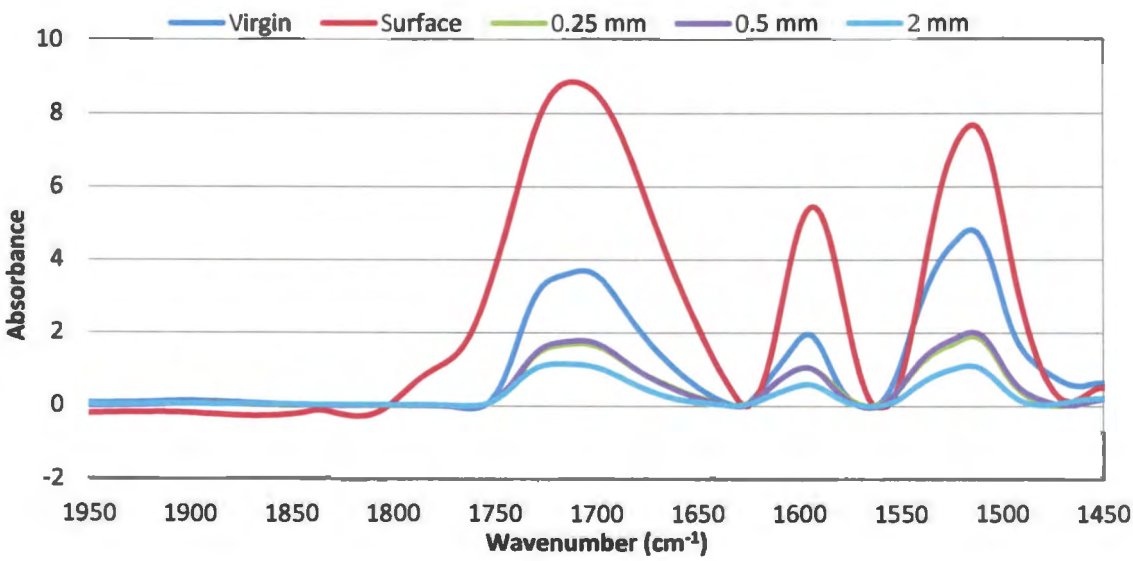

Figure 66: FTIR spectra of neat PU foam at 1700 cm^{-1}.

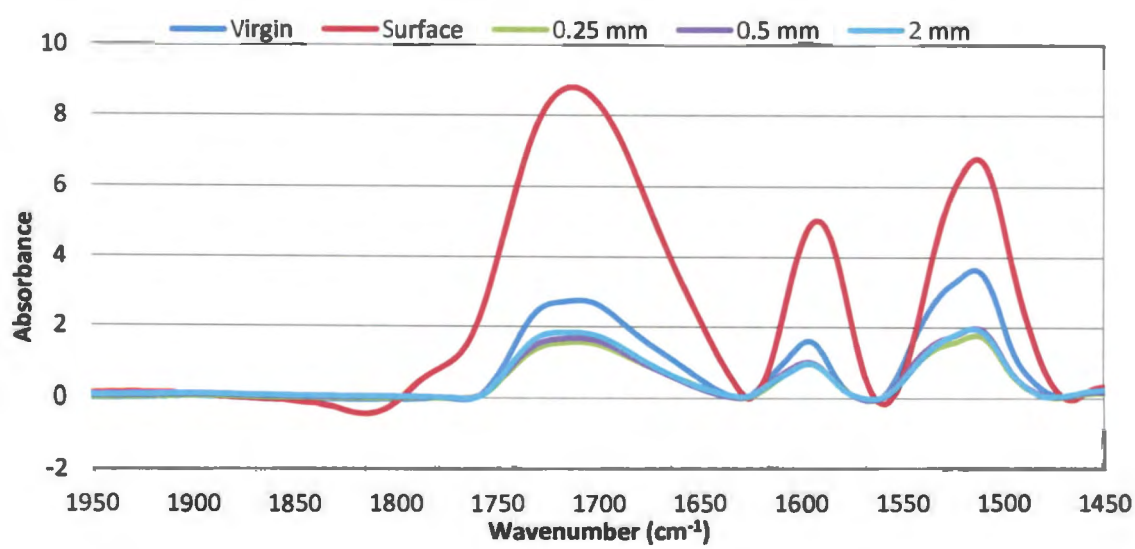

Figure 67: FTIR spectra of CB-filled PU foam at 1700 cm^{-1}.

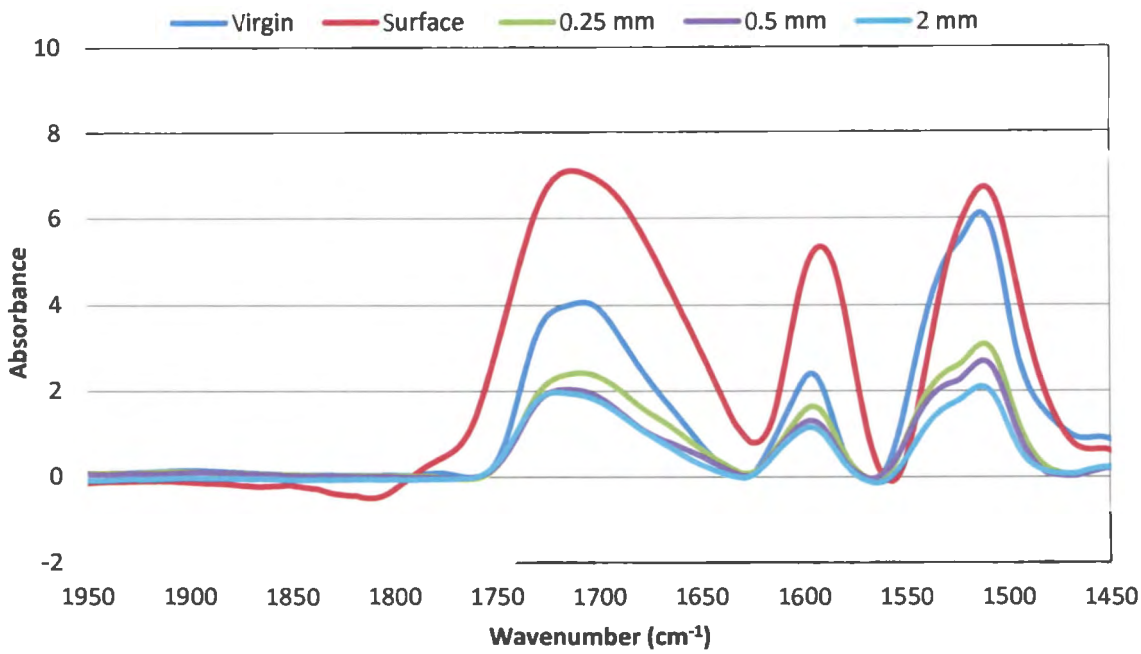

Figure 68: FTIR spectra of SF-filled PU foam at 1700 cm^{-1}.

Compositional changes have been indicated to occur upon exposure to UVA. It is likely to induce chain scission which would presumably lead to re-association of polyurea molecular segments. It is also possible that the surface species are oxidized leading to the formation of carbonyl groups, predominantly formation of polyurea [36].

5.4.5. Depth of UV/Condensation Penetration

Since it is confirmed that there are compositional changes within the polymer structure, the next step was to determine how far the UV irradiation penetrates the surface. Figure 69, 70, and 71 show plots of the absorbance intensity as a function of the sample depth for the three panels exposed to the QUV environmental chamber. For all three figures, it is apparent that most of the compositional changes occur within the first 0.25 mm of the material. Figure 93 shows a very slight change of intensity after 0.25 mm, showing that the UV penetration has minimal impact on the carbonyl stretching region.

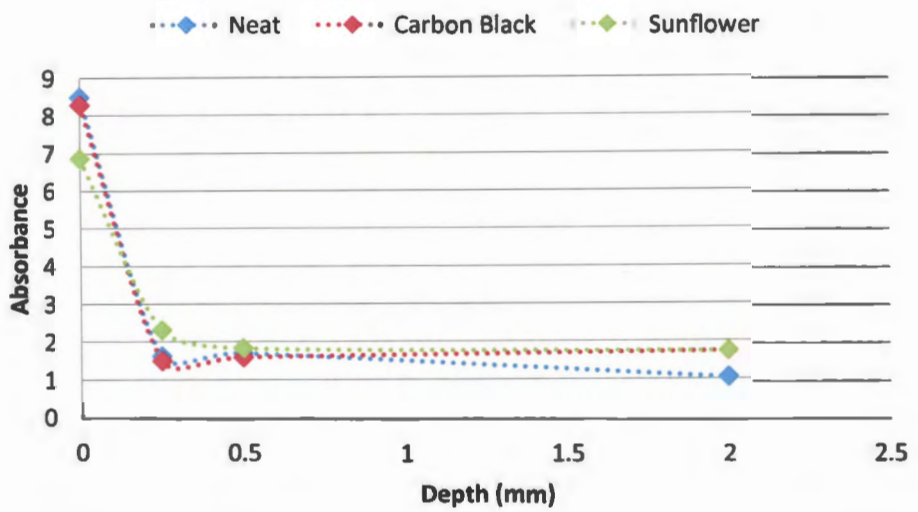

Figure 69: FTIR intensity vs. UV penetration depth @ 1700 cm^{-1} band.

Figure 70 shows the NCO region at the NCO 2260 cm^{-1} band which is related to the amount of isocyante cure. It can be seen for the sunflower filled panel how the amount of cure is highest on the surface, then drastically reduces up to 0.25 mm and then slightly increases within the bulk of the material. This could be a result from the sunflower filler blocking the UV radiation or due to the irregular distribution of sunflower filler causing processing difficulties. However, the intensity is fairly similar for the neat and carbon black filled PU foam.

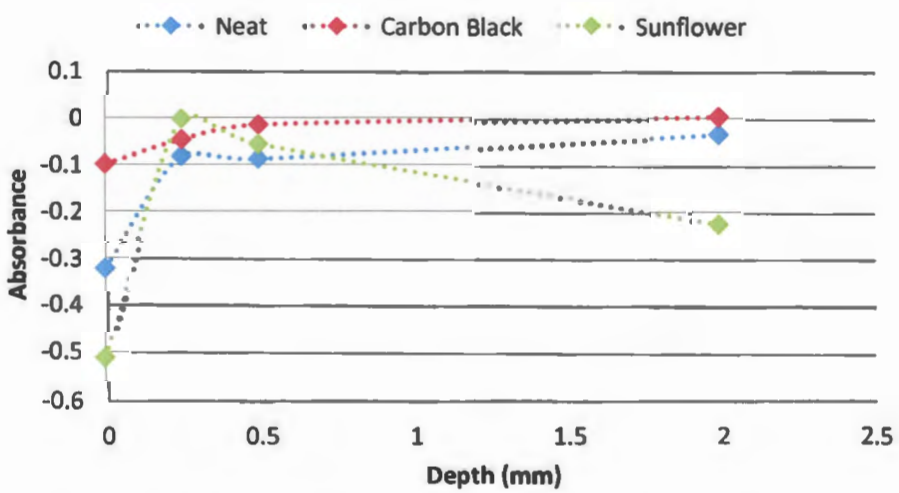

Figure 70: FTIR intensity vs. UV penetration depth @ 2260 cm^{-1} band.

Figure 71 shows the FTIR absorbance versus the sample depth when conditioned in the accelerated weather chamber at the 3300 cm^{-1} N-H band. The plot shows similar results to Figure 69 above where the majority of intensity change occurs within the initial 0.25 mm of the material. However, Figure 70 does show that minimal compositional changes continue to occur for the neat PU and sunflower filled PU, whereas a equilibrium has occurred for the carbon black filled panel.

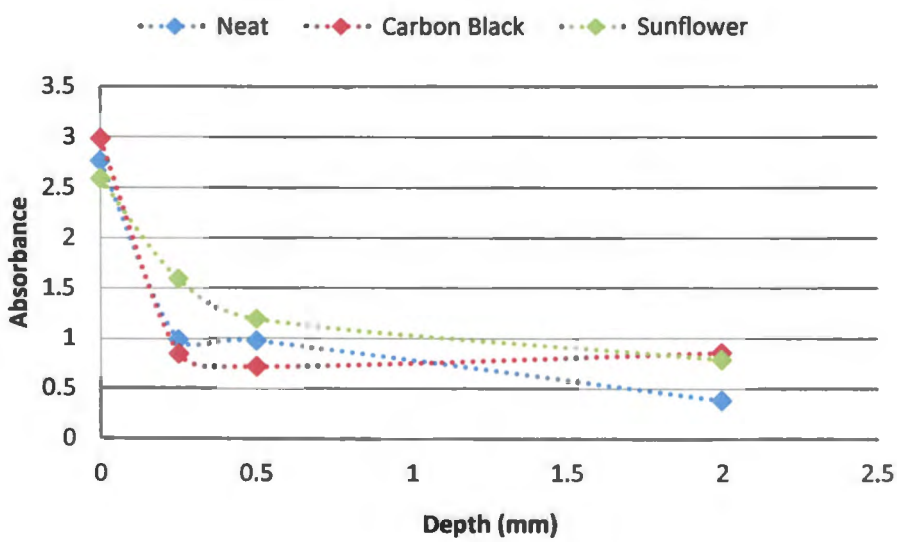

Figure 71: FTIR intensity vs. UV penetration depth @ 3300 cm^{-1} band.

The next set of Figures (72, 73, 74) show the FTIR intensities as a function of exposure time for the three QUV exposed panels within the same band regions as the absorbance versus UV depth. Figure 72 shows a very similar pattern for both the neat and carbon black filled panels, whereas the sunflower filled panel has slightly higher absorbance initially but a lower absorbance after 252 h of exposure. This lower absorbance after exposure shows that the sunflower filler has the highest resistance to UVA within the carbonyl stretching region within the first 252 h of exposure and does have the ability to help inhibit the affects that UV has on the SAS composites.

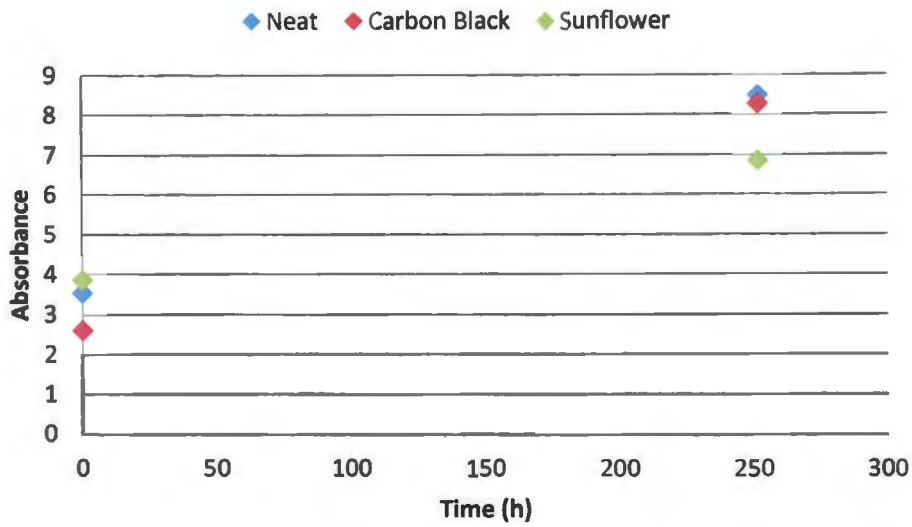

Figure 72: FTIR intensity vs. UV exposure time @ 1700 cm^{-1} band.

Figure 73 shows the cure rate of the isocyanate with polyol as a function of time (hours). FTIR intensities were measured at the NCO band at 2260 cm^{-1}. Figure 73 shows that the sunflower-filled PU panel had the largest change in intensity which showed that the cure rate for the sunflower-filled panel is faster than that of the carbon black filled and neat reinforced PU foam panels.

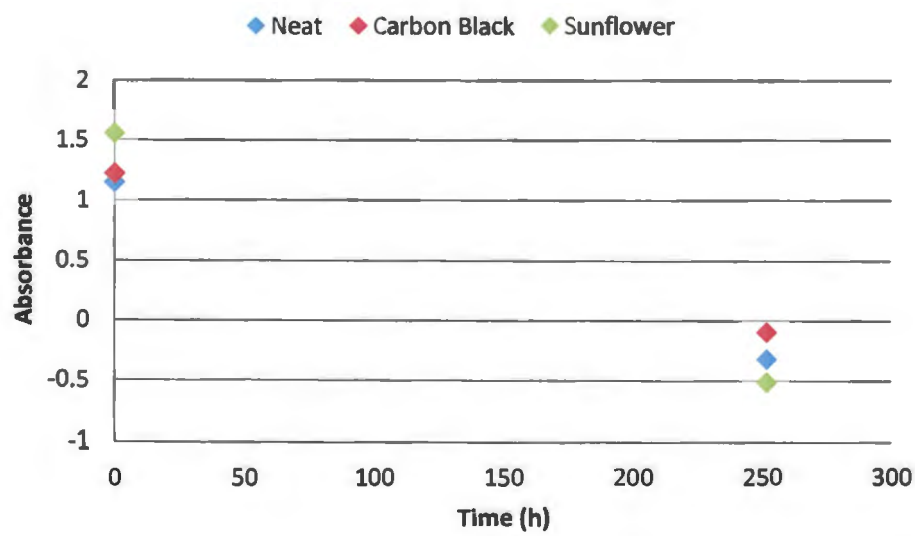

Figure 73: FTIR intensity vs. UV exposure time @ 2260 cm^{-1} band.

Figure 74 shows the NH band located at 3300 cm^{-1} band. It can be seen that all three panels have a similar effect from UVA at the N-H region. All intensities increase with exposure time, where the sunflower filled panel has the highest resistance to UV irradiation, shown by the slightly lower difference between the intensity before and after exposure.

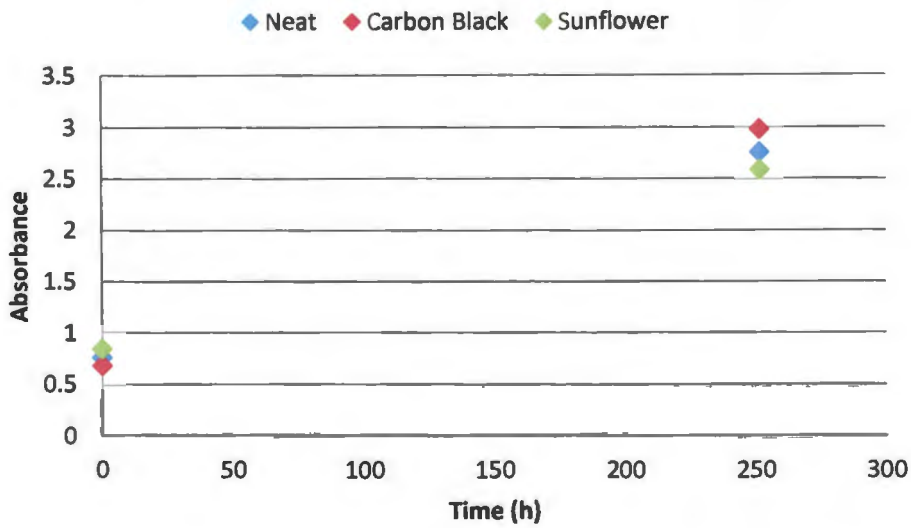

Figure 74: FTIR intensity vs. UV exposure time @ 3300 cm^{-1} band.

The FTIR tests did prove that UV irradiation does have an impact on the reinforced PU foam. Compositional changes were observed, predominately on the surface of the material and steadily decreasing to approximately 0.25 mm into the surface. The more significant compositional changes consist of both cross-linking (additional cure) and chain scission, whereas less important changes were also seen.

5.5. Thermal Properties

In order to fully understand how SAS composites respond to different environmental conditions, certain thermodynamic properties needed to be studied. The properties were analyzed using differential scanning calorimetry (DSC), thermogravimetric analysis (TGA), and post cure tensile tests. The material tested consisted of the foam only

with no glass loading, as the fiberglass would potentially alter the results from testing. The thermodynamic properties to be investigated for this part of the study were:

- Determine glass transition temperature with no secondary post cure process.
- Determine glass transition temperature with a secondary post cure process.
- Determine the two material degradation temperatures.
- Investigate the effect of post cure process on the mechanical performance.

5.5.1. Thermogravimetric Analysis

The degradation temperature is determined using thermogravimetric analysis (TGA) which gradually heats the sample while changes in the weight of the material are observed. The weight changes are associated with the volatilization or decomposition of components of the sample. The large weight percentage drops represent a breakdown within the PU foam and is known as the degradation temperature. The TGA samples were heated to 800 °C at a rate of 20 °C/min. The TGA results for the eight samples are shown in Figure 75. The degradation temperatures are represented by the drastic reduction in weight at approximately 290 °C and 620 °C for the first and second degradation temperatures, respectively.

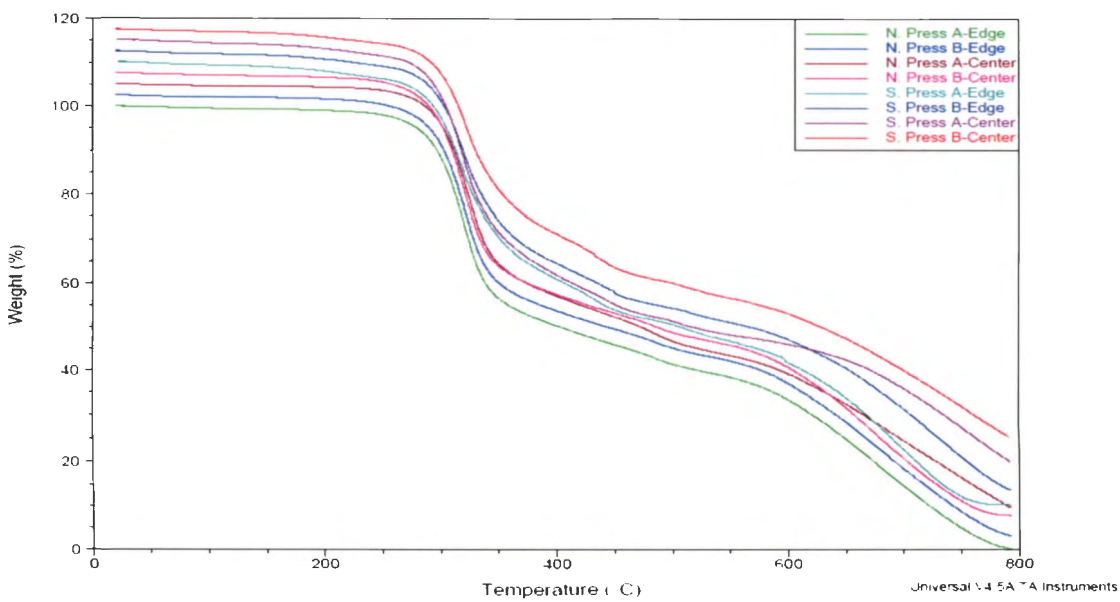

Figure 75: TGA comparison on PU foam.

Table 15 shows the values for the 8 samples' degradation temperatures along with a mean and standard deviation. It is noted that the first degradation temperature is 292 ± 3 °C and a second degradation temperature of 618 ± 22 °C. The first degradation temperature is the one primarily used when determining properties as this is the point where the material begins to break down, which ultimately will hinder the mechanical performance.

Table 15: TGA Degradation Temperature

Sample	TGA 1st Degradation Temp(°C)	TGA 2nd Degradation Temp(°C)
S. Press A-Center	291	650
S. Press A-Edge	286	626
S. Press B-Center	292	631
S. Press B-Edge	295	639
N. Press A-Center	296	608
N. Press A-Edge	293	587
N. Press B-Center	292	600
N. Press B-Edge	292	604
Mean	**292**	**618**
STDV	**3**	**22**

5.5.2. Differential Scanning Calorimetry

The glass transition temperature, T_g, is the thermal transition associated with long-range molecular motion. Below this temperature, the material is rigid and hard and when above, the material will become more flexible and ductile. DSC measures temperature and heat flow associated with thermal transitions in material. The DSC testing performs three cycles (heat, cool, heat). The samples were heated from -50 °C to 175 °C, followed by a cool cycle to -50 °C, and finally heated to 175 °C. The T_g is characterized by a slight change in slope of the final heat cycle and can be seen as approximately 125 °C in Figure 76 for the eight PU foam samples. The first heat cycle and the cool cycle are not shown due to the insignificance in determining the T_g. The heat flow for the curves below is offset so each of the eight samples can be seen in the same figure.

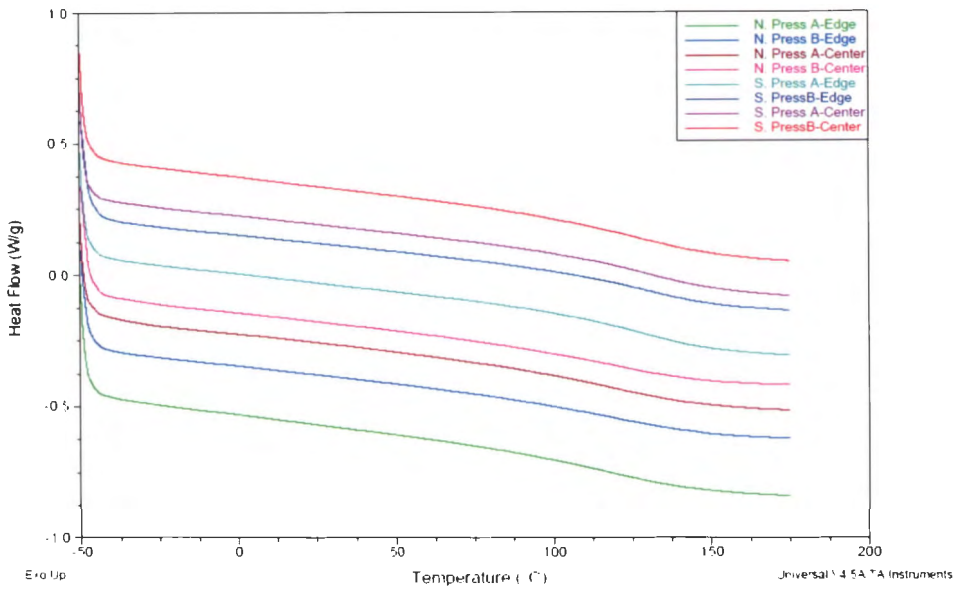

Figure 76: DSC comparison on PU foam.

Table 16 shows the results of the DSC test. Glass transition temperature value was calculated using the TA Universal Analysis vendor software and determines the change in the slope of the DSC curve. It is shown that the south manufacturing press has a mean T_g of 127 ± 2 °C compared to the north manufacturing press at SAS of 121 ± 4 °C. This slight discrepancy is a result of different mold materials and slight variation of the foam used.

Table 16: DSC Glass Transition Temperature

Sample	DSC Glass Transition Temp(°C)
S. Press A-Center	127
S. Press A-Edge	129
S. Press B-Center	126
S. Press B-Edge	125
Mean	127
STDV	2
N. Press A-Center	117
N. Press A-Edge	126
N. Press B-Center	120
N. Press B-Edge	119
Mean	121
STDV	4

The next step after testing the as received PU foam was to incorporate a post cure process. Prior testing of post cured SAS PU foam has shown that a secondary post cure process has induced off gassing. This post cure process induced further cross linking within the PU foam leading to an increase in the T_g. Table 17 shows the results of four different post cure temperatures all with four hours of exposure at the specified temperature. Each test consisted of evaluating the foam at the top, center, and bottom of panel "A" for both the North and South presses at SAS. This was conducted to examine the variation through the thickness of the panel. The T_g variation through the thickness is a result of the bottom of the press having different tool surface than the top tool surface. The differing tool surfaces will insulate the material at diverse rates causing a inconsistent amount of cure within the polymer structure. The north SAS press consists of a MDF wood board for the bottom half and steel tool surface for the top half. Where the south SAS press has a steel tool surface for both the top and bottom.

Table 17: Post Cured PU Foam DSC Glass Transition Temperature.

Sample	Control Material	Post Cured 4 hr @ 100°C	Post Cured 4 hr @ 125°C	Post Cured 4 hr @ 150°C	Post Cured 4 hr @ 175°C
South Press Top	117	126	125	128	120
South Press Center	130	139	130	139	140
South Press Bottom	111	111	112	112	112
Mean	119	125	122	126	124
STDV	10	14	10	13	15
North Press Top	113	111	118	116	121
North Press Center	117	130	138	125	121
North Press Bottom	125	150	139	153	147
Mean	118	131	131	131	130
STDV	6	20	12	19	15

As shown from the table above, the T_g trend does increase with a post cure process. The T_g increased 5.4% from 119 ± 10 °C to 125 ± 14 °C for a post cure temperature of

100 °C on the South press and a 10.5% increase on the North press. However, the post cure temperature does have inconsistencies on the T_g which is better exemplified in Figure 77. The figure shows the mean T_g for each the north and south presses. Each post cure T_g is within standard deviation of each other with slight differences between the means. This is a result of the post cure temperature only promoting so much additional cross linking, resulting in the T_g to not increase between post cure temperatures. However, a increase in T_g is noted from a post cure process versus no post curing.

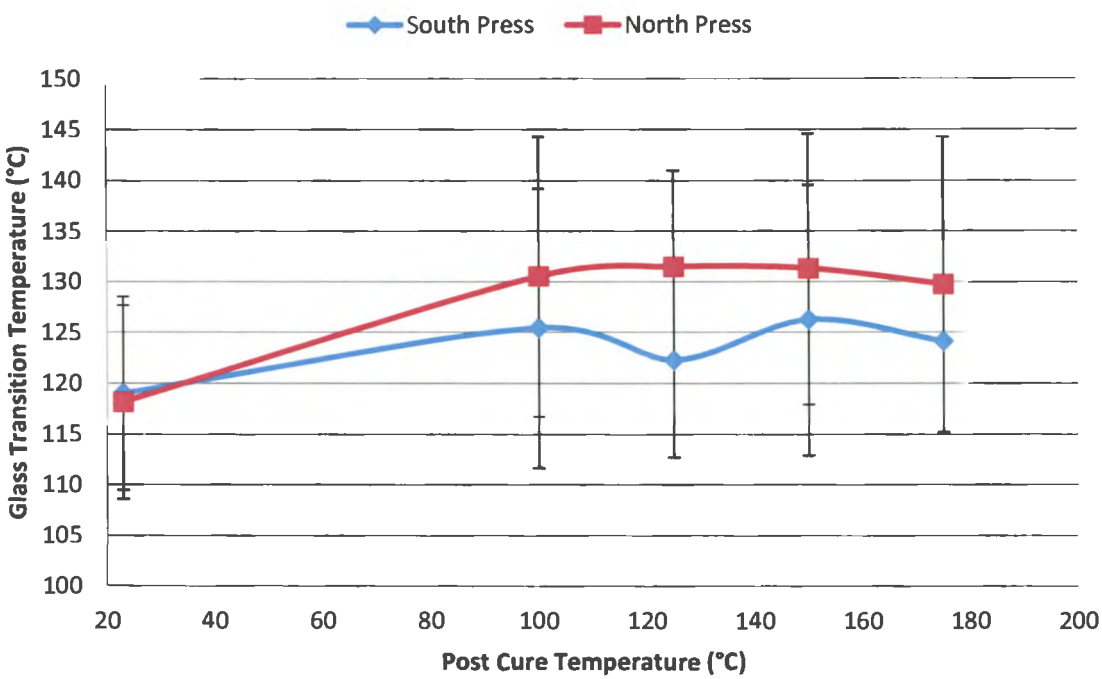

Figure 77: Comparison of glass transition temperature of post cured PU foam.

5.5.3. Post Cure Mechanical Tensile Performance

The final test was to determine how the post cure on the reinforced PU foam affected the mechanical properties, specifically tensile strength and modulus. Previous post cure study did show additional cross-linking within the PU foam and was suspected to increase even with the addition of fiberglass reinforcement, which will not be affected from the secondary post cure procedure. Table 18 shows the results of the tensile test containing ultimate tensile strength and modulus.

Table 18: Post Cure Tensile Test Results on 450-12.7-wr Series

Baseline Material			Post Cure 4 hr @ 80 °C		
Sample	σ_{ult} (MPa)	E (MPa)	Sample	σ_{ult} (MPa)	E (MPa)
1	41.9	2264	1	53.7	2499
2	43.9	2094	2	55.4	2515
3	41.4	2078	3	53.8	2468
4	42.1	2238	4	55.0	2456
5	40.9	2344	5	55.4	2385
Mean	42	2204	Mean	55	2465
STDV	1.2	114	STDV	0.9	51

It is shown from Table 18 that the ultimate tensile strength and the Young's modulus increased after the PU foam was post cured. The post cured panel resulted in an ultimate tensile strength of 55 ± 0.9 MPa, resulting in a 30% increase in tensile strength from 42 ± 1.2 MPa for the baseline panel. The modulus of elasticity also increased from 2204 ± 114 MPa to a 2465 ± 51 MPa resulting in an increase of 12%. The increase in performance is resulted from the additional cross-linking or "cure" that is occurring due to the secondary post cure process. However, the additional cure was not clearly correlated with T_g as initially hypothesized.

CHAPTER 6. CONCLUSIONS AND FUTURE RECOMMENDATIONS

Polyurethane (PU) foam has a vast range of applications due to its many different forms, making PU foam a very common material for everyday applications. Polymeric materials operate in a variety of environmental conditions that could have pronounced impact on their performance [2], consisting of extreme temperatures, moisture, ultraviolet (UV) light, mechanical loads, and combinations thereof [1,9]. These conditions can degrade the polymeric material similar to corrosion in metals. The polymer structure determines how significant of impact the environmental conditions have on polymers.

This study consisted of closed-cell, rigid PU foam as the matrix material with fiberglass reinforcement. In this work, environmental conditions (i.e moisture, UV light, extreme temperatures, or a combination of all three) were investigated through means of physical and mechanical experimentation. Polyurethane foam density, panel thickness, and reinforcement orientation were varied to identify the effects various environmental conditions have in performance as a function of exposure duration or temperature. Mechanical tensile tests, fourier transform infrared spectroscopy (FTIR), differential scanning caliorimetry (DSC), thermal gravimetric analysis (TGA), and colorimetry were used to characterize the performance, degree of degradation, glass transition temperature, degree of cure, decomposition temperature, and color change. The characterization process involved accelerated testing to induce property changes and assure long term integrity [4].

Incorporating fiberglass into the rigid PU foam gives far superior mechanical performance than compared with the neat foam alone. The degradation of rigid PU foam material can occur from several factors: loss of strength of the fibers, loss of interfacial bond strength, chemical degradation of the matrix material, temperature effects on the modulus and strength of the matrix material, and accelerated degradation as a combination of multiple factors [8]. The degradation of the composite occurs as an interaction between the constituents along with each of the individual components [8].

This research topic arose from U.S. Navy / SpaceAge Synthetics Spartan Scout project, where some work is subcontracted to North Dakota State University. The project involves designing and testing of components that have the potential to be used by the U.S. Navy in the Spartan Scout. The trouble with the Spartan Scout is the weight of the vessel is too heavy, whereas SpaceAge Synthetics materials incorporate lightweight structures while having high specific strength and specific stiffness. It is these strong, yet lightweight structures that have the advantage to use in the Navy over many existing monolithic structures with the intention to reduce weight while maintaining strength and integrity.

In order to ensure SAS materials remain structurally sound during use, testing had to be executed to fully characterize the performance and modifications of the PU foam reinforced with fiberglass. As the Spartan Scout is in service, the vessel will be exposed to moisture, extreme temperatures, UV light, and combinations of each. Therefore the importance to study SAS material under natural, environmental operating conditions is essential.

Subsequent to being exposed to various environmental conditions, the reinforced PU foam material did show performance shifts and compositional changes due to exposure. Each conditioning criteria had a different effect on the material, where both an improvement and reduction in properties were seen. Temperature had the largest influence in mechanical performance drop, whereas an increase in performance was noted for the secondary post cure process. Moisture absorption had a pronounced effect in mechanical properties and caused plasticization, whereas UV exposure mainly resulting in compositional changes which slightly altered the mechanical performance.

6.1. Temperature Test Conclusions

After being subjected to a temperature, it was apparent that the strength and Young's modulus decreased as the temperature increased. This is because the PU foam matrix material became more ductile with increasing temperature. As the matrix becomes

more ductile, more molecular movement is permitted within the polymer chains. This increase in molecular motion allows the polymer chains to slide past one another with less restriction, which ultimately reduces the strength and modulus. This decrease in strength and modulus was noted for both the 385-12.7 and 450-12.7-wr series. The temperature testing experienced a temperature range from –40 to 121 °C resulting in a 52% decrease in strength for the 385-12.7 series with a 21% decrease in strength from -40 °C to ambient temperature (28 °C). The 450-12.7-wr series exhibited a 48% decrease in strength over the entire temperature range from 61 ± 1.0 MPa at -40 °C to 32 ± 3.1 MPa at 121 °C. Similar to the strength parameter, the modulus decreased 49% and 40% respectively for the 385-12.7 and 450-12.7-wr series over the temperature range. Temperatures that deviate from ambient conditions show an increase in strength properties with a temperature below ambient and a decrease in properties with a temperature above ambient conditions. However, the strain-to-failure reduces with a decrease in temperature.

The addition of the extra fiberglass was hypothesized to help reduced the impact temperature had within the SAS composite, but it was shown to have just as determintal effect as the non-woven roving series did. A trend was fitted to previous data for strength and modulus for both series and empirical expressions were generated from the data trend. The next step would consist of extending the temperature ranges further to demonstrate if the material would continue to embrace the linear trend or if the strength and modulus would plateau at a certain temperature. Also, the material density would be altered to show the effect of the foam density.

6.2. Moisture Test Conclusions

Similar to the effects of temperature, the material is also affected by moisture but to a lesser extent. The fiberglass-reinforced PU foam did in fact absorb moisture, which caused plasticization throughout the material. This plasticization effect causes the material to soften and slightly swell, which ultimately should reduce the mechanical performance.

As expected, the material absorbed moisture continuously until the saturation point was reached. The 25.4 mm samples took a longer exposure duration to reach full saturation than the 12.7 and 9.5 mm samples. The 350-9.5 series absorbed the largest percentage moisture content of 13.12% and the 515-25.4-wr-n series absorbed the least amount of 6.11%. The 515-25.4-wr series had the fastest diffusivity rate of 7.09E-5 ± 6.08E-6 mm^2/s and the 515-9.5 series had the slowest rate of 1.28E-5 ± 1.95E-6 mm^2/s, resulting in a difference of approximately a factor of 5.5.

It was also shown that the diffusivity depended upon the material thickness, foam density, and void content. As the thickness and density increases, the diffusivity also increased. In addition, increasing the void content decreased the diffusivity rate and the void content increased with a decreasing foam density, which was the driving factor for the max saturation content. A confidence level of 95% was determined for the mechanical performance test data. After being subjected to moisture, the tensile performance didn't show any statistical difference from the control sets. The 95% confidence level show good correlation to the test data allowing one to consider the test data valid. However, a performance decrease was shown after the samples were conditioned in the boiled water for 2 h. For example, the 515-9.5 series showed a 28% decrease in tensile strength and a13% decrease in tensile modulus. Likewise, the 350-9.5 series had less of an impact due to the boiling water. The series showed a 7% decrease in strength and 1% decrease in stiffness. The 515-9.5-wr showed a similar decrease in properties with a drop of 34% in strength and 22% decrease in stiffness, showing the additional reinforcement had slight improvement in mechanical properties.

Due to the long exposure durations, future work would consist of determining the diffusivity coefficient and max saturation level at a RH less than 100% (i.e. 80% RH). This would result in a diffusion rate and saturation level less than that of 100% RH. In addition, it would be of interest to examine the reversible and irreversible effects once exposed to

moisture then dried to demonstrate how the mechanical performance is affected. Along with a one-dimensional diffusion, a three-dimensional diffusion could greatly affect increase the rate of diffusion but maintain similar max saturation levels. Lastly, the T_g could be determined as a function of moisture uptake, whereas the T_g is suspected to decrease with increasing temperature which could be a result of plasticization.

6.3. Ultraviolet Irradiation Conclusions

However, unlike demonstrating mechanical performance loss when being subjected to extreme temperatures or moisture, the PU foam material responded differently to UV exposure. Similar to being exposed to high temperatures, UV also induces cross-linking or additional cure. This is a result of the material not being fully cured during the processing procedure. This additional cross-linking initially increased the mechanical performance. However, as cross-linking is occurring, chain scission is also taking place, which results in a breakdown of the polymer chains and decomposes the material. After some time, the cross-linking is likely to stop and chain scission will continue which will than drop the mechanical performance. Also, unlike moisture causing plasticization and softening the material, UV increased the brittleness on the surface, which will locally increase the strength and stiffness. However, UV only penetrates the surface and slightly lower than the surface. This slight penetration and localized performance change does not affect the material to as high of extent as other environmental conditions (i.e. temperature and moisture).

The 515-9.5 series displayed a 11.7% increase in strength and 9.6% increase in modulus after 240 h of exposure; although, the standard deviation greatly increased for the exposed samples. The 515-9.5-wr series showed a slight increase in properties at 240 h and then decreases at 480 h of exposure. This is attributed to first, the cross-linking increasing the properties followed by chain scission decreasing the properties. The 515-9.5-wr resulted in a 2.7% and 3.2% decrease in strength and stiffness respectively. These slight

decreases fall in standard deviation with the baseline panels and the discrepancy could also be a result of slight processing variations. Again, a 95% confidence level was determined for each sample set to verify the test data is valid (good correlation between confidence level and standard deviation).

6.4. Ultraviolet/Condensation Conclusions

FTIR results confirm that UV does in fact provide additional cross-linking of the reinforced PU foam through the disappearance in intensity of the 2260 cm^{-1} NCO band. This band results in the additional curing of the isocyanate with the polyol. The signal at the 3300 cm^{-1} peak is characteristic of the stretching vibration of the N-H group. The decrease of the intensity of the band corresponding to the N-H group stretching vibration indicates a decomposition of urethane structures as a result of UV irradiation. Compositional changes have been indicated to occur upon exposure to UVA. It is likely to induce chain scission which would presumably lead to re-association of polyurea molecular segments. It is also possible that the surface species are oxidized leading to the formation of carbonyl groups, predominantly formation of polyurea [36]. The results of FTIR also confirm that the majority of the compositional changes occur primarily on the surface and within the first 0.25 mm of material from the surface.

Color and compositional changes were noted very quickly within the reinforced PU foam (less than 240 h). The discoloration is a result of photoxidation occurring on the surface due to the aromatic ester structure of the urethanes via a quinonoid route. This structure is a strong chromophore, which results in the yellowing of the polymer. The discoloration was characterized through colorimetry and calculating the YI. The non-woven roving series exhibited a 418% increase YI after only 240 h of exposure. However, the mechanical properties were hardly affected within the first 240 h and further exposure to UVA should be conducted to better demonstrate the overall material performance when subjected to UV long-term. Further testing would continue to cause

chain scission and further break down the polymer structure. Compositional changes should be monitored by FTIR and microscopy for functions of time duration and depth. In addition, it would be interesting to determine the rate of cross-linking versus chain scission. Lastly, testing should be done to determine what amount of cross-linking is caused by the exposure to UV versus elevated temperature.

Besides being subjected to UV and elevated temperature, a series of panels were subjected to a combination of UV, elevated temperatures, and condensation. The testing consisted of three panel variations including: no filler, carbon black filler, and sunflower hull filler. The addition of sunflower was to utilize an agricultural by-product as a filler to hinder the degradation effects of UV with the lignin component of the natural fibers, while also sustaining similar properties. The addition of carbon black is to resist degradation to UV but has an insignificant effect on the mechanical properties.

The neat PU showed the lowest drop in mechanical strength of 3.7% compared to 13.7% and 17.0% for the carbon black and sunflower filled respectively. However, the sunflower filled exhibited the lowest decrease in strength resulting in a 9.3% drop versus a 13.6% and 17.6% respectively for the neat PU and carbon black filled. This goes to show that agricultural by-products could have the potential to be used for UV stabilizers. Additional testing would need to be done to further investigate the effects of the sunflower filler in PU foam composites. These very slight decreases in performance are a result from the UV penetration being near the surface and the bulk of the material unaffected.

The materials were tested at ambient temperature and oven dried to mitigate the effects of the temperature and moisture. However, further testing is needed to be executed to show if the effects from the temperature/moisture are reversible or irreversible. Exposure time to UV, temperature, and condensation also needs to be carried out longer to further demonstrate the effects UV have on the performance of the material. Besides the combination effects, the panels should be exposed to only UV for multiple durations. FTIR

and microscopy should be conducted after being exposed for longer durations to UV radiation in order to determine the depth of penetration along with any compositional changes that may occur throughout the material. After the extended exposure, the materials should be tested for mechanical properties as the previous panels were.

6.5. Fourier Transform Infrared Spectroscopy

The FTIR spectroscopy determined that the reinforced PU foam did not fully cure during processing which is common for the material. It was suspected that a secondary process to fully cure the material would improve the material properties. The post cure procedure consisted of placing the processed panel in an oven at an elevated temperature and did in fact promote additional cross-linking with the polymer chains (cure). The tensile test comparisons did also improve the mechanical performance by 30% increase in strength and 12% increase in modulus. The post cured panel resulted in an ultimate tensile strength of 55 ± 0.9 MPa versus a tensile strength of 42 ± 1.2 MPa for the neat panel. The modulus of elasticity also increased from 2204 ± 114 MPa to a 2465 ± 51 MPa due to the post cure.

6.6. Differential Scanning Calorimetry Conclusions

After the post cure tensile specimens were tested, it was important to determine the glass transition temperature along with the degradation temperature of the foam. The T_g and degradation temperature were determined using neat foam only, whereas the reinforcement would cause complications during testing and provide invalid test results.

6.7. Thermogravimetric Analysis Conclusions

The degradation temperature is defined as when the structure in the polymeric backbone breaks down, resulting in a drastic weight loss and a decrease in properties. It is determined using TGA where weight changes are observed and associated with the decomposition of the structure. The PU foam exhibited a first degradation temperature of

approximately 292 °C and a second degradation temperature of 618 °C. The T_g is the point where above this temperature, the material behaves in a more brittle behavior and below, the material is more ductile and is determined using DSC. The DSC measures temperature and heat flow associated with thermal transitions. The DSC measured a T_g of 127 ± 2 °C for the south press and 121 ± 4 °C for the north press. The discrepancy is a factor of the two presses having different mold materials. The next step was to show how the cross-linking would affect the T_g. It went to show that the mean T_g increased due to a secondary post cure procedure. A post cure process of 4 h at 100 °C resulting in a T_g increase from 119 ± 10 °C to 125 ± 14 °C accounting for a 5% increase.

Now after the tests are completed and the results are interpreted, it is apparent that the reinforced, rigid PU foam does is in fact very susceptible to environmental conditions. Each of the conditioning criteria had a different influence on the material which is determined by the structural backbone. The extreme temperatures appeared to have the largest influence on mechanical performance, whereas the UV and UV/condensation had the largest impact on visual properties. Now that the reinforced PU foam is characterized and a better understanding for how the material responds to the various environmental conditions, the material is more applicable for marine when considering the exposure conditions throughout the design process.

REFERENCES

[1] Strong, Brent A. Plastics: Materials and Processing. 3rd ed. Upper Saddle River: Pearson Education Inc., 2006.

[2] Daniel, Isaac M., Ishai, Ori. Engineering Mechanics of Composite Materials. 2nd ed. New York: Oxford University Press, 2006.

[3] Gibson, Ronald F., Principles of Composite Material Mechanics. New York: McGraw-Hill, Inc., 1994.

[4] Davies, Peter and Evrard, Guy. "Accelerated Ageing of Polyurethanes for Marie Applications" Polymer Degradation and Stability 92 (2007): 1455-1464.

[5] "QUV Accelerated Weathering" Q-Lab Corp. LU-0805.3-EN (2006).

[6] Ministry of Defense, Singapore. 06 December 2010. <http://www.mindef.gov.sg/cyberpioneer/images/today_17052005_IMDEX_img3.jpg. >

[7] "SpaceAge Synthetics." SpaceAge Synthetics, RV Repair, Plywood Replacement, Composite, Flooring, Rot Free, Truck Floor. 2008. Web. 09 Sept. 2010. <http://www.spaceagesynthetics.com/products/products.html>

[8] Agarwal, Bhagwan D., Lawrence J. Broutman, and K. Chandrashekhara. Analysis and Performance of Fiber Composites. 3rd ed. Hoboken: John Wiley & Sons, 2006.

[9] Pegoretti, Alessandro, Penati, A., "Effects of Hygrothermal Aging on the Molar Mass and Thermal Properties of Recycled Poly(ethylene terephthalate) and its Short Glass Fibre Composites" Polymer Degradation and Stability 86 (2004): 233-243.

[10] Mahieux, Céline A., "Effect of Temperature on Polymer Matrix Composites" Environmental Degradation of Industrial Composites, 2005.

[11] Strong, Brent A. Fundamentals of Manufacturing Materials, Methods, and Applications. 2nd ed. Dearborn, Michigan: Society of Manufacturing Engineers, 2008.

[12] Tang, Xiaodong, Whitcomb, J., Li, Y., Sue, H., "Micromechanics Modeling of Moisture Diffusion in Woven Composites" Composites Science and Technology 65 (2005): 817-826.

[13] Bao, Li-Rong, and Yee, A.F., "Moisture Diffusion and Hygrothermal Aging in Bismaledimide Matrix Carbon Fiber Composites-part II: Woven and Hybrid Composites" Composites Science and Technology 62 (2002) 2111-2119.

[14] Thomason, J.L., "The Interface Region in Glass Fibre-Reinforced Epoxy Resin Composites: 2. Water Absorption, Voids and the Interface" Composites 26 (1995): 477-485.

[15] Sutherland, L.S. and Soares, C.G., "Impact Behaviour of Typical Marine Composite Laminates" Composites Part B 37 (2006): 89-100.

[16] Compston, P., Jar P., and Davies, P., "Matrix Effect of the Static and Dynamic Interlaminar Fracture Toughness of Glass-Fibre Marine Composites" Composites Part B 29B (1998): 505-516.

[17] Johnson, H.E., Louca, L.A., Mouring, S., and Fallah, A.S., "Modeling Impact Damage in Marine Composite Panels" International Journal of Impact Engineering 36 (2009): 25-39.

[18] Veazie, David R., Robinson, K.R., and Shivakumar, K., "Effects of the Marine Environment on the Interfacial Fracture Toughness of PVC Core Sandwich Composites" Composites Part B 35 (2004): 461-466.

[19] Gellert, E.P., and Turley, D.M., "Seawater Immersion Ageing of Glass-Fibre Reinforced Polymer Laminates for Marine Applications" Composites Part A 30 (1999): 1259-1265.

[20] Mourtiz, A.P. and Mathys, Z., "Post-Fire Mechanical Properties of Marine Polymer Composites" Composite Structures 47 (1999): 643-653.

[21] Baral, N., Davies, P., Baley, C., and Bigourdan, B., "Delamination Behaviour of Very High Modulus Carbon/Epoxy Marine Composites" Composites Science and Technology 68 (2008): 995-1007.
[22] "Polyurethane Foam Gas-Producing Reaction." Dow Answer Center. Web. 11 Aug. 2010. <http://dow-answer.custhelp.com/cgi-bin/dow_answer.cfg/php/enduser/std_adp.php?p_faqid=5656&p_created=1168886940&p_topview=1>
[23] Schueneman, G. T., Lesser, A. J., Hobbs, T., and Novak, M., Evaluation of the Termal Degradation of Polymer Matrix Composites via Ultrasonic Spectroscopy and Fracture Toughness. ANTEC Papers Conference, 1999, New York, NY.
[24] Tsenoglou, Pavlidou, Papaspyrides. "Evauluation of Interfacial Relaxation Due to Water Absorption in Fiber-Polymer Composites" Composites Science and Technology 66.15 (December 2006): 2855-2864.
[25] Yang, Bin, Huang, W., Li, C., and Chor, J., "Effects of Moisture on the Glass Transition Temperature of Polyurethane Shape Memory Polymer Filled with Nano-Carbon Powder" European Polymer Journal 41 (2005): 1123-1128.
[26] Crank, J. The Mathematics of Diffusion. 2nd ed. London: Oxford University Press, 1975.
[27] Sabbahi A., Vergnaud J.M., "Absorption of Water at 100°C by Polyurethane Foam" European Polymer Journal 27.8 (1993): 845-850.
[28] Braun, Klein, Bernarding, Leitner, Mika. "Non-destructive, Three-Dimensional Monitoring of Water Absorption in Polyurethane Foams Using Magnetic Resonance Imaging" Polymer Testing 22 (2003): 761-767.
[29] Woo M, Piggott MR. "Water Absorption of Resins and Composites: IV Water Transport in Fiber Reinforced Plastics" Journal of Composite Technology and Research 10.1 (1988): 20-24.
[30] Sabbahi A., Vergnaud J.M., "Absorption of Water at 100°C by Polyurethane Foam" European Polymer Journal 27.8 (1991): 845-850.
[31] Sabbahi A., Vergnaud J.M., "Absorption of Water by Polyurethane Foam Modelling and Experiments" European Polymer Journal 29.9 (1993): 1243-1246.
[32] Leveque, David, Schieffer, A., Mavel, A., and Maire, J., "Analysis of How Thermal Ageing Affects the Long-Term Mechanical Behavior and Strength of Polymer-Matrix Composites" Composites Science and Technology 65 (2005): 395-401.
[33] Rosu, Dan, Rosu, L., and Cascaval, C., "IR-Change and Yellowing of Polyurethane as a Result of UV Irradiation" Polymer Degradation and Stability 94 (2009) 591-596.
[34] Singh, R.P., Tomer, N., and Bhadraiah, S., "Photo-Oxidation Studies on Polyurethane Coating: Effect of Additives on Yellowing of Polyurethane" Polymer Degradation and Stability 73 (2001): 443-446.
[35] Abu-Zeid, Nofal, Tahseen. "Photoacoustic Study of UV, UV-Thermal, and Weathering Degradation of Rigid Foam Polyurethane" Journal of Applied Polymer Science 29.8 (1984): 2443-2452.
[36] Yang, X.F., Vang, Tallman, Bierwagen, Croll, Rohlik. "Weathering Degradation of a Polyurethane Coating" Polymer Degradation and Stability 74 (2001): 341-351.
[37] "UV Properties of Plastics: Transmission & Resistance." Cole-Parmer Technical Library. 13 March 2009. <http://www.coleparmer.com/techinfo/print.asphtmlfile=Zeus_UV_properties. >
[38] White, J.R. and Shyichuk, A.V. "Effect of Stabilizer on Scission and Cross-linking Rate Changes During Photo-Oxidation of Polypropylene" Polymer Degradation and Stability 92 (2007) 2095-2101.